Ing. Stefan Wagner, BSc

High - Security and Privacy Ensuring Patient Locating System in Health Care Environment

Master's Thesis

to achieve the university degree of

Diplom-Ingenieur

Master's degree programme: Biomedical Engineering

submitted to

Graz University of Technology

Supervisors: Univ.-Prof. Dipl.-Ing. Dr.techn. Christian Baumgartner

Institute of Health Care Engineering
Stremayrgasse 16/II
A - 8010 Graz, Austria

Ass. Prof. Dipl.-Ing. Dr.techn. Peter Söser

Institute of Electronics
Inffeldgasse 12/I
A - 8010 Graz, Austria

in Cooperation with

Infineon Technologies Austria AG

Advisor: Dipl.-Ing.Ing. Georg Skacel, BSc

Affidavit

I declare that I have authored this thesis independently, that I have not used other than the declared sources/resources, and that I have explicitly indicated all material which has been quoted either literally or by content from the sources used. The text document uploaded to TUGRAZonline is identical to the present master's thesis.

Date

Signature

Acknowledgements

I would like to express my sincere thanks to both of my supervisors, Univ. - Prof. Christian Baumgartner and Ass. Prof. Peter Söser for always having an ear and eye open. At this point I also would like to thank my employer Infineon Technologies Austria AG for giving me the opportunity to write my master's thesis under such professional conditions.

My special thanks also go to my colleague and mentor at Infineon Technologies, Georg Skacel, for his professional and personal support. His very broadly based knowledge was important for pointing the way into the right direction, be it in a good or rather unpleasent situation of this master's thesis.

Special thanks goes to my parents, Maria and Alois, and to my siblings, Jasmin and Alexander, for the continuous support and encouraging words in all situations of my life and studies.

Abstract

In the hospital sector it is important to be able to correctly identify and assign patients. Additionally, to know the current whereabouts of the patient is a key role for the regular procedure and is the ideal statement, but leaving the hospital sector earlier and being undetectable is becoming more common than expected. There may be several reasons, for example an arbitrary disappearance or disorientation due to dementia. Currently, the task is performed by clinical staff which is a potential weakness.

The aim of this master's thesis is to find potential solutions and improvements to decrease weak spots and to automate this process in an easy way. According to this, currently technologies for applications are evaluated and major parameters for clinical applications for a smart wearable device for patient locating are defined.

Kurzfassung

Im Krankenhausbereich ist es wichtig Patienten richtig zu identifizieren und zuweisen zu können. Zudem spielt der aktuelle Aufenthaltsort des Patienten eine wichtige Rolle für einen geregelten Ablauf. Es kommt jedoch immer häufiger vor, dass Patienten den Krankenhausbereich verlassen und nicht mehr auffindbar sind. Diese Gründe können verschiedenster Natur sein, sei es beispielsweise durch eigenwilliges Verschwinden oder durch Desorientierung verursacht durch eine Demenzerkrankung. Die derzeitige Umsetzung erfolgt durch das Personal, jedoch stellt diese Art eine potentielle Schwachstelle dar.

Das Ziel dieser Masterarbeit ist es, potentielle Lösungen und Verbesserungen zu finden um diese Schwachstelle zu minimieren und den Vorgang zu automatisieren. Dementsprechend werden aktuelle Technologien evaluiert und die wichtigsten Parameter für den Einsatz im Krankenhausbereich für ein handliches, stabiles und tragbares Lokalisierungsystem definiert.

Glossary

AC Alternating Current
ADS® Advanced Design System
AIDC Automatic Identification and Data Capture
ATT Attribute Protocol
BLE Bluetooth Low Energy
Bluetooth SIG Bluetooth Special Interest Group
BR Basic Rate
CE Conformité Européenne
CL Contactless
CRC Cyclic Redundancy Check
DC Direct Current
DoF Degree of Freedom
EAS Electronic Article Surveillance
EC European Commission
EDR Enhanced Data Rate
EEC European Economic Commission
EMI Electromagnetic Interference
FDA Food and Drug Administration
GAP Generic Access Profile
GATT Generic Attribute Profile
GFSK Gaussian Frequency Shift Keying
GPIO General Purpose Input Output
GPS Global Positioning System
GSM Global System for Mobile Communications
GUI Graphical User Interface
HCI Host Controller Interface
HFSS® High Frequency Electromagnetic Field Simulation
HIPAA Health Insurance Portability and Accountability Act
IC Integrated Circuit
ID Identifier
IDE Integrated Development Environment
I2C Inter-Integrated Circuit
ISM industrial, scientific, medical
IoT Internet of Things
IO Input Output
LAN Local Area Network
LED light-emitting diode
LL Link Layer

L2CAP Logical Link Control and Adaption Layer
MAC Medium Access Control
Mbps Megabit per second
MDD Medical Device Directive
MOSFET metal - oxide - semiconductor field - effect transistor
NFC Near Field Communication
PHY Physical Layer
PCB Printed Circuit Board
PCD Proximity Coupling Device
PICC Proximity Integrated Chip Card
QR Quick Response
RF Radio-Frequency
RFID Radio-Frequency Identification
SE Secure Element
SMP Security Manager Protocol
SoC System on Chip
TEG Thermoelectric Generator
UART Universal Asynchronous Receiver/Transmitter
UUID Universally Unique Identifier
USB Universal Serial Bus
WEP Wireless Equivalent Privacy

Contents

List of Figures

List of Tables

1 Smart Wearables

The smart wearable chapter will brief highlight the current state of affairs in the area of smart wearable and smart medical devices designed as a wristband. The leading focus is set on sensing vital parameters, secure data storage and the offering of technology for localisation. Interesting is also the possibility of data encryption for such devices. Afterwards, a short introduction and a summary of all advantages and disadvantages of the common wireless technologies should give an understanding for the chosen wireless technology at the end. Decisive for this is the ability of usage with counterparts in a system, the communication range and the aspect of energy consumption. Finally, licensing fees and software costs are taken into account.

1.1 State of the Art

Indeed, every year smart devices gain increasing popularity, which, of course, can be attributed to the technology process in miniaturization of integrated circuits, increased performance with most simultaneous reduction in power consumption and the tolerable price range for the market.[18] [17] Nowadays, smart wearable devices are used more and more for health promotion in the private sector and enjoy the increasing popularity due to sensing vital parameters. [43]

The application of smart wearable wristbands in the hospital sector keeps within limits. Other and, of course, higher regulations must be observed in this market, rather than in the customer market. In addition, the system integration in the existing health care IT - system makes the life not easier.

Nowadays, outpatients waiting in a wheelchair or on a hospital bed for examination and inpatients get a medical plastic wristband for identification. Figure 1.1 shows an example of a medical plastic wristband from Mediaform® for the health sector which contains the Conformité Européenne (CE) marking and meets the essential requirements of the Medical Device Directive (MDD) 93/42/European Economic Commission (EEC) and 2007/47/European Commission (EC), therefore it is classified as a Class I medical device. The medical plastic wristband contains various informations of the patient, for example the first and last name, the birth date and can also be printed with a barcode and Quick Response (QR) - code to get access to the patient record. Additionally, the wristband can be printed with colour coding which helps doctors and nursing staff to immediately identify risk factors, for example allergies or hepatitis disease. [32]

Another company, who offer medical wristbands, is Honeywell with the Inband II wristband or Infant Inband II Bracelet / Tag for patient identification which is compareable

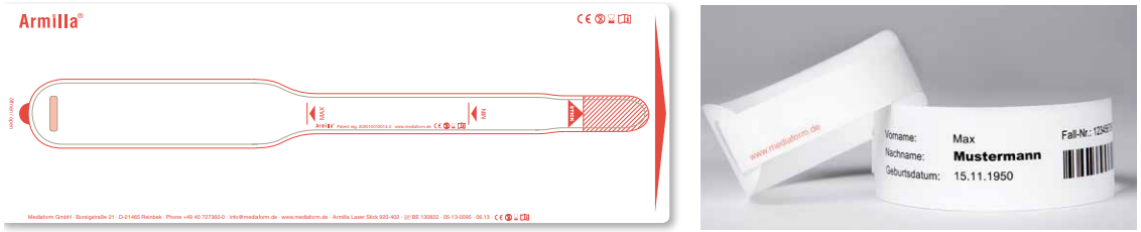

Figure 1.1: Armilla® Laser Stick Erwachsene [32]

to the Armilla® wristbands. Informations are printed onto the wristband with a desktop printer and are compliant to the Health Insurance Portability and Accountability Act (HIPAA) regulation to ensure the security of patient-related data. [22]

1.1.1 Smart Wearable Wristband Devices

Smart wearable devices for motion tracking were one of the first developments for the customer market. People should be motivated by wearing those devices by tracking the daily walking distances or do daily workouts and perform exercises. During walking or doing exercises, sensors on the device will measure physiological parameters and store all the information local on the device or make them available on a cloud storage. Resulting data shows the activity and routine of the person and can take a part on motivation to maintain a healthy life. [7] [20]

Motion detection can be measured by adding 3-axis accelerometers and auxiliary combination of magnetometers or gyroscope sensors in the system. By using only the 3-axis accelerometers, the system maintain 3 Degree of Freedom (DoF), which can detect movements in three directions, by adding all three mentioned devices, the result is a system for 9 DoF detection. [15] [20]

1.1.1.1 Customer Oriented

1.1.1.1.1 CARE Medical History Bracelet The CARE™ medical history bracelet is a small bracelet with up to 2 GB of memory storage and a Universal Serial Bus (USB) interface to write or read data, which works with the CARE e-Manager Software. Accordingly, the person always carries its own medical history with it and the records can be viewed in emergency cases. [4] Due to the system approach there is no communication technology included in this bracelet, so there is no possibility for sensing vital parameters or locating the person in a given range. Furthermore, no details were found by encrypting the personal-related data in the device itself.

1.1.1.1.2 Smart Watches Companies like Apple, Fitbit and Samsung provide smart watches and fitness tracker in their portfolio with various communication technologies inside. All of them contain a heart rate sensor, one or more gyroscope sensors, accelerometers and in most cases different wireless technologies, for example Bluetooth, Wi-Fi,

Cellular network or Global Positioning System (GPS). [3] [15] [45] A more detailed analysis is not carried out here because of different types of fitness trackers and smart watches. Additionally, all of them use nearly the same technologies and each device has no Food and Drug Administration (FDA) clearance.

1.1.1.1.3 Verily Study Watch The Study Watch from Verily, formerly Google Life Sciences, is a device designed with sensors for heart rate and skin resistance measurements and includes a cloud infrastructure to analyze and collect personal-related physiological and environmental data. All data is encrypted on the watch itself to increase security. The design is harmonized for the daily use, so the user is able to see the current time on a display and it looks like a accessory and not like a medical device. With a Wi-Fi interface or by using a cellular network, data from the watch can be transferred into the cloud and will be analyzed afterwards by backend algorithms and machine learning tools. Currently, the watch is used in clinical studies but has no FDA clearance. [48]
The utilized encryption method on this watch is unknown and since this watch is currently only used in several observational studies it is difficult to get more informations about.

Figure 1.2: Verily Study Watch [48]

1.1.1.2 Medical Device Oriented

Smart wearable devices have already found their way into the health care sector and this market is properly growing. An important part is the ability of self-monitoring and preventive medicine for chronically ill and elderly people, which hardly relates to the Internet of Things (IoT) to support the aspect of telemedicine. Telemedicine was originally developed to reach remote patients living in rural areas far away from physicians or health care facilities. The incentive is to develop technologies and applications, which are able to reduce overall costs for prevention, monitoring and also prevent or reduce hospitalization. [20] [43] [29] In order to achieve this, smart wearable devices must be able to constantly monitoring health indicators. Examples are continuous monitoring the blood pressure or glucose level. [29] Furthermore, not only the sensor part plays a major role for these devices. The ability to handle connections to other devices like a blood pressure monitor or weighing scale via wireless technologies is crucial for telemedicine

technology. The technical implementation of telemedicine is separated into two units. The telemedicine unit is located at the patient's site and the base station unit is located at the health care facility or physician's site. Therefore, an example is that measured information will be immediatly transfered from a blood pressure monitor to a smartphone and afterwards transmitted via Global System for Mobile Communications (GSM) or other communication technologies to the base station. [47] [24]

A look at the current wearable market shows that the majority of commercially available smart wearable devices are able to measure different vital signs, but they are not qualified for medical use. Therefore, these devices are not suitable for monitoring physiological parameters of high risk patients.

1.1.1.2.1 Philips Health Watch The Philips Health Watch, figure 1.3, is a medical device for home use and is also listed in the FDA. It is classified as a Class IIa medical device and fulfills the requirements of MDD 93/42/EEC and 2007/47/EC. A combination of a tri - axial accelerometer to measure motion and green light - emitting diode (LED) with a photodiode to create a photoplethysmogram enables tracking of vital physiological parameter like heart rate and movements. With these physiological parameters it is possible to derive the resting heart rate and the energy expenditure of persons who suffer under lifestyle related disease like cardiovascular disease and diabetes type 2. The daily monitoring of these parameters reflects the physical activity of the person and heart rate changes over the monitoring time.

According to used technologies within the watch, personal - related data will be transfered via Bluetooth by using the Philips HealthSuite health app on a smartphone. Afterwards, all relevant data will be analyzed on the smartphone and not on the watch itself. All calculated information is based on clinically validated algorithm. Locating several Health Watch users is possible due to the Bluetooth Technology, but it is not designed for this use case. Besides, informations about an continuous advertising mode cannot be found. With a durable life time of at least four days with one battery charge, the watch itself has good preconditions for the locating use case. [41]

Figure 1.3: Philips Health Watch [41]

1.1.2 Wireless Communication Technologies

1.1.2.1 Bluetooth Low Energy (BLE)

BLE is a low - power wireless technology, which uses the 2.4 GHz industrial, scientific, medical (ISM) band with 40 different RF channels. Depending on the output power and the sensitivity power from the receiver, BLE can send data packets from a few meters up to 100 meters in ideal environmental conditions. [21]
BLE SoC solutions are designed for lower - power consumption. [12] Measurements from Nordic Semiconductor shows that the nRF52832 BLE SoC draws approximately 30 μA in a 500 ms advertising event under defined specifications. [37] Nowadays, the price on low volume devices is mostly less than EURO 10 for such SoC solutions and rapidly decreases by high volume order. In addition, designing BLE applications has benefits due to the free access to programming tools and the core specification without any licensing costs or fees. Also the counterparts, such as smartphones or notebooks, are highly spread.

1.1.2.2 Wi - Fi

The IEEE Standard 802.11 includes the results from the development of wireless Local Area Network (LAN) networking and offers specifications for the Medium Access Control (MAC) and Physical Layer (PHY). [10] Wi - Fi implemented systems can communicate via the 2,4 GHz, 3,6 Ghz, 5 GHz and 60 GHz frequency bands. [11] The stream data rate vary between a few Mbit and 6,75 Gbit per seconds and data can be transmitted in different ranges. Therefore, a distinction is made between indoor communication with a range of 20 m and outdoor communication up to 100 m. [43] The power consumption of Wi - Fi depends on data rates and the utilized chipset. Additionally, with the utilization of a powerful microprocessors to control the power management of the Wi - Fi module a lower power consumption can be reached. [55] For high data rate applications Wi - Fi is a sufficient solution if the provided higher data rate is compared to the higher energy consumption. [9]

1.1.2.3 Zigbee

Zigbee is a wireless technology which uses the 868 MHz, 915 MHz and the ISM band of 2.4 GHz with a transmission range up to 100 m and is designed as BLE to maintain the communication between devices over a short distance. [36] The protocol supports the mesh network to extend the communication via mesh topology and is classified as a low power consumption technology. The main utilization is to handle the data transfer between sensor nodes. [2] According to the power consumption, Zigbee has only slightly higher current consumption in the sleep, receiving and transmitting mode than BLE. [36] One common application is the smart home automation. One example is the smart lamp Hue from Philips, which uses the Zigbee technology. [41]

1.1.2.4 Decision between Wireless Technologies

Dementyev A. et al. has shown that the BLE and Zigbee protocol are real low-power consumption technologies, whereby BLE has a small edge compared to Zigbee. The current consumption is significantly lower and was measured for 60 packet transmissions with five different sleep intervals and a packet transfer of 8 Byte per transmission interval. [12] Nair K. et al. has tested both wireless standards for energy consumption with the result that BLE draws less current and also connected faster than Zigbee. [36]

In comparison to Wi-Fi, BLE has much lower bit rates than Wi-Fi and can only send small data packets. According to the energy consumption, a Wi-Fi module with an additional microprocessor can have a smaller power consumption than a BLE SoC. Measurements were taken for comparing both technologies by connection handling and data transfers from a sensor. [55] From the security point of view Wi-Fi uses 256 bit encryption by using the Wireless Equivalent Privacy (WEP) and WPA2-AES security accesses, whereas BLE can handle only 128 bit encryption by using AES-CCM. [6]
The decision now falls on the BLE technology due to the required low data rates, the free software, a good BLE community, the low power consumption and a sufficient range for transmitting data or locating other devices. A Wi-Fi solution sounds interesting, but due to the conclusion from [55], another controller is needed to decrease the power consumption. Therefore, a Wi-Fi module, a powerful controller and a SE should be used to fulfill the requirements instead of only two controllers. Furthermore, with three controllers another programming effort and a source for issues exists in the system.

Goal of the Thesis

The goal of this master's thesis is to design a smart wearable wristband with the cabability to correctly identify and assign patients and to determine the current whereabout in the hospital sector. An implementation of two wireless communication technologies enable the identification and localization of patients. Therefore, a SE enables the secure data storage of information and provides an encrypted data transfer via a Near Field Communication (NFC) interface to a reader device. Authorized medical staff can read and change the patients data accordingly in case of an upcoming medical procedure or control. A BLE controller enables the localization of patients in the hospital sector and provides data to be sent over longer distances up to 100 m. A suitable base station should be implemented into the system to fulfill the function of locating patients indoor and outdoor.

Since the energy consumption is a limiting factor for the life time of such devices, possibilities need to be found to enhance the life time of this wristband.

2 Basics

2.1 Bluetooth Low Energy Basics

In this chapter, readers will get a brief introduction to the wireless technology of BLE, which started as a part of the Bluetooth 4.0 Core Specification, by including the system architecture, the controller, host and application properties.

2.1.1 Introduction

Bluetooth Low Energy was designed by Nokia and was adopted by the Bluetooth Special Interest Group (Bluetooth SIG) in 2011 to offer a wireless technology for ultra-low power applications in a new way. Consequently, the BLE technology plays a major role for the big wave of IoT devices nowadays due to the big market segment growth in smartphones and tablets.[57] The classic Bluetooth technology was developed to offer a link to communicate with peripheral devices and separate the parts of computing and communication in such applications. Some examples can be seen in the music streaming to wireless headsets, calling via the hands-free car kit or data transfers between smartphones. These applications can only be handled with higher data rates started with the Basic Rate (BR) of 1 Megabit per second (Mbps), to the Enhanced Data Rate (EDR) of 3 Mbps and with an additional version even up to hundreds of Mbps.

The BLE technology was not developed to reduce the current consumption of such systems. It is more of a rethought of the technology to make it easier for developers and to penetrate new market segments. The goal is to develop applications for a life time of months or years, only powered by a small coin cell, instead of Bluetooth systems, which works only a few hours. Furthermore, BLE systems should work in a robust way all over the world and reduce the costs due to the high volume design approach. [21]
But how can this new wireless technology provide such goals? The three key elements are the proper selection of the:

- Frequency band
- IP license
- System components or materials within an application

Starting with the frequency band for the communication, the 2,4 GHz ISM band was chosen to reduce the costs instead of paying for a licensed spectrum. According to the IP license, Nokia has chosen the Bluetooth SIG to reduce the cost for patent licensing instead of joining the Wi-Fi Alliance. And finally, for high volume markets, devices has to be cheap and this requirement can only be satisfied with small numbers of components

which are in a low price range. As mentioned above, a coin cell to power a BLE application for a few months or even years is price worth. The other side of a coin cell powered BLE device can be the smartphone and this is significant to be successful with this wireless technology. [21]

2.1.2 Components of BLE Systems

Figure 2.1 shows the architecture which roughly consists of the controller, host and at least the application. [21] [49] [56]

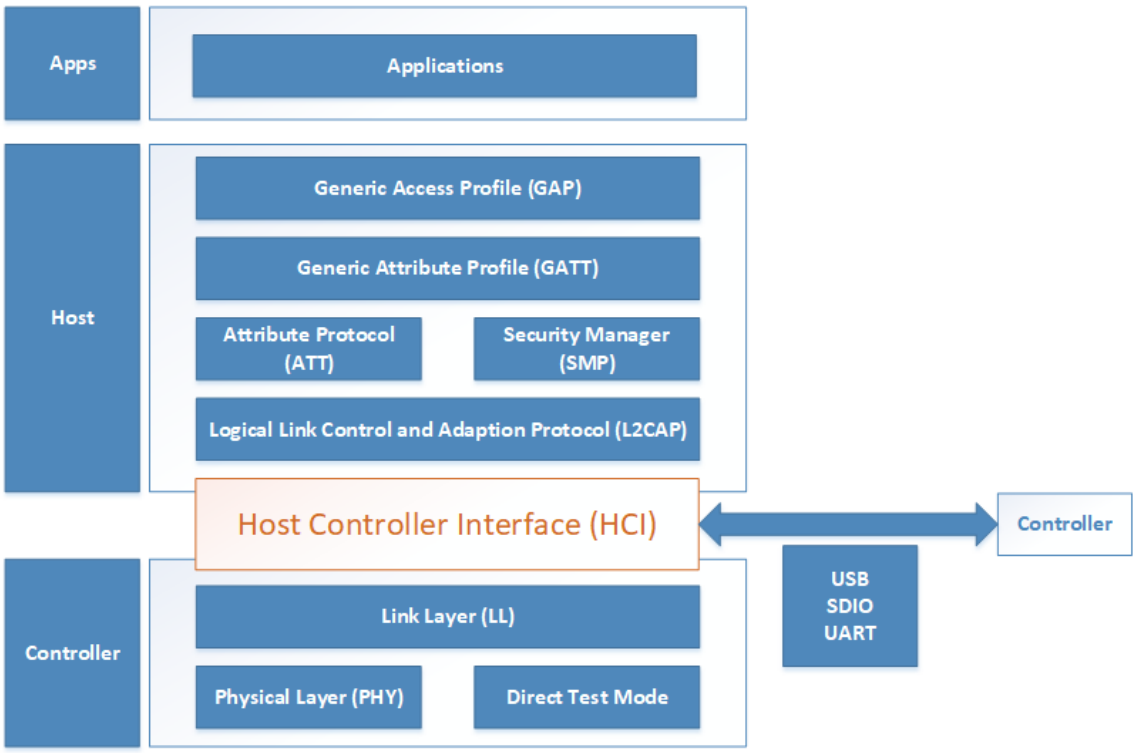

Figure 2.1: Bluetooth architecture overview.

2.1.2.1 BLE Architecture - Controller

The controller is the only physical part of the architecture to handle the radio signals for transmitting or receiving data packets. It contains interfaces for two separated tasks - the antenna interface to connect an external antenna or chip antenna component and on the other side the host Host Controller Interface (HCI), which is the only interface to the host. The HCI plays an important role in handling the communication within the chip or to an external microprocessor. The controller part in the architecture also embeds the Link Layer (LL), the PHY, the Direct Test Mode and as mentioned above the HCI. [21]

2.1.2.1.1 Physical Layer The Physical Layer handles the transmission and the reception of radio signals and uses the Gaussian Frequency Shift Keying (GFSK) modulation scheme to modulate data from the host on the radio signal base band of 2,4 GHz. The range of RF channels reaches from 2,40 GHz to 2,48 GHz. Therefore, the 2.4 GHz band is split up into 40 RF channels with operating channel frequency of 2 MHz, whereupon 3 RF channels are only for advertising and the other 37 channels are for data transmission in the connection mode. An adaptive frequency-hopping engine enables RF channel switching when interferences are detected on the transmission channel. [56]

2.1.2.1.2 Direct Test Mode The Direct Test Mode in the layer allows raw RF tests with the Physical Layer to control wether compliance with the Bluetooth specifications is guaranteed. This mode will be mainly used for production and certification tests. [21]

2.1.2.1.3 Link Layer The LL manages two different channel modes. One channel is for advertising, this means that no connection will be created between two devices and the second channel is the data channel for active connections. As mentioned above, only three of 40 RF channels are reserved for advertising, the rest will be used for connection handling. Furthermore, this layer is responsible for advertising, scanning and the part of connections handling between devices. [56]

2.1.2.2 BLE Architecture - Host

The Host is the next scope in BLE which takes a part in multiplexing layers and handling of different protocols and procedures which are shown in figure 2.1.

- Logical Link Control and Adaption Layer (L2CAP)
- Security Manager Protocol (SMP)
- Attribute Protocol (ATT) [21]

2.1.2.2.1 Logical Link Control and Adaption Layer (L2CAP) Bottom up, the L2CAP takes over the task of multiplexing layer of channel and signaling commands. In BLE the channel for signaling, SMP and the ATT are fixed and uses only one packet structure format for each channel as shown in figure 2.2. Therefore, the packet structure contains the length of the data payload, followed by the channel Identifier (ID) and at least the data payload. [21] [56]

2.1.2.2.2 Security Manager Protocol (SMP) The SMP handles the authentication and secure connection between devices. The protocol itself defines rules for pairing, which includes the authentication process to trust the other device, followed by the link encryption to handle the key distribution between devices. The key is generated by a series of of security algorithm. [56]

2.1.2.2.3 Attribute Protocol (ATT) The last protocol of the Host is the ATT, which defines the data access on a peered device, where data is stored as so called attributes by a dedicated address and label. Each attribute can be uniquely identified by the Universally Unique Identifier (UUID), which comprises of 128 Bits. [56] When such a device will read some attributes from an peered device, the device, storing data as attributes, is called server and on the other site the reading device is called client. To read data from the server, it is necessary to send a request and the server replies with a response message. With this procedure the client get all attributes from the server. [21]

Figure 2.2: Link Layer packet structure (adapted from [49])

Now the focus is set on the Host profiles, which are listed below.

- Generic Access Profile (GAP)
- Generic Attribute Profile (GATT)

2.1.2.2.4 Generic Attribute Profile (GATT) The GAP is set one level higher than the ATT and is therefore described as a layer to offer high - level services, which includes one or more characteristics, or in other words subtasks. [57] The GATT has the purpose of managing the data transfer process and defines the role of the device in a connection. As mentioned above, the device can therefore be a client or server. When a client will read data from a server, it sends a request to the server and except a response. This procedure will now packed into a service. [56]

2.1.2.2.5 Generic Access Profile (GAP) The GAP defines how devices can be discovered, connected or actively maintained a connection. Besides, the name of the device can also be determined, which is important for the connection handling. [21] The GAP includes different roles for the device, such as Broadcaster, Observer, Central or Peripheral which were briefly described below. [56]

Broadcaster In the broadcasting role, the device sends advertising packets continuous or in interval. These packets include data from a service, which will be send to other devices that eventually are in the observer role. All devices have the ability to receive the advertising packets except transmit - only device. [56]

Observer An observer describes the counterpart of the broadcaster. This device can read advertising packets and listen to the incoming data but does not support incoming connection requests. [56]

Central and Peripheral The central and peripheral role only exists if a connection appears between two BLE devices. This role is compareable with a master - slave architecture, where the master acts in the central role and the peripheral vice versa. Devices in the central role are able to handle more than only one connection to a device at the same time and can also only initiate a connection request. Peripheral devices can send advertising packets followed by being discoverd by the central device but can not start a connection request. [56]

For the Application Layer, which is above the GATT and GAP, theGAP also groups up the different attributes from the GATT server to create characteristics and profiles. [56]

2.1.2.3 BLE Architecture - Application

The last stack in the BLE architecture is the Application Layer, which presents different applications that uses grouped attributes. All three properties of the Application Layer were listed below:[56]

- **Profiles**: set of services
- **Services:** set of characteristics
- **Characteristics:** labeled with a UUID

2.2 Radio-Frequency Identification (RFID) Basics

2.2.1 Introduction

RFID is a contactless communication technology, which will be used in many various applications these days. One of the common use cases is probably the Electronic Article Surveillance (EAS) which is used to prevent shoplifting in nearly every retail store or in libraries nowadays.[14] A further example in our daily working routine is the access control, which can be handled by card to get entry in several rooms or not.

Technologies like RFID typically considered as part of the AIDC, which includes for example smart cards, barcode systems, biometrics or optical character recognition. [23] Figure 2.3 shows an overview about the AIDC included technologies.

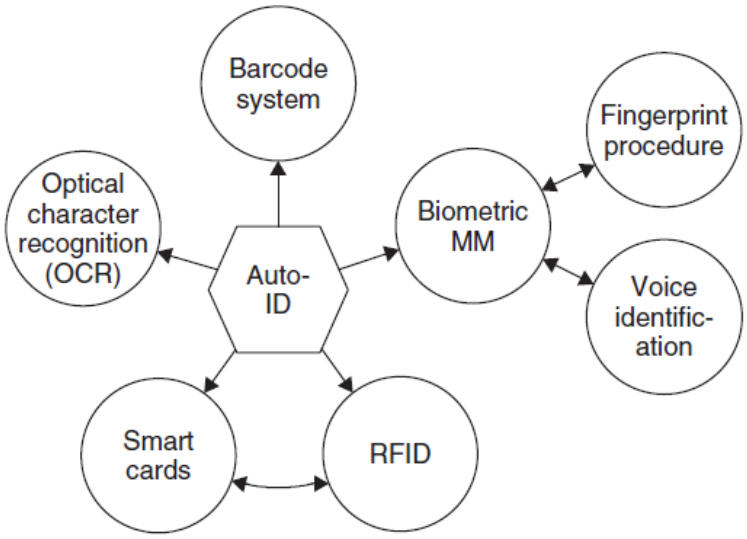

Figure 2.3: Overview of AIDC systems [14]

Fundamentally, RFID systems are contactless systems, which means that the system will be supplied by energy from electric, magnetic or electromagnetic fields of a reader. Also the data exchange between a RFID system and a reader is only possible via external fields, like mentioned before.

Furthermore, a distinction can be made between RFID systems in their application level. So called EAS systems are assigned to low - level applications and do not need a memory for a huge amount of data. These systems take up most of the RFID market. On the other hand, high - level applications, like cards for access control, credit cards and also passports contains a memory for personal - related data. Depending on the reading range all systems were additionally classified into three different ranges, the so called low - end, mid - range and high - end systems. [14]

2.2.2 Components of RFID Systems

RFID systems for 13,56 MHz always consist of two main components to fulfill a communication system, which includes a reader and a transponder (tag), shown in figure 2.4. The reader acts as main station and transmits the electric, magnetic or electromagnetic field for physical coupling. Therefore, the emitted field provides an energy supply for a present transponder to establish the communication towards it. The readers main part is therefore to control the communication for receiving and transmitting data from the transponder in the field. However, there are exceptions for writing data to a transponder which depends on the application on the transponder. [14]

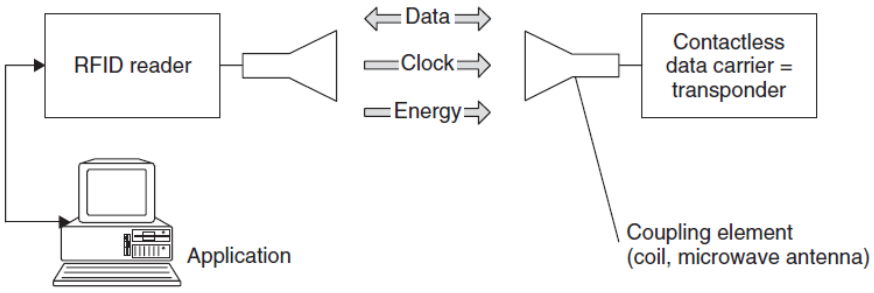

Figure 2.4: Main components of a RFID system [14]

2.2.2.1 Reader

The reader acts as transmitter and receiver in the communication path and provides a reader field, the so called interrogation zone, for the transponders. Like in any communication system, one device acts like a master and the second device as slave, therefore the reader handles the commands for communication with the transponder. Furthermore, a reader usually contains an additional interface for communication or command handling

via personal computer. Such interfaces can be a RS 232 oder RS 485 interface. [27] Modern devices often provide a USB interface for communication handling.

2.2.2.2 Transponder

The transponder is the data - carrying device in the RFID system and consists of a coupling element, which is an antenna and a controller or a microprocessor, both components are shown in figure 2.5. In a low - level system, a transponder only includes an identification or serial number, which can be read by the reader. This will be commonly used in EAS systems, where only the presence of the transponder in the reader field will be detected. [14]

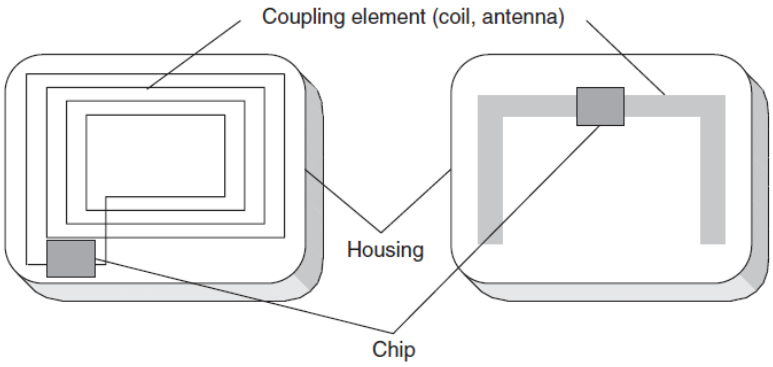

Figure 2.5: Basic layout of the RFID data-carrying device, the transponder. Left, inductively coupled transponder with antenna coil; right, microwave transponder with dipolar antenna [14]

2.2.2.2.1 Active Transponder Active transponder include a energy storage device, usually a small battery or a solar cell to power itself. Therefore, the transponder does not need the reader field as power supply but for data modulation, because they work as a slave in this system. This system can enhance the communication range in comparison to passive transponder only when the weak reader signal can be detected in higher distances. [14]

2.2.2.2.2 Passive Transponder Passive transponders has no energy storage device and all power required for communication must be drawn from the reader field in the interrogation zone. Once the device is within the interrogation zone, it acts totally passive and is the device within the interrogation zone, but far away from the reader, the device can operate with the drawn power but only with a very low performance. To transmit data from the transponder to the reader, the transponder modulates the field from the reader via load modulation or modulated backscatter. Naturally, the transponder can also store energy from the reader field for a short time. [14]

2.2.3 Classification

Systems for RFID applications can be separated into different classes, therefore it can be differentiated in frequency transmission, in the coupling range and in the system classification.

2.2.3.1 RFID Operating Frequency

RFID systems can be separated into three reader transmission frequency classes, shown in the list below. [27]

- **Low Frequency (LF):** range from 30 to 300 kHz
- **High Frequency (HF):** range from 3 to 30 MHz
- **Very High Frequency (VHF):** 300 MHz to 3 GHz

2.2.3.2 Ranges and Basics of Coupling

A distinction is also made in the coupling range, therefore close-coupling devices are able to communicate over a distance from 0 to a maximum of 1 cm. The next enhanced range is the remote-coupling range with a distance of 0 to 1 m and the last one, is the long-range, where 1 m is the lowest distance for communication (up to 15 m). [14]

2.2.3.2.1 Close-Coupling Close-coupling provide RFID only over a very small distance up to 1 cm. The coupling can be performed by electric and magnetic fields from DC to 30 MHz. Systems for this coupling type are often applications with higher security level, for example passports or electronic door lock systems. [14]

2.2.3.2.2 Remote-Coupling With distances up to 1 m, remote-coupling devices are working to a high percentage with inductive (magnetic) coupling and only a small amount of them with capacitive (electric) coupling. Frequencies below 135 kHz or exactly 13,56 MHz can be used for such system. Common standards are the ISO 14443 (proximity coupling) for contactless smart cards or the ISO 15693 (vicinity coupling) for smart label and contactless smart cards. [14]

2.2.3.2.3 Long Range Long range RFID frequency systems have ranges above 1 m and uses electromagnetic waves for transmission. Therefore, these systems operate with the UHF frequency of 868 MHz in Europe and with a slightly higher frequency of 915 MHz in the USA. Such microwave applications use frequencies of 2,5 GHz and 5,8 GHz. [14]

2.2.3.3 System Classification

Transponder can be separated into three different classes, as mentioned above. So called low - end systems are 1 - bit transponders with only a microchip, but no additional memory for data storage. With exactly 1 - bit the reader has only two different states. The first one is that the transponder is in the field and the other one is that no transponder can be detected in the field.

The next classification contains transponders with an only readable memory which can include an ID number.

The third classification contains a memory and a microchip or microprocessor to process more complex reader commands. [14]

2.2.4 Physical Fundamentals of Antennas

This chapter explains the physical principles on basic level for proximity coupling RFID systems. However, only the inductive coupling transponders is dealt with due to the system approach for this master's thesis. Therefore, a separation of the transmitting electromagnetic field from the reader can be done into two parts. The first part is called near field, which dominates close to the antenna. The second part is called far field. A separation can be done, when the distance between the transponder and the reader is smaller than the transmitted wavelength of the reader field frequency divided by two times of π. Otherwise, if the distance is bigger in comparison to the mathematical expression below, the existing field in this distance is called far field. As an example, the mathematical expression for the near and the far field are mentioned below. [14]

Table 2.1: Units and abbreviations used

Variable	Symbol	Unit	Abbreviation
Lightning Speed	c	Metre	m
Wavelength	λ	Metre	m
Frequency	f	Hertz	Hz
Distance to Reader	d_r	Metre	m
Magnetic field strength	H	Ampere per meter	A/m
Magnetic flux density	B	Tesla	T
Magnetic flux	ϕ	Weber	Wb
Electric current	I	Ampere	A

$$d_r = \frac{\lambda}{2\pi} \tag{2.1}$$

$$\lambda = \frac{c}{f} \tag{2.2}$$

Due to the carrier frequency of 13,56 MHz for used RFID transponder in this thesis, the maximum reader distance for the near field is expressed below. The reason for this 13,56 MHz high - frequency alternating field is the NFC interface of the chip with the LA and LB pads for the coil or antenna. As the name near field communication suggests, the communication range will therefore be in the electromagnetic near field part.

$$\lambda = \frac{c}{f} = \frac{3 * 10^8\, m}{13,56\, MHz} \cong 22,12\, m$$
$$d_r = \frac{\lambda}{2\pi} = \frac{22,12\, m}{2\pi} \cong 3,52\, m$$

The result of the distance calculation with 3,52 m is much higher than the needed distance between the transponder and reader. Therefore, the reading distance with the NFC interface will be in a range of a few centimetres depending on the antenna parameters. With the given carrier frequency, the transponder is located in the near field of the reader.

2.2.4.1 Inductive Coupling

The basic principle of inductive coupling is that each current flow through a conductor creates a circular magnetic field around this conductor. By moving a conductor through a magnetic field, the field induces a voltage and by extension a current flow in this conductor. This procedure is called electromagnetic induction and can be increased by forming the conductor to a coil with one or more windings. The coupling principle is the placing of two conductors together on a common axis. Now with this placement the magnetic field of one coil, caused by an alternating current, can now pass through the second coil that generates a current, which can be seen in figure 2.6. Nevertheless, a current is generally only possible when one coil is under motion or the magnetic field in a coil is alternating. A distinction must, therefore, be made between whether this induction is wanted or not. In this case of RFID systems and proximity coupling, this coupling is, of course, wanted and intentional for the function. Unintentional coupling refers to Electromagnetic Interference (EMI) in nearby located circuits, which is called cross - talk. [27]

With only passive powered transponders, inductive coupling is the way to supply the chip on the transponder with energy from the 13,56 MHz magnetic field of the reader. The chip on the transponder does even need a rectified voltage supply, therefore, a diode is inside to rectify the induced voltage. Furthermore, a capacitor mentioned as C_1 in figure 2.6 is needed to form a resonant circuit with the inductance of the coil that corresponds with the frequency of the reader field. The reader part forms a parallel resonant frequency circuit with the inductance and the capacitor C_r. [14]

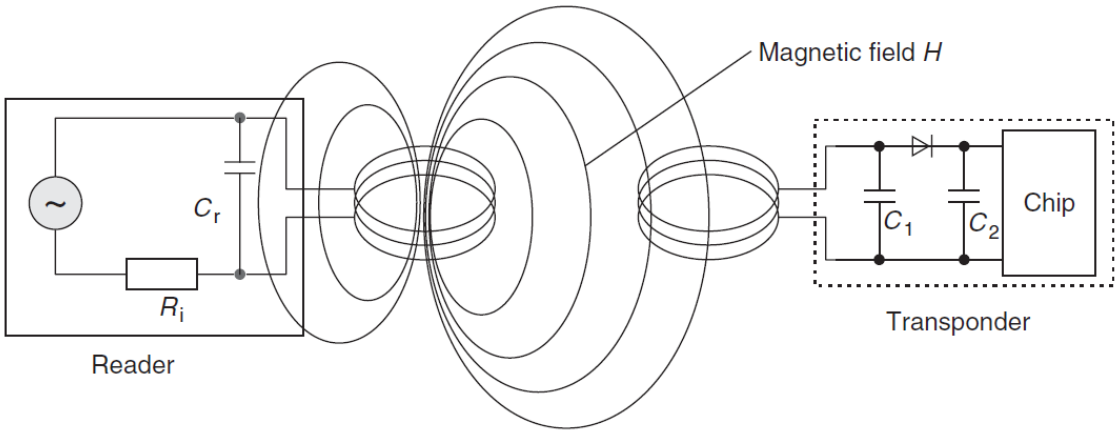

Figure 2.6: Power supply to an inductively coupled transponder from the energy of the magnetic alternating field generated by the reader [14]

2.2.4.2 Inductive Coupling Fundamentals

The energy transfer between two coils can only be provided by the magnetic field. Therefore, a few basics will follow to enable the understanding of the physical principle. As mentioned above, a current, which flows in a conductor creates a circular magnetic field round this conductor. Each magnetic field has a direction, which can be seen in figure 2.7, and an intensity which decreases with the distance to the wire. The magnetic field direction can be determined by using the right hand grip rule, where the direction of the thumb presents the current and that of the fingers the magnetic field. [27]

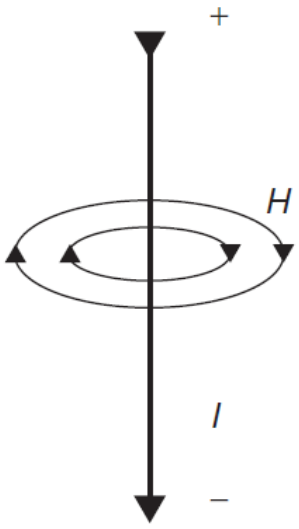

Figure 2.7: Magnetic field direction by presented current move [14]

By forming a coil with the wire, the magnetic field will be concentrated in the middle

of the coil and decreases at the outside of the wire, which can be seen in figure 2.8. The magnetic lines of force of the magnetic field decrease by higher distances to the coil, therefore at a certain distance the transponder can not be powered anymore. [14]

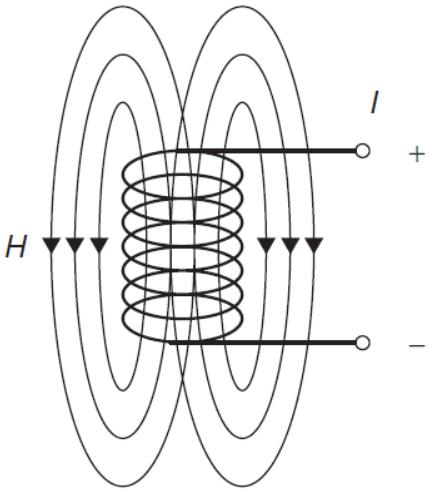

Figure 2.8: Magnetic field direction and concentration by presented current move in a coil [14]

To calculate all the current, which flows through a defined area, Ampere's law gives a relation between the strength of a magnetic field and the current in this area with the following equation. Therefore, an integration of the field strength of the magnetic field along a closed loop gives the sum of currents in this area. [14]

$$\oint \vec{H} \cdot \vec{d} = \sum I_n \tag{2.3}$$

To determine the magnetic field strength H, the following equation can be taken to calculate the field strength in a certain distance to a round conductor coil in the x - axis, where N represents the number of windings of the coil and R the coil radius. [19]

$$H = \frac{I \cdot N \cdot R^2}{2\sqrt{(R^2 + x^2)^3}} \tag{2.4}$$

The equation below can be taken to determine the magnetic field strength H of a rectangle antenna where a and b represents the edge lengths. [19]

$$H = \frac{I \cdot N \cdot a \cdot b}{4\pi\sqrt{(\frac{a}{2})^2 + (\frac{b}{2})^2 + x^2}} \cdot \left[\frac{1}{(\frac{a}{2})^2 + x^2} + \frac{1}{(\frac{b}{2})^2 + x^2} \right] \tag{2.5}$$

Equation 2.6 describes the magnetic field by using the *magnetic flux* ϕ and the *magnetic flux density* B. Comparable to the current density, the magnetic flux density represents the total number of lines of a magnetic field passing through a defined area, which is shown in figure 2.9. [14]

$$\phi = \int_A B \cdot dA \tag{2.6}$$

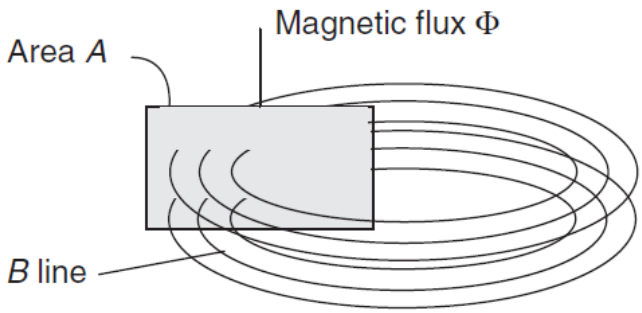

Figure 2.9: Relation between magnetic flux ϕ and magnetic flux density B [14]

Assuming that the magnetic flux density passing perpendicular through the area and also the area that is remaining constant, the equation from above can be simplified by using:

$$\phi = B \cdot A \tag{2.7}$$

To determine B, the equation 2.8 can be taken as a function of the magnetic field constant μ_0, which describes the magnetic conductivity, the relative permeability μ_r and the magnetic field strength H. [14]

$$B = \mu_0 \cdot \mu_r \cdot H = \mu \cdot H \tag{2.8}$$

$\mu_0 = 4\pi \cdot 10^{-7} \frac{Vs}{Am}$

$\mu_{r,Air} = 1$ (taken for air as example)

Since the equation 2.7 only describes the simple case with one coil, the total magnetic flux can be determined by including the winding number N of the coil which can be seen in formula 2.9. [14]

$$\Psi = \sum_{N} \phi = N \cdot \phi = N \cdot \int_{A} B \cdot dA = N \cdot \int_{A} \mu \cdot H \cdot dA \tag{2.9}$$

$$\Psi = \sum_{N} \phi = N \cdot \phi = N \cdot \mu \cdot H \cdot A \tag{2.10}$$

The inductance L is described as self - induction in the case that a self - generated magnetic field will be induced into the own coil. Therefore, a relation between the magnetic flux ϕ and the alternating current in the coil, which generates the magnetic field, determines the inductance L. Besides the capacitance and resistance of a coil, the inductance is the third characteristic value for antenna calculations. In equation 2.11 the relation will be shown between both physical values. By given antenna geometries and winding number N, L can be approximated as shown in equation 2.11. [14]

$$L = \frac{\Psi}{I} = \frac{N \cdot \phi}{I} = \frac{N \cdot \mu \cdot H \cdot A}{I} \tag{2.11}$$

If the magnetic flux Ψ will be induced in an other coil in the closer environment, this sort of induction is called mutual induction M, which is the main physical principle for transformers and inductively coupled RFID systems. Therefore, both coils are connected together by coupling flux, which depend on the coil radius, distance between both coils and the magnetic properties, described by the permeability. In equation 2.12 the relation between the partial flux Ψ_{21} and the current from the first coil I_1 is given. The mutual inductance M_{21} represents the relation of both physical values, which can be seen in figure 2.10. The other way around, the mutual inductance outgoing from the second coil is called M_{12}. [14]

$$M_{21} = \frac{\Psi_{21}(I_1)}{I_1} = \oint \frac{B_2(I_1)}{I_1} \cdot dA_2 \tag{2.12}$$

$$M = M_{21} = M_{12} \tag{2.13}$$

In RFID systems the reader and the transponder are coupled inductively in the proximity coupling range with the physical principles of mutual induction. Each coil (antenna) design depends on the application.

Therefore, dimensions differ between a credit - card format and a small wearable device, where the antenna is included in the small wristband. Changing the antenna geometry results in a change of antenna parameters. Afterwards, parameters must be adjusted for the ideally energy transfer between reader and transponder.

Figure 2.11 shows the equivalent circuit diagram of a RFID system containing two inductively coupled antennas. The first conductor loop L_1 represents the reader antenna and L_2 is therefore the transponder antenna. The resistance R_2 is the coil resistance of the transponder antenna and R_L represents the load. [14]

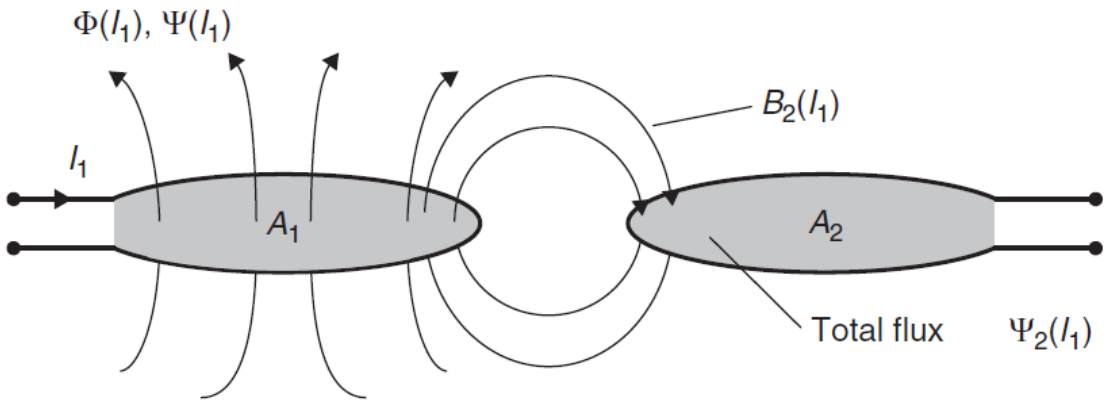

Figure 2.10: The definition of mutual inductance M_{21} by the coupling of two coils via a partial magnetic flow (adapted from [14])

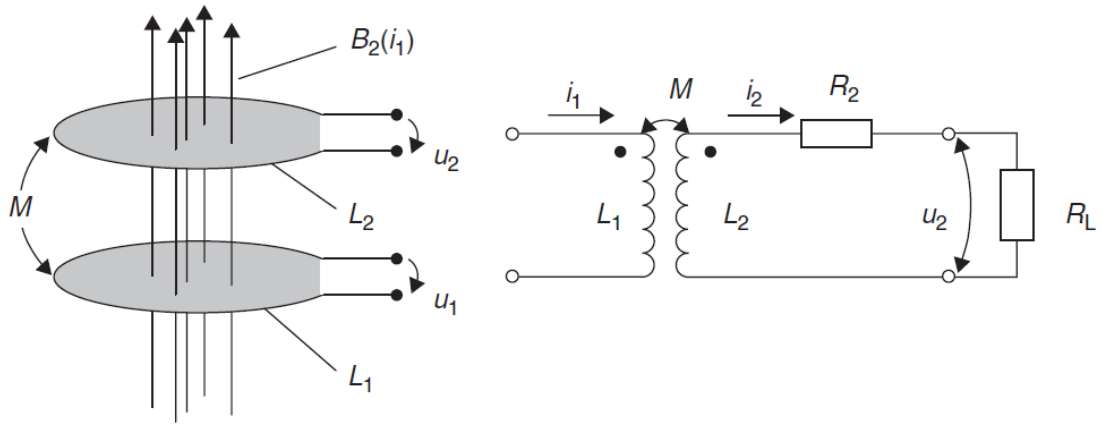

Figure 2.11: Left, magnetically coupled conductor loops; right, equivalent circuit diagram for magnetically coupled conductor loops [14]

2.2.5 Energy Transfer and Equivalent Circuit

Now the transponder is called Proximity Integrated Chip Card (PICC) and the reader is the Proximity Coupling Device (PCD). With so called resonant circuits, both the PICC and PCD can be optimized for the energy transfer. This section will give a brief overview about the resonant circuits and further possibilities to enhance both systems.[14]

In a resonant circuit electrical resonance will occur by decreasing the imaginary part of the impedances ideally to zero by mutual cancellation of capacitance and inductance in the circuit. Usually, the real part, which depends on the resistance of the conductor coils, and a slightly deviated imaginary part from zero remain. To maximize the magnetic field in the antenna when all geometries are fixed, the induced voltages and therefore the current must be maximized. By a given circular antenna, the inductance L can be determine with the assumption above in equation 2.11. The resonant frequency for the

PCD and for the PICC can be determined with the Thomson's formula 2.14 for resonant circuits, where C is the tuning capacitor.[19]

$$f_{RES} = \frac{1}{2\pi\sqrt{L \cdot C}} \tag{2.14}$$

Consequently, as mentioned before, the impedance $\underline{Z}(j\omega)$ of the equivalent resonant circuit has only a real part and is a non-existing or even extremely low imaginary part. This causes the induced voltage and the current to be in phase. This becomes visible by the following expression 2.15 when both impedances of L and C are cancelling each other. [19]

$$\underline{Z}(j\omega) = R_s + j(X_L - X_C) \tag{2.15}$$

2.2.5.0.1 Quality Factor Q The quality factor Q defines the absorbation of power from the resonance band of the PCD field. In equation 2.16, Q will be determined for a serial resonance circuit, figure 2.12 by the relation between the inductance of the antenna and the serial loss resistance R_s, which however contains the Alternating Current (AC) and the DC resistance part of the antenna. For a parallel resonance circuit, figure 2.12, the Q factor can be determined with the equation 2.17. The AC resistance part results in the skin - effect phenomena which appears in higher frequency applications due to the current flow concentration. Therefore, the current flows only at the edge of the conductor and not through the entire cross section. A high R_s value caused to a lower Q value. High Q values are recommended, but can also take some problems with it. Only a small deviation in the resonant frequency affects due to environmental influences leads to a higher change of the Q value. The bandwidth between ω_2 and ω_1 can be determined with the -3 dB limit which can be seen in figure 2.13. Other problems may be, that a high Q value causes to conflict with the PCD bandpass characteristics or create some bit timing problems in the protocol. [27]

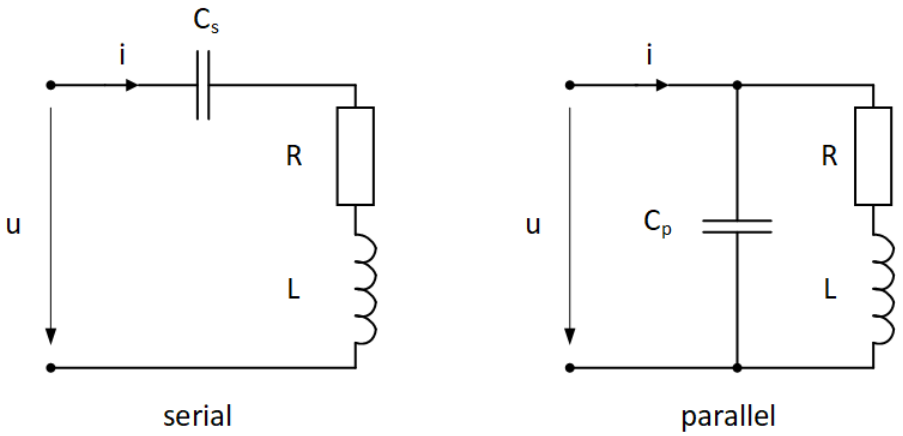

Figure 2.12: Left, serial resonance circuit; right, parallel resonance circuit

Serial resonant circuit:

$$Q_{Res} = \frac{\omega_{Res} L}{R_S} = \frac{1}{\omega C R} = \frac{1}{R}\sqrt{\frac{L}{C}} = \frac{\omega}{\omega_2 - \omega_1} \tag{2.16}$$

Serial resonant circuit:

$$Q_{Res} = \frac{R_P}{\omega_{Res} L} = \omega_{Res} R C = R\sqrt{\frac{L}{C}} \tag{2.17}$$

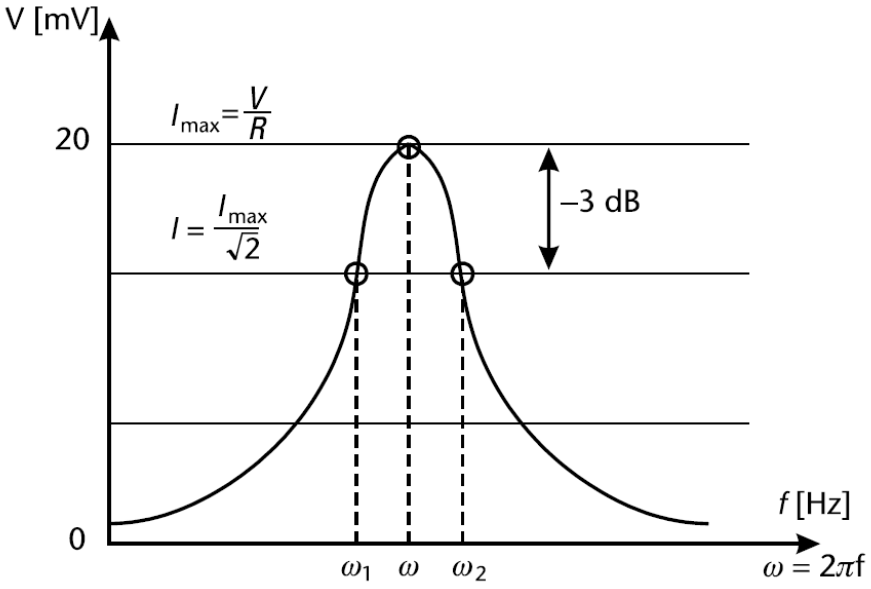

Figure 2.13: Frequency response curve for resonant tank circuit [27]

2.3 Energy Harvesting

Nowadays, smart wearables can operate as sensor nodes to measure the temperature, skin humidity or even motion. The limitation is not the aspect of processing power, it is even the aspect of power supply. [35] Acting as a sensor node, the power consumption keeps within limits, when measurements and short communication are periodically taken. In case of power consuming calculations or even data encryption for secure data transfer, the battery can be a limiting factor. [1] Therefore, solutions must be found, no matter whether in the power consumption of the system or the extension of battery lifetime with harvesting ambient energy. [35] Energy can be harvested from different sources and stored in conventional batteries, thin film batteries or goldcaps, also known as supercaps. A general distinction is made between the following types of sources: [1]

- light
- thermal
- vibration / motion
- radio frequency

In table 2.2 all common energy storage devices dedicated for smart wearable devices are listed. For applications with microchips and sensors, average sleep and operating states and also receive - poll - transmit cycles can estimate in the concept phase and accordingly the storage device can be selected due to these requirements.

Supercaps may be the right choice for simple sensor nodes but are not suitable for higher power consumption applications due to the small energy density [34], which is

shown in the table below. All in all, by discounting the costs, only three requirements are used filtering these storage devices in place of batteries, where lifetime, size and finally the environment must be evaluated. The evaluation of the environment can be the most important part for some applications. Here, a distinction should be made between the battery chemistry and its specified self - discharge value, the appearance of high current peaks in the application and the temperature exposure range.[42]

Table 2.2: Power available from different energy sources (adapted from [1])

Comparison	**Conventional batteries**	**Thin film batteries**	**Supercaps**
Recharge cycles	100's	5–10k	Millions
Self-discharge	Moderate	Negligible	High
Charge time	Hours	Minutes	Sec-minutes
Impedance	Low–high	High	Low
Physical size	Large	Small	Medium
Capacity	$0,3$–$2500\,mAh$	12–$220\,\mu Ah$	10–$100\,\mu Ah$

2.3.1 Energy Harvesting Methods

The next sections will describe the different energy sources for energy harvesting in a brief way.

2.3.1.1 Piezoelectric

One of the most common energy harvesting techniques in the mechanical area is the piezoelectric mechanism based on materials which exhibit piezoelectricity. Thus, materials like polarized ferroelectric ceramics, like *PZT* and barium tritanate. Otherwise, zinc - oxide(ZnO) is also a suitable material for the use as harvesting materials. [8] The mechanism will be described with the change from an undisturbed state of the material to an disturbed state by applying an external force. A mechanical strain results from the force and leads to a separation of charges in the material which creates an electric field with a dedicated output voltage. Figure 2.14 shows the procedure by showing the steady state, first with the non - polarized condition on the left side of part (b) and the disturbed state by applying a force F, which can be seen in (a), in the middle of part (b). [5]

This mechanism convert the mechanical energy into electrical energy which is shown in figure 2.15. The magnitude of the resulting force depends on the force or the mass in figure 2.15, thus a higher force leads to a higher magnitude.[13]

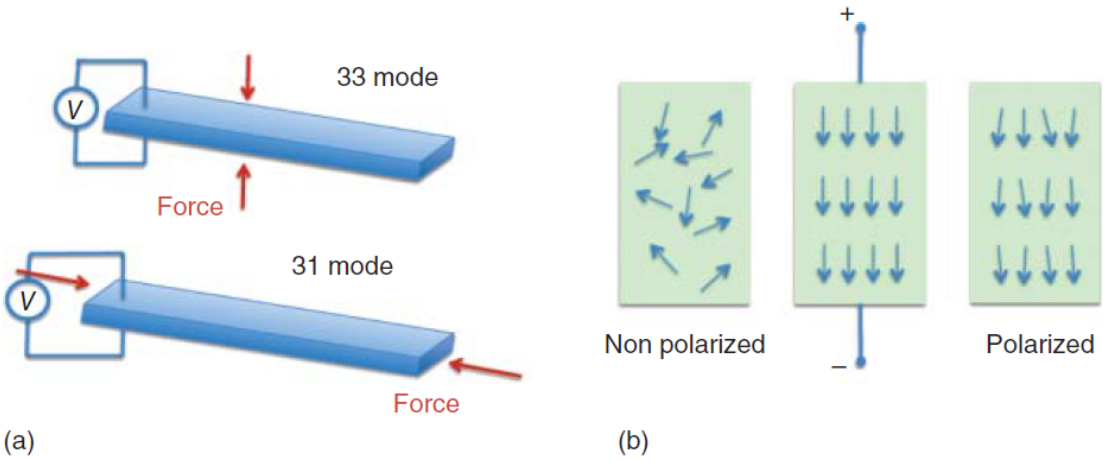

Figure 2.14: Piezoelectric effect in a beam [5]

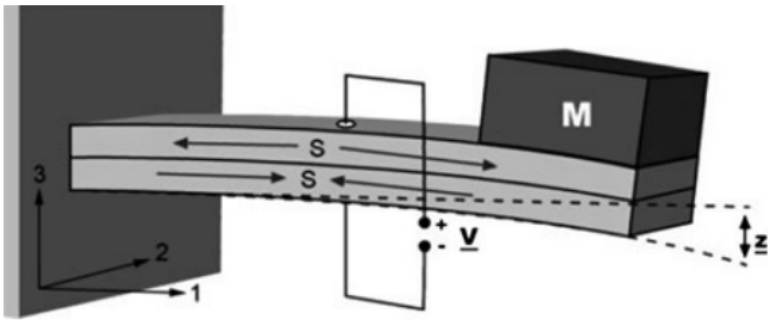

Figure 2.15: Piezoelectric effect in a beam [13]

2.3.1.2 Thermoelectric

The thermoelectric energy harvesting method will be described by the use of a TEG to generate electricity from a temperature gradient. The underlaying effect is called Seebeck effect in which a temperature gradient between two different electrical conductor materials produces a voltage. Requirements to build up a temperature gradient are the properties of the used materials. Both of them must have a high electrical conductivity σ and a low thermal conductivity κ. These parameters are important to build up a thermal gradient to ensure that one side is hot and the other side stays cold. The Seebeck coefficient S represents the magnitude of the electrons flowing across the materials. The figure of merit ZT can be determined by equation 2.18. [1] Figure 2.16 shows a TEG construction, where both materials are connected together at one end, one n-type semiconductor with a negative charge and, on the other hand, the p-type semiconductor with a positive charge. Due to the low thermal conductivity, both materials are arranged thermally in parallel but electrically in series. By applying one side to a heat source, the cold side must be cooled to increase the temperature gradient in this system. [5]

$$ZT = \frac{S^2 \cdot \sigma \cdot T}{\kappa} \tag{2.18}$$

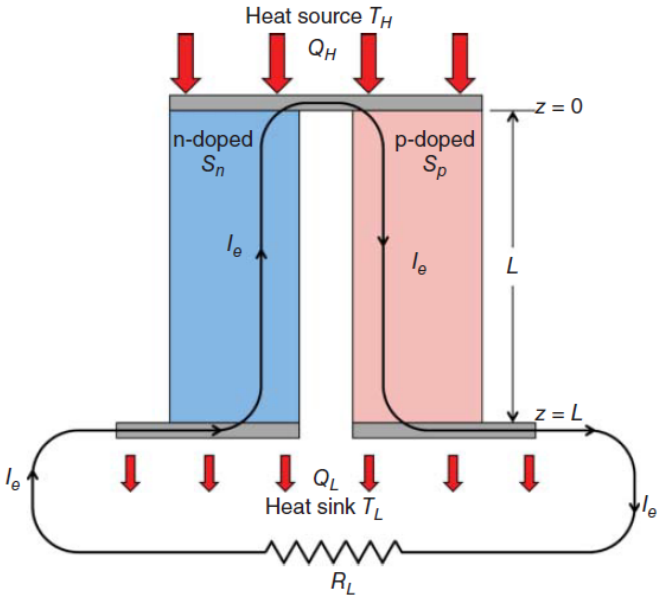

Figure 2.16: p-n leg in TEG device [5]

2.3.1.3 Photovoltaic

Energy from ambient light can be harvested by photovoltaic solar cells in various geometries and is based on the photoelectric effect. If a photon will be absorbed by the p-n

junction, ideally a electron - hole pair will be generated in the semiconductor material, but only if the photons energy is larger than the bandgap energy of the used semiconductor material. Figure 2.17 depicts the structure of a solar cell, including an anti - reflection layer, a material to increase the absorption of photons. [1]

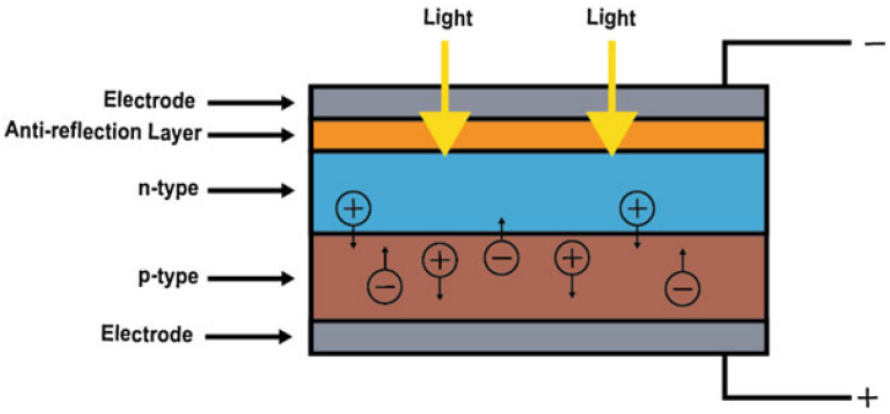

Figure 2.17: Operating principle of solar cell [1]

The energy of a photon can be determined with the Planck's constant h, the lightning speed c and the wavelength λ of the incident light which can be seen in the equation below. [1]

$$E = \frac{h \cdot c}{\lambda} \tag{2.19}$$

In figure 2.18 the circuit - equivalent model of a photovoltaic solar cell is shown as a Norton - equivalent current source. The maximum current i_{PH} will not reach the output connectors due to the recombination of charge carries on his way there and the parallel structured diode diverts also a small amount of i_{PH} to i_D. Furthermore, the load resistance R_R takes a part of the current.[42]

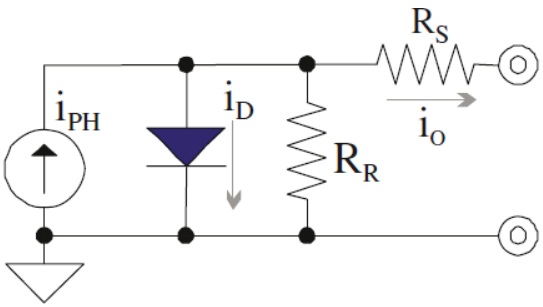

Figure 2.18: Photovoltaic circuit - equivalent model [42]

2.3.1.4 Radio Frequency

Radio frequency harvesting is the scavenging of energy from transmitted communication signals at certain radio frequency bands that will be converted into electricity. Common RF bands in Europe are the 433 MHz, 868 MHz and the ISM band at 2.4 GHz.[40] The harvesting structure contains a RF antenna, specially tuned for the operating frequency, to receive the signal strength from the signals in the air. By increasing the antenna size, the signal strength can also be increased but there is a trade - off between antenna size and the used operating frequency, therefore the higher the frequency the smaller the RF antenna can be. [1]

A typical RF harvester block diagram shows figure 2.19 and contains the RF antenna, an impedance matching network, a filter section and the rectifier. The AC signal will be rectified by single diode or diode bridge rectifier to a DC signal for suitable use to load storage devices like batteries or supercaps. In the filter section low - pass filters were used to prevent the reflection of harmonics generated by the diodes in the rectifier section back to the antenna. [40]

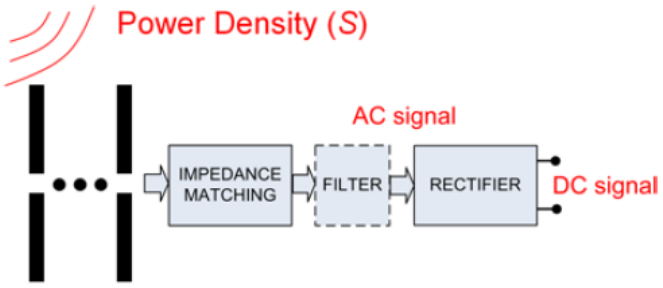

Figure 2.19: General block diagram of an RF harvester [40]

2.3.2 Selection

According to the application in this master's thesis with the smart wearable wristband only small photovoltaic solar cells can contribute the best in case of energy harvesting. For thermoelectric harvesting, the temperature gradient will be too low because an active cooling is not possible for this small wearable. Energy harvesting from motions or vibrations is not efficient due to less movements in the everyday life of a patient in the health care environment. RF harvesting sounds good at first sight, but can not be utilized due to the small geometry of a wristband. According to the geometry, there is no place for big antennas besides the RF antenna for the NFC interface.

The yield of energy, which can be ideally taken from ambient sources will be shown in table 2.3. Additionally, the harvesting method with solar energy has the lowest energy yield per cm^2 in comparison to other methods in the table.

Table 2.3: Comparison table between batteries and capacitors (adapted from [1])

Source	**Source power**	**Harvested power**
Ambient light		
Indoor	$0.1\,mW/cm^2$	$10\,\mu W/cm^2$
Outdoor	$100\,mW/cm^2$	$10\,mW/cm^2$
Vibration/motion		
Human	$0.5\,m$ at $1\,Hz$	
	$1\,m/s^2$ at $50\,Hz$	$4\,\mu W/cm^2$
Industrial	$1\,m$ at $5\,Hz$	
	$10\,m/s^2$ at $1\,kHz$	$100\,\mu W/cm^2$
Thermal energy		
Human	$20\,mW/cm^2$	$30\,\mu W/cm^2$
Industrial	$100\,mW/cm^2$	$1-10\,mW/cm^2$
RF		
GSM base station	$0.3\,\mu W/cm^2$	$0.1\,\mu W/cm^2$

3 Hardware Design

3.1 Design

This chapter gives a deeper insight into the hardware design of the system. The first section describes the system followed by each component.

3.1.1 System Overview

The smart wristband and the base station creates a whole system and is realized with the prototype and one Raspberry Pi. Therefore, the system consists of two parts, the wristband represents the patient unit and the base station represents the locating system unit in a health care facility. In the first system approach Infineon's SLE70 controller is the key component and acts as the master. It provides the necessary interfaces like NFC, Inter-Integrated Circuit (I2C) and UART. The NFC interface is used for data transfer between the wristband and a reader device. The heart rate sensor from Infineon is controlled via I2C interface by the SLE70. A communication between the HCI of the Texas Instruments CC2564 SoC and the SLE70 will be established via UART interface.

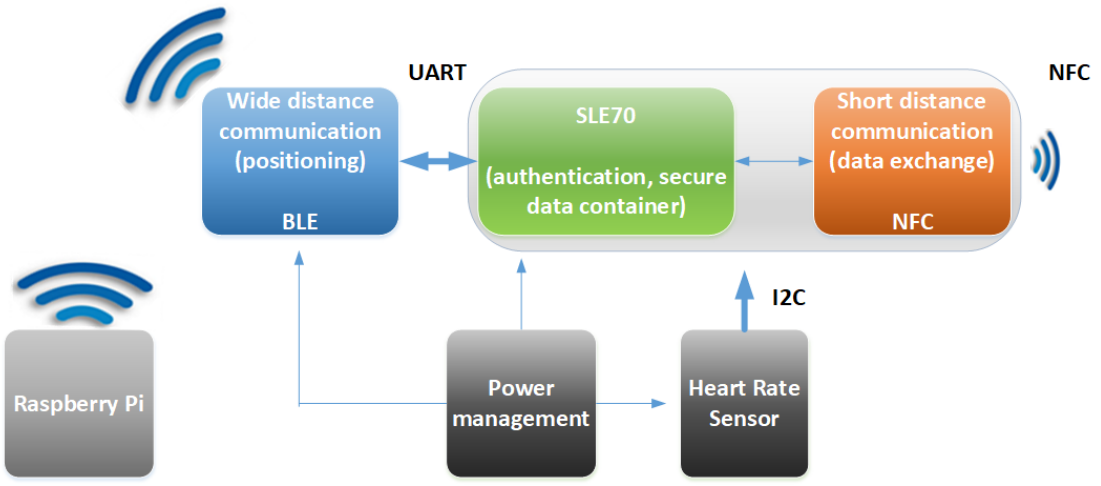

Figure 3.1: First system approach of the patient locating system

Due to several issues of the first prototype the system approach was changed. Several changes have been made in the second system approach. Figure 3.2 shows the new

system. A Nordic Semiconductor nRF52832 SoC replaces the Texas Instruments CC2564 SoC and Infineon's SLE70 was also replaced. The SLE70 has now less interfaces and a reduced capability of performance, which results in a lower power consumption. Now, the Nordic BLE SoC acts as master device, whereas the SLE70 is now the slave device. Furthermore, the BLE SoC controls the heart rate sensor via the I2C interface instead of the SLE70. At least, the energy consumption is reduced by the given system, which benefits the life time of the smart wristband.

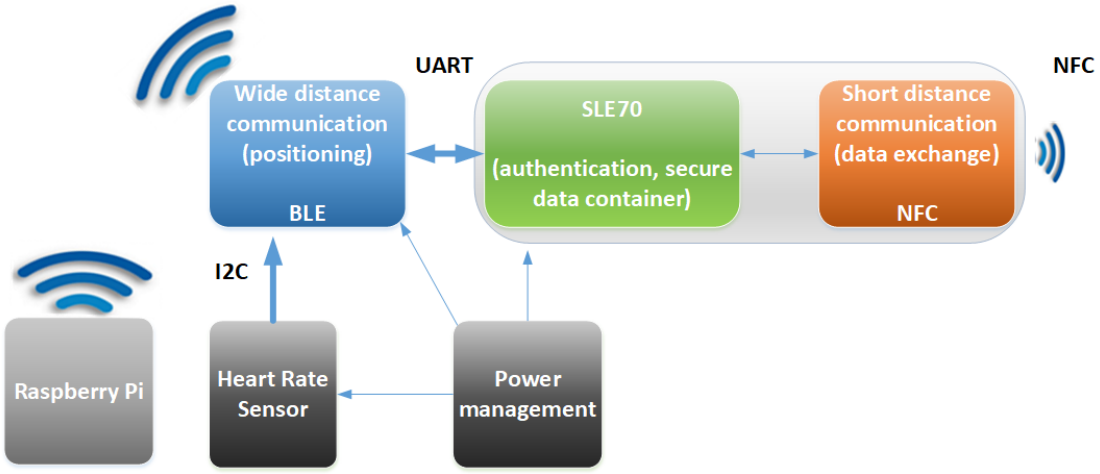

Figure 3.2: Second system approach of the patient locating system

3.1.2 Requirements

The smart wearable wristband concept and the various applications behind lead to the following requirements.

The requirements are listed below:

- The wristband shall be equipped with a SE for secure data storage and to provide a NFC interface and further interfaces for potential sensor integration
- An antenna is required to utilize the NFC interface.
- A BLE SoC shall be integrated to perform the patient locating part and to provide data transfer to the SE.
- The power management shall be designed to provide a life time of a at least 6 days
- The resulting design should fit in a wristband
- The final system shall include a base station for locating the wristbands

Due to the fact that the heart rate sensor was added in the course of the work, it is not included in the requirements, but can be implemented. Further sensors, like gyroscopes or accelerometers, can be implemented as well.

3.1.3 System Components

This chapter describes all blocks and components of both concepts. The following datasheets were used in this chapter: [51] [53] [50] [52] [30] [31] [44] [39] [26] [33] [38] [54]

3.1.3.1 Block Diagrams

The following diagrams give an overview about the various system blocks of the dedicated concepts.

3.1.3.1.1 First Concept Figure 3.3 contains all blocks of the system and additionally the current consumption of each component. An example for the current consumption of the heart rate sensor with two external LEDs can be seen below. Therefore, the supply current of the sensor is $300 \mu A$ and the average current consumption of one LED with a supply current of 100 mA and a on / off duty ratio of 1/320 results in $925 \mu A$.

$$I_{CC} = 300\,\mu A + 2 \cdot 100\,mA \frac{1}{320} = 925\,\mu A \tag{3.1}$$

The estimation of the supply current of the BLE SoC depends on the selected mode. Therefore, the difference between an active advertising and a connection mode is considerable. Summing up all values by excluding the SLE70 and consider that the BLE SoC operates in the continuous connection mode, results in a total current consumption of $I_{total} = 21,52\,mA$. With the chosen accumulator the life time of the wristband is therefore 4 hours and 39 minutes. Even in this estimation the SLE70 controller was not included.

$$t = \frac{C}{\sum I_{CC}} = \frac{100\,mAh}{21,52mA} = 4,65\,h \tag{3.2}$$

Operating the device in an active advertising mode results in a life time of 12 hours and 30 minutes for the whole system by excluding the SLE70 controller. Additionally, the energy harvesting part is not active.

$$t = \frac{C}{\sum I_{CC}} = \frac{100\,mAh}{8\,mA} = 12,5\,h \tag{3.3}$$

The results show that a solution is required to enhance the life time of the system.

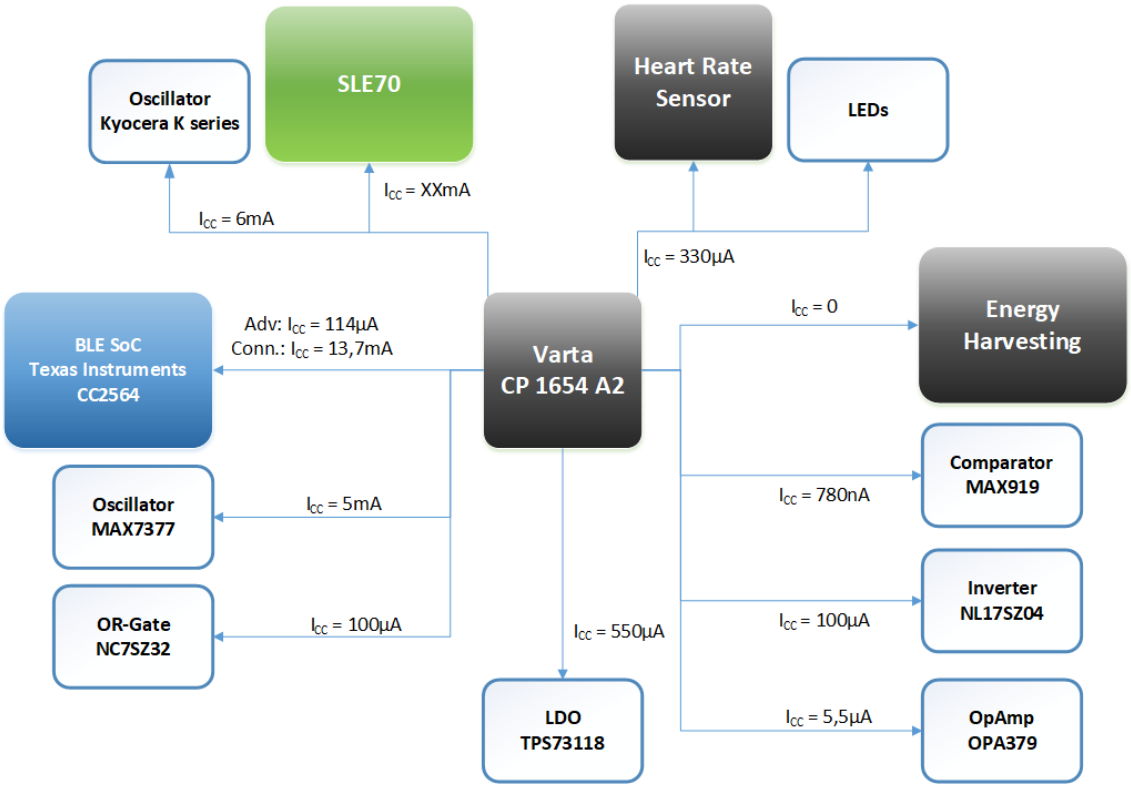

Figure 3.3: First concept: block diagram and current consumption

3.1.3.1.2 Second Concept The second concept was reduced to a minimum of components. The following calculations show the current consumption of the system.

$$t = \frac{C}{\sum I_{CC}} = \frac{100\,mAh}{5,734\,mA} = 17,45\,h \tag{3.4}$$

The supply current value from the BLE SoC represents an active receiving mode. The resulting current consumption is 17 hours and 27 minutes for the whole system by excluding the SLE70 controller. By implementing a continuous advertising mode and a connection mode every once in a while, the life time increases. In this system concept, the SLE70 controller acts as slave, therefore the current consumption increases only by data transfer between both controller.

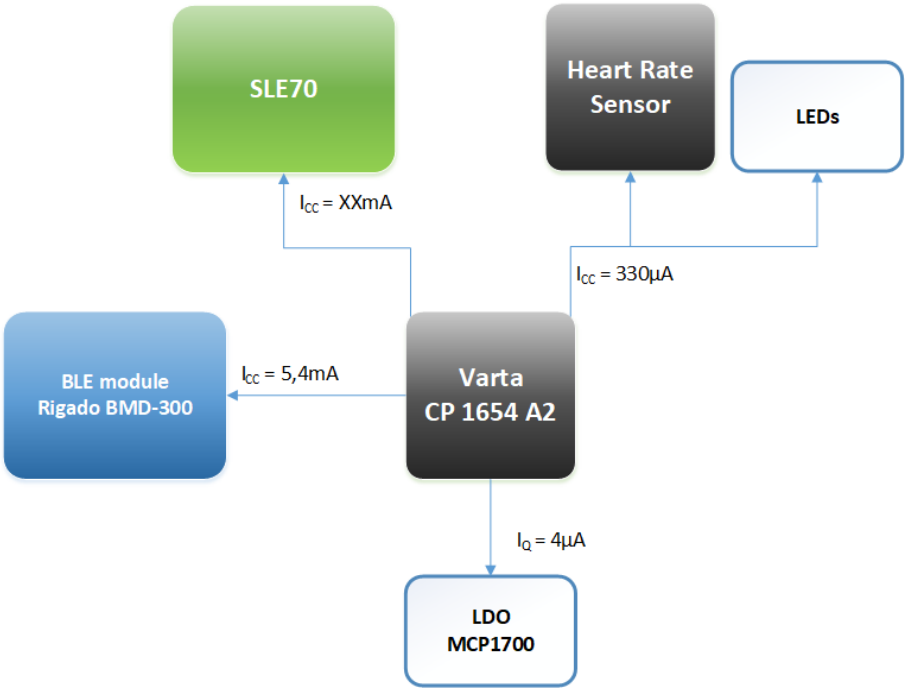

Figure 3.4: Second concept: block diagram and current consumption

3.1.3.2 Power Management

One requirement for the prototype is to design the power management for a long life time. Once powered, the system should provide his function for 6 days. To provide this, all components like controllers, low - dropout regulators and oscillators should be well selected due to the quiescent current and maximum current consumption. Also the software has a big optimization potential. An active power saving mode and a deacreased polling time on an interface are two common parts.

3.1.3.2.1 Accumulator A small rechargable battery which fits in a wristband and provides a suitable nominal voltage and a high capacity should be implemented. Samsung SDI provides accumulators for wearables and especially for wristbands with a curved and a flat cell type. According to the geometries, these types provide suitable capacity values of 210 mAh (curved) and 300 mAh (flat). [46] The acquisition of these two components is only possible if high quantities are ordered.

Varta offers also a small accumulator type with coin geometries. The CoinPower® CP 1654 A2 lithium - ion accumulator provides a nominal voltage of 3,7 V and a capacity of 100 mAh with dimensions of 16,1 mm in diameter and 5,4 mm in height. The charging voltage is limited to 4,2 V. [58] This choice is suitable for testing the first prototype by including the energy harvesting part in the system.

All components should be now chosen due to the accumulator parameters. Therefore, the highest voltage is presented by the upper limit of 4,2 V from the charging voltage parameter of the accumulator. The implementation for the second concept can be seen in figure 3.12. Two possibilities to connect different batteries are included, therefore the CP1654 and a CR2032 battery can be applied.

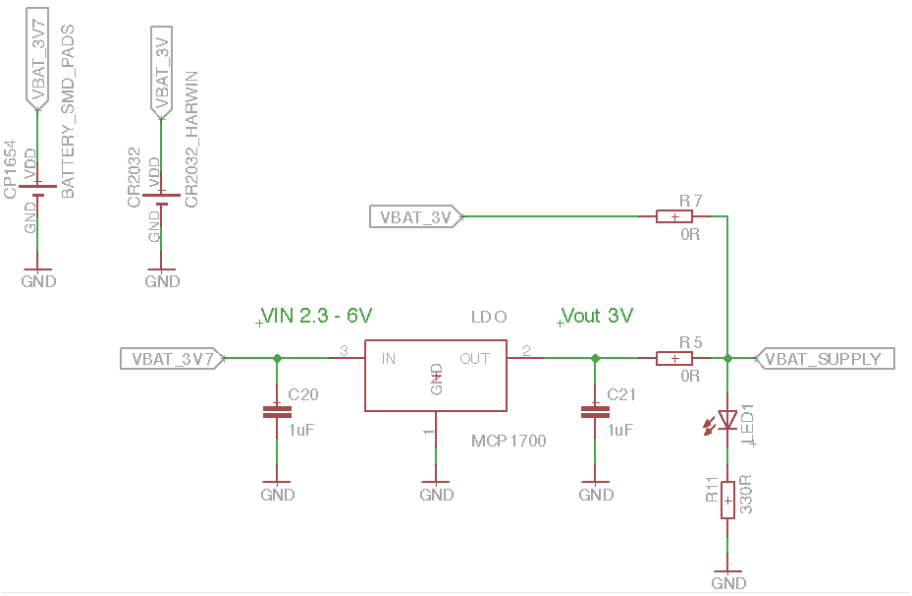

Figure 3.5: Second concept: battery supply

3.1.3.3 Energy Harvesting

An energy harvesting technology is integrated into the system with the expectation to derive energy from a photovoltaic cell. After a few considerations according to the application two cells were chosen. When wearing the wristband, it is to be noted that arm movements and possible rotations of the wristband have an influence on the light irradiation of the cell. Therefore, two cells are implemented to have the capability in several arm positions that at least one cell detect an incidence of light.

3.1.3.3.1 Photovoltaic cell The chosen photovoltaic cell is shown in figure 3.6 below. All cell parameters are listed below.

- Geometries: 19,5 x 30 x 0,3 mm (width, height, thickness)
- Nominal voltage: $V_N = 0,5\,V$
- Nominal current: $I_N = 200\,mA$
- Maximum power: $W = 100\,mW$
- Crystalline structure: mono - crystalline [25]

Due to the thickness the cell is very fragile and shatters by applying pressure. Furthermore, the surface is very sensitive to dirt, therefore cleaning when stained is necessary to maintain the efficacy, especially by such a low nominal voltage.

To increase the output voltage photovoltaic cells can be combined in series configuration, figure 3.7, therefore the output voltage becomes the sum of each cell in the configuration. In a parallel configuration it is possible to increase the output current.

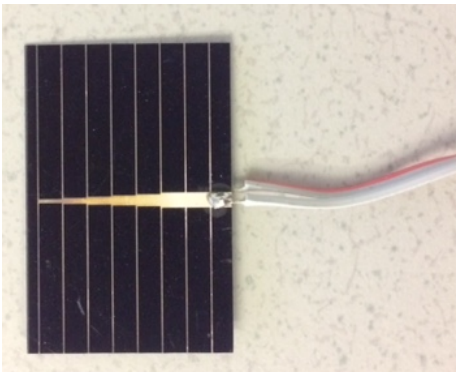

Figure 3.6: Single photovoltaic cell

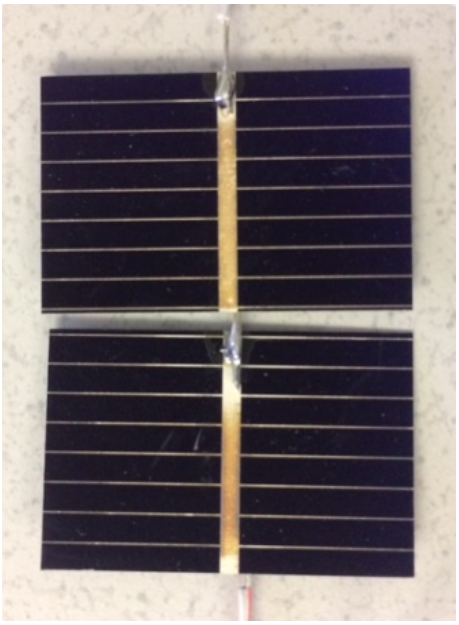

Figure 3.7: Series connection of two photovoltaic cells

Two cells are implemented in the system and are distributed attached at the wristband. To get the highest output voltage from one of the two cells, a comparator section and a switch is needed. Therefore, two n - channel MOSFET are implemented to switch through the cell with the highest voltage, figure 3.8.

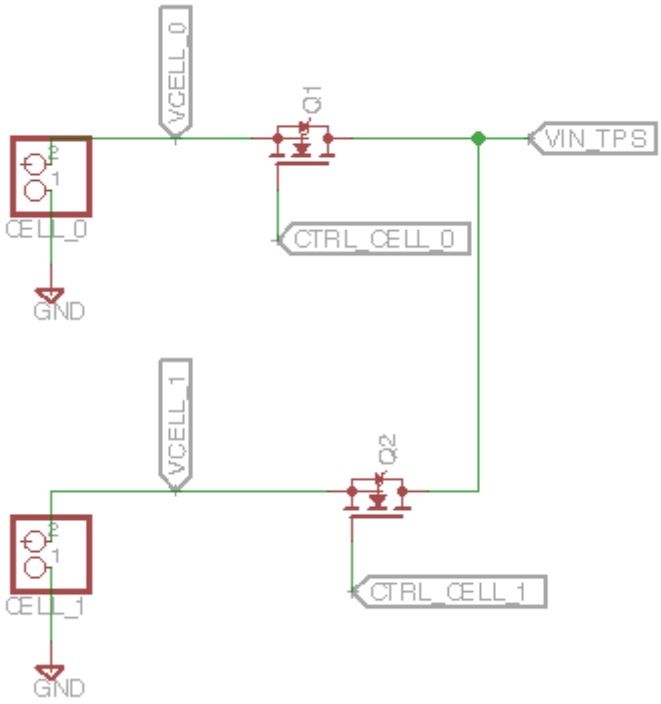

Figure 3.8: N - channel MOSFET controlled photovoltaic cells

For switching only one cell with a n - channel MOSFET, a comparator section with an additional converter is implemented. Figure 3.9 shows the mentioned section. The Maxim Integrated MAX919 comparator is a nanopower beyond - the - rails comparator with two input pins.

To switch between both photovoltaic cells the threshold must be set. The comparator offers a 4 mV internal hysteresis band, which is not suitable for this application. An additional hysteresis can be set with external resistors. The calculation of resistor values and selection of input parameters can be seen below. The threshold voltage for the rising signal was set due to the input voltage minimum of the energy harvesting IC in the next section of the design. It is to consider that the reference voltage changes with the output voltage from the cell, so the reference value is dynamic.

- Supply voltage: $V_{CC} = 3,7\,V$
- Threshold for rising signal: $V_{THR} = 0,31\,V$
- Hysteresis band: $V_{THB} = 20\,mV$
- Voltage of second input pin: $V_{REF} = V_{CELL1} = 0,3\,V$
- Leakage current: $I_{R16} = 200\,nA$ (recommendation from datasheet)

$$R_{16} = \frac{V_{REF}}{I_{R16}} = \frac{0,3\,V}{200\,nA} = 1,5\,M\Omega \tag{3.5}$$

$$R_{14} = R_{15} \cdot \frac{V_{HB}}{V_{CC}} = 1,5\,M\Omega \cdot \frac{20\,mV}{3,7\,V} = 8,33\,k\Omega \tag{3.6}$$

$$R_{15} = \frac{1}{\left[\frac{V_{THR}}{V_{REF} \cdot R_{14}} - \frac{1}{R_{14}} - \frac{1}{R_{16}}\right]} = \frac{1}{\left[\frac{0,31\,V}{0,3V \cdot 8,33\,k\Omega} - \frac{1}{8,33\,k\Omega} - \frac{1}{1,5\,M\Omega}\right]} = 300\,k\Omega \tag{3.7}$$

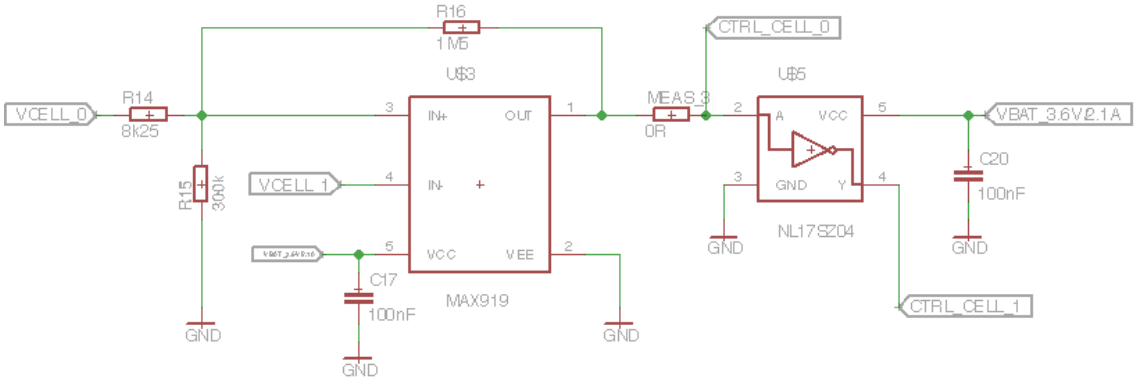

Figure 3.9: Comparator section with additional inverter

3.1.3.3.2 Energy Harvesting IC section The chosen energy harvesting IC is a low input voltage synchronous boost converter from Texas Instruments. With an input operating range of 0,3 V to 5 V, the harvesting IC, the lower input voltage limit of 0,3 V is a suitable value for the selected photovoltaic cells. The output voltage of the IC can be programmed via the voltage divider. It is recommended that R_{11} should be in the range of 200 $k\Omega$. All selected parameters can be seen below.

- Resistor: $R_{11} = 200\,k\Omega$
- Feedback voltage: $V_{FB} = 0,5\,V$
- Output voltage: $V_{OUT} = 4,2\,V$

$$R_{10} = R_{11} \cdot \left(\frac{V_{OUT}}{V_{FB}} - 1\right) = 200\,k\Omega \cdot \left(\frac{4,2\,V}{0,5\,V} - 1\right) = 1,48\,M\Omega \tag{3.8}$$

The value for R_{10} is set to 1,5 $M\Omega$ due to the preferred values in the E series of electronic components.

The maximum power point tracking (MPPT) unit was skipped in this application due to the lack of improvements in the output signal.

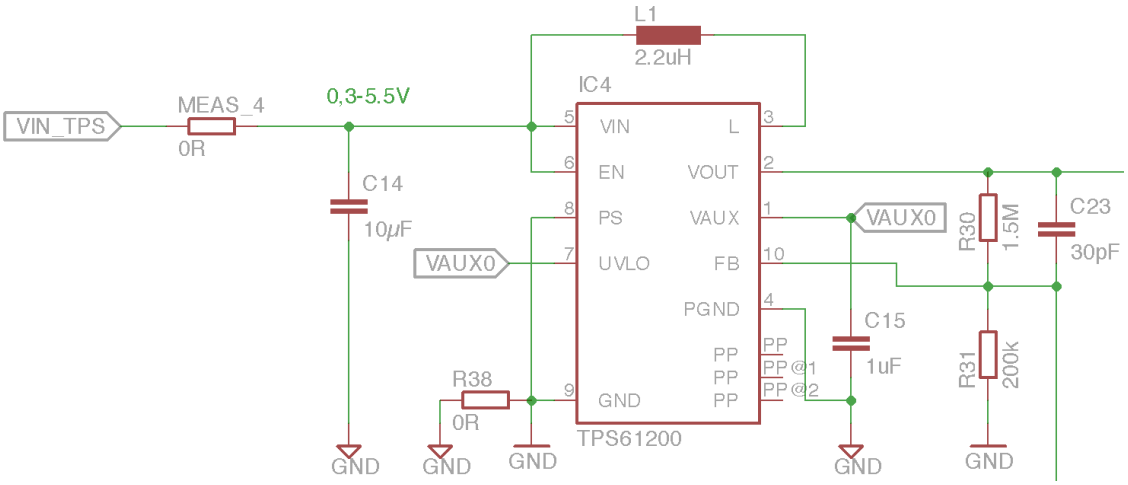

Figure 3.10: Energy harvesting IC section

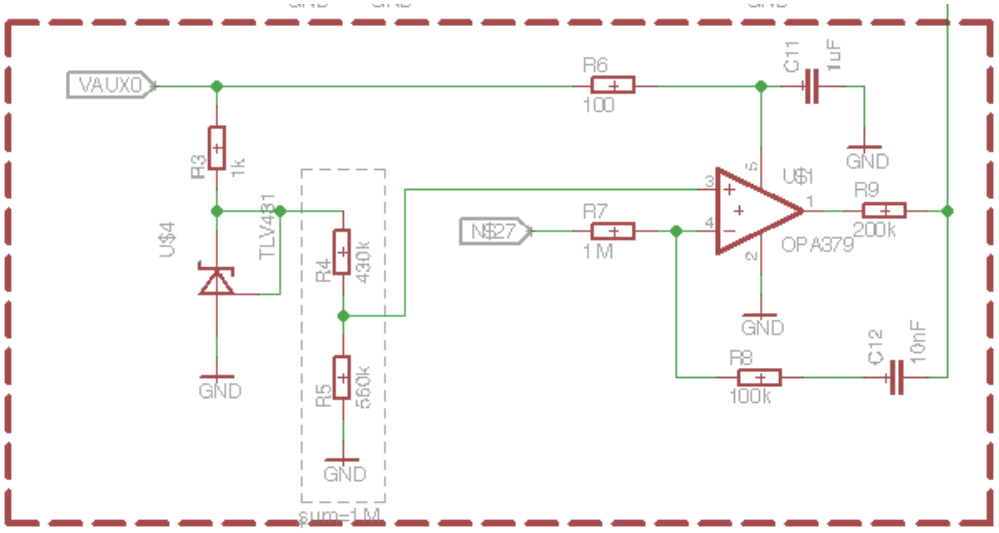

Figure 3.11: Maximum power point tracking section

3.1.3.3.3 Battery charging IC The battery charging IC was chosen due to the internal overvoltage protection and for the utilization as backup if the boost converter may have issues to boost the low input voltage up to the 4,2 V charging voltage.

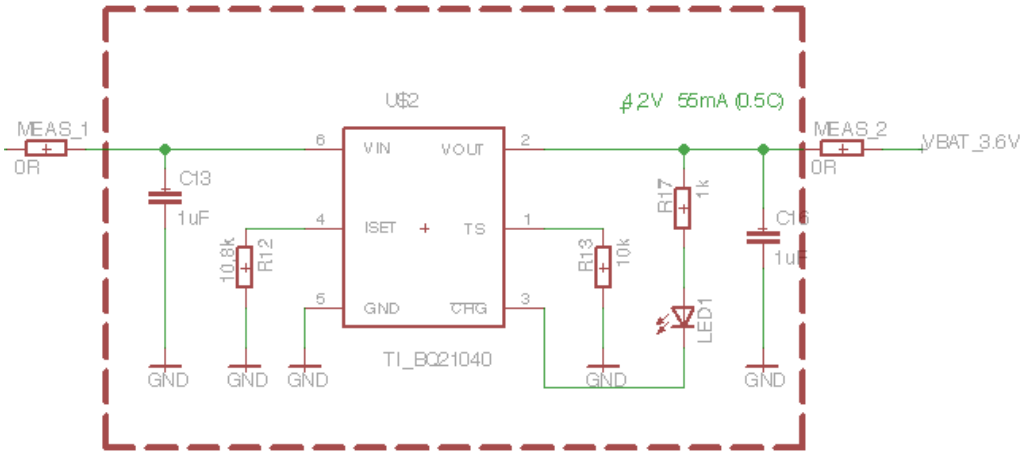

Figure 3.12: Battery charging IC

3.1.3.4 Secure Element

The SLE70 controller for both concepts are capable of operating in a dynamic voltage range. Therefore a supply voltage of 4,2 V by active energy harvesting presents no circumstances. Both controllers provide a chip input capacity of 56 pF. Figure 3.13 shows the SLE70 symbol for the chip package and a second possibility for a smart card module. The smart card module footprint provides to implement various SE types for testing. According to the schematic diagram, the LA and LB pad includes a parallel capacitor C7. For antenna tuning to 13,56 MHz this capacitor may be exchanged, more detailed informations can only be provided after a resonant frequency measurement procedure in the measurement and result chapter.

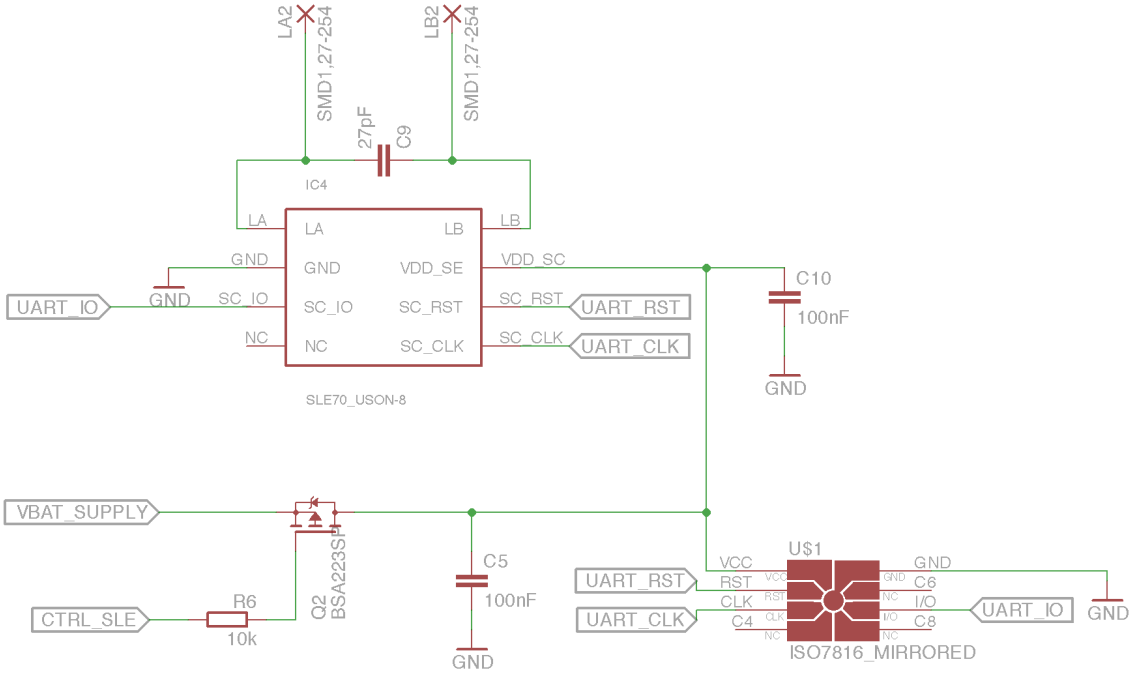

Figure 3.13: Second concept: SLE70 package and smart card module

3.1.3.5 BLE SoC

The Texas Instruments CC2564 is a dual-mode SoC which is assembled in the first concept. With an additional HCI interface, the controller offers all features to fulfill the requirements. An external oscillator supplies the controller with a clock frequency of 32,768 kHz. An external chip antenna is implemented to provide a BLE interface.

For the second system concept a Rigado BMD-300 BLE SoC module with integrated oscillator and antenna is assembled. The chosen Rigado BMD-300 module based on the nRF52832 with a compliant 2,4 GHz transceiver antenna. Both are connected via UART interface to the SE.

3.1.3.6 PALS - 2

The PALS-2 is a proximity and ambient light sensor can be utilized due to the built - in LED driver, a photo - pin - diode and a signal processing IC to determine the heart rate of a person. Three external LEDs can be controlled with the LED driver section. Furthermore, a 16 bit resolution is provided for both modes, the ambient light and the proximity mode. Data can be transfered via I2C interface between the built - in signal processing IC and an external controller. The LED driver section can be utilized to switch between current values of 10 mA up to 200 mA for three LEDs. The resulting current consumption depends on the number of measurements per second and the driving LED current. According to the proximity sensor, the relative spectral sensitivity in comparison to the wavelength has its maximum in the range of 750 nm and 950 nm, which represents infrared light. Therefore, three LED footprints are available and one of them should be utilized for an infrared LED. For the ambient light sensor, the relative spectral sensitivity has its peak in the range of 500 to 600 nm, which includes the spectral colors green and yellow.

According to the host programming, the sensor provides 27 registers with 8 bit length to set parameters for the ambient light and the proximity mode.

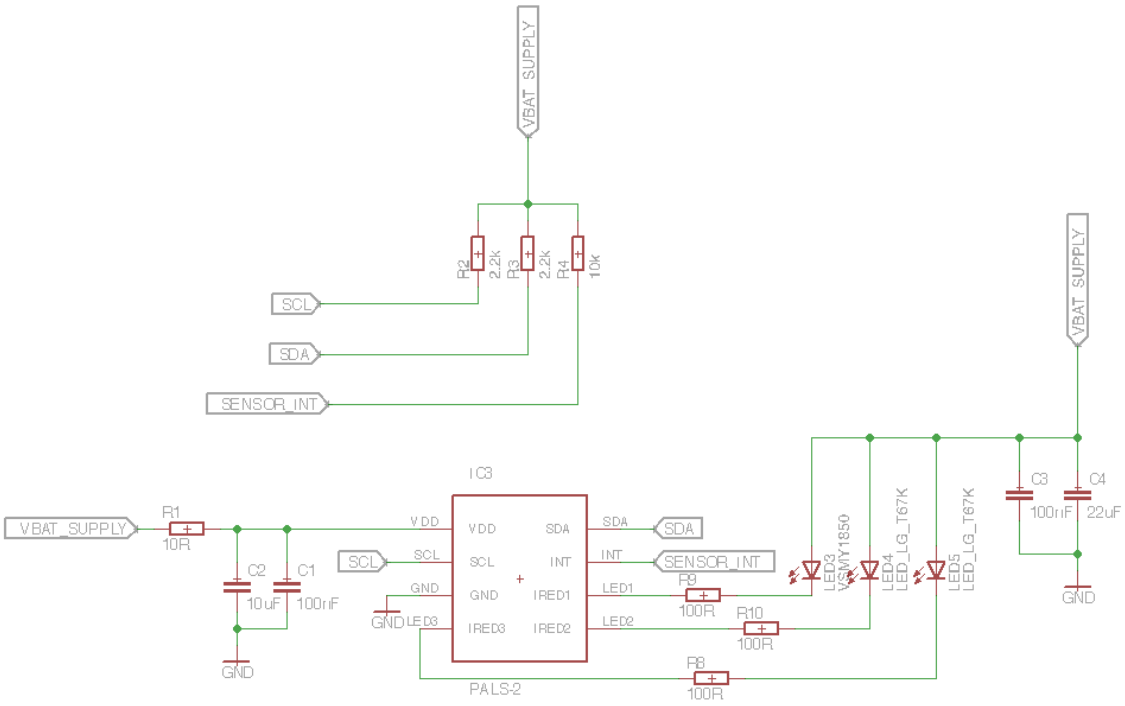

Figure 3.14: PALS-2 schematic

3.1.3.7 Raspberry Pi Base Station

After the design and development procedure of the wristband, a base station is required to fulfill the function of locating patients indoor and outdoor. The Raspberry Pi provides a BLE and Wi-Fi interface and contains an ARM-Cortex processor , which is sufficient for normal desktop work. For this application, this devices is a meaningful decision between the costs, provided interfaces and size. [16]

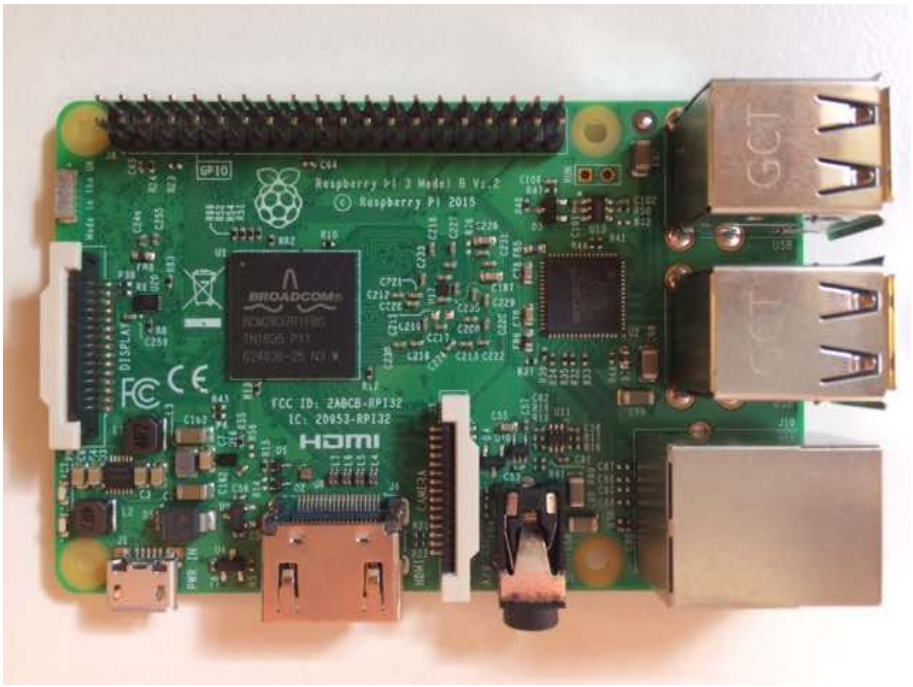

Figure 3.15: Raspberry Pi 3 Model B

3.1.3.8 NFC System

A suitable SE is chosen due to the required interfaces, as mentioned at the beginning of this chapter. For contactless communication via NFC interface, the standard ISO/IEC 14443 is used with a carrier frequency of 13,56 MHz and with an ISO/IEC 14443 class 6 antenna. The antenna provides the smallest antenna geometry from the standard ISO/IEC 14443. It is implemented at the PCB and connected to the Contactless (CL) - interface pins LA and LB. In addition, a capacitor Cp is applied between the LA and LB pin for resonant frequency tuning. For the second system concept a new antenna was designed to optimize the performance with respect to the wristband geometry.

In section 2.2 for RFID basics, a short introduction was given to physical fundamentals of RFID devices and antenna basics. With these basics a small antenna for the chosen wristband was designed with the Keysight Technologies software Advanced Design System (ADS®).

All important antenna properties for the common design are listed below.

- **Dimensions:**
  - **Width:** 16 mm
  - **Height:** 20 mm
- **Windings:** 5
- **Track width:** 200 μm
- **Track height:** 200 μm
- **Gap:** 200 μm

3.1.3.8.1 Wired Antenna Design The size of the antenna is chosen due to the width of the wristband. A coated wire with 200 μm in diameter was attached to the design, see figure 3.16. Figure 3.17 shows the attached antenna design onto the wristband.

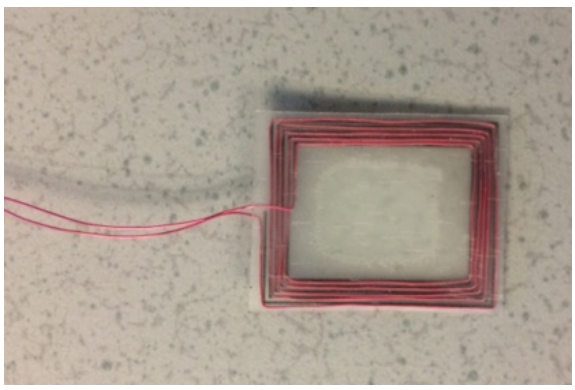

Figure 3.16: Antenna design printed and wired on paper with adhesive layer

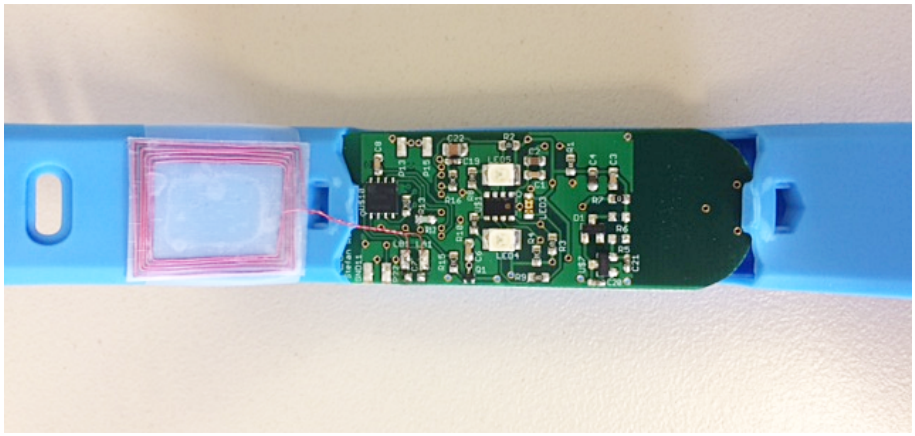

Figure 3.17: Antenna design attached on the wristband

3.1.3.8.2 Antenna Design Simulation The antenna design from ADS® was imported into the software ANSYS High Frequency Electromagnetic Field Simulation (HFSS®) to simulate the design in 3 D. Figure 3.18 shows the antenna and an additional PCD antenna with dimensions from 70 mm width and 50 mm height. All simulation and measurement results are shown in section 5.2.

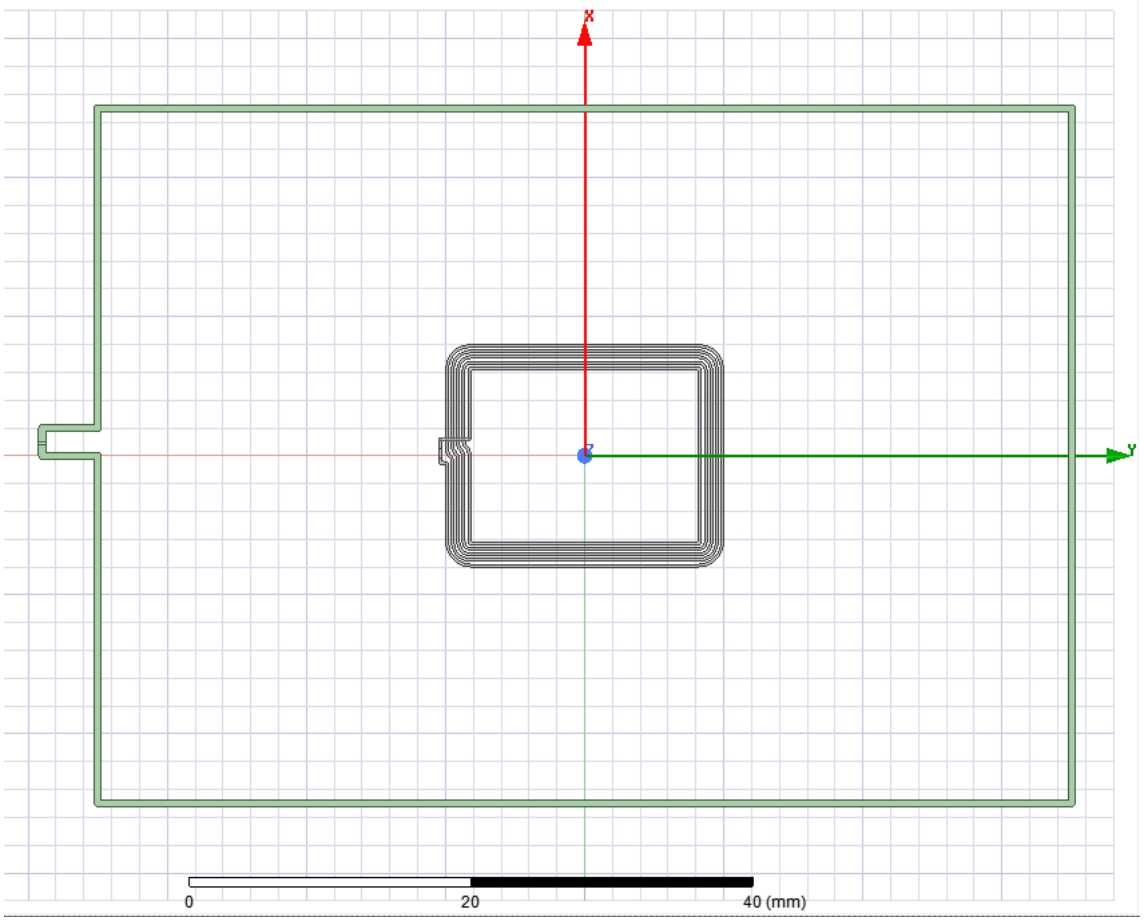

Figure 3.18: Antenna 3D design with addtitional reader antenna below to simulate voltage inducing at a given reader distance

3.1.4 Prototypes

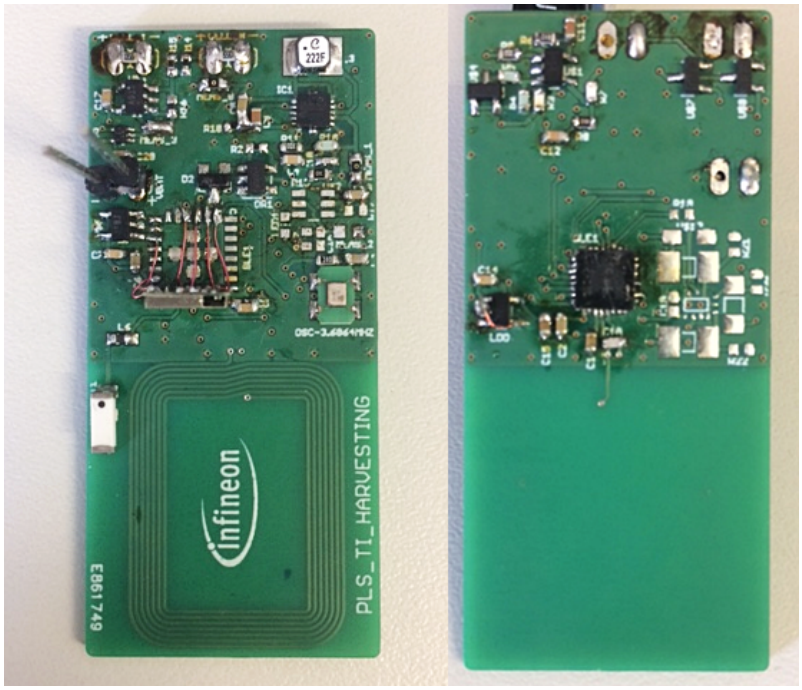

Figure 3.19: First concept prototype assembled as PCB

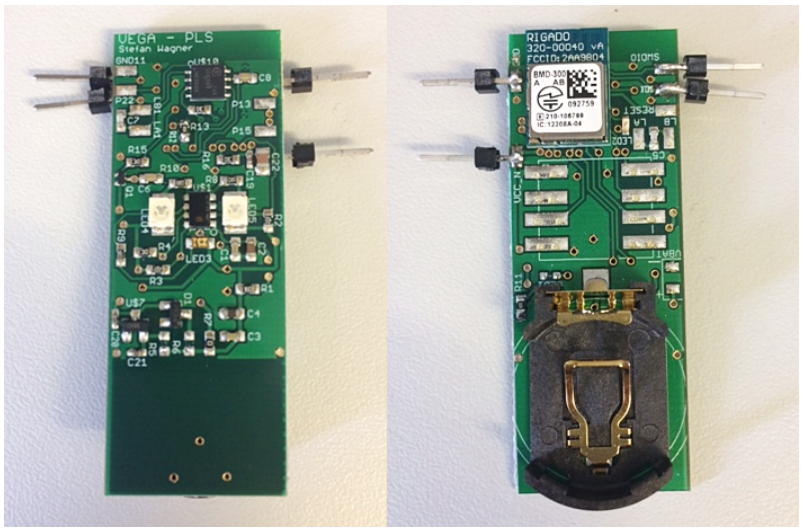

Figure 3.20: Second concept prototype assembled as PCB

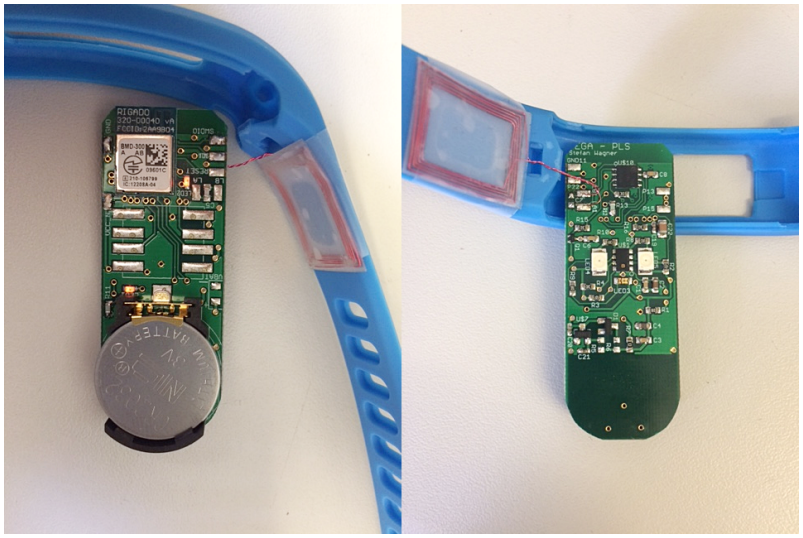

Figure 3.21: Prototype with antenna - top and bottom view

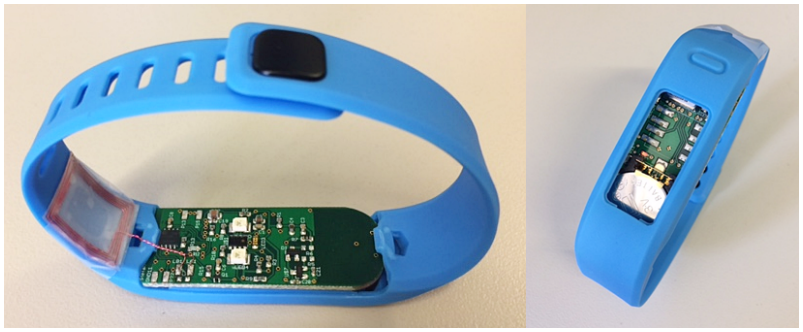

Figure 3.22: Prototype integrated in wristband

4 Software

4.1 Software

This chapter describes the requirements and implementation of the software of the SE, the BLE SoC and the Raspberry Pi. For proper function of the energy harvesting block no software is required.

4.1.1 Requirements

The subsection 3.1.1 describes two different system approaches due to problems with the first prototype and a subsequent rethink of the patient unit. All requirements have been splitted into two parts, the basic requirements and advanced requirements.

4.1.1.1 Basic Requirements - First System Approach

The patient unit should include the SE and the BLE SoC. Only the essential functions of each device should be implemented to enable a communication between both devices. The locating system unit, represented by the Raspberry Pi, should be able to locate and list BLE devices afterwards in a GUI.

4.1.1.1.1 Basic requirements for SE

1. UART interface: Start communication between SE and BLE SoC
2. Advertising Mode: Test if BLE SoC is locatable with the BLE development kit

4.1.1.1.2 Basic requirements for BLE SoC

1. Acts as slave in the master / slave system

4.1.1.1.3 Basic requirements for Raspberry Pi

1. Detect BLE devices
2. Create GUI
3. Show all detecting devices in the GUI

4.1.1.2 Basic Requirements - Second System Approach

4.1.1.2.1 Basic requirements for SE

1. CIPURSE data container
2. Write/ Read Data via NFC interface

4.1.1.2.2 Basic requirements for BLE SoC

1. Advertising Mode: Test if BLE SoC is locatable with the BLE development kit
2. UART interface: Start communication between SE and BLE SoC

The requirements for the Raspberry Pi does not change for the second system approach.

4.1.1.2.3 Basic requirements for Raspberry Pi

1. Detect BLE devices
2. Create GUI
3. Show all detecting devices in the GUI

4.1.2 Secure Controller

Infineon's SLE70 controller acts as master device in the first concept and is connected to the HCI of the Texas Instruments CC2564 via UART interface. This BLE SoC was chosen due to the standardized HCI to reduce the effort for programming of two different controller.

In addition, the SLE70 has a multi-tasking operating system and can deal with different tasks simultaneous. This is important for connection handling, data transfer with the BLE SoC and the heart rate sensor. Therefore, applications for a BLE handler, a NFC handler and a handler for the heart rate sensor data are required.

4.1.2.1 Flow-Diagram

The first steps include the initialization of all relevant parameters and registers for the advertising and sleep mode, which can be seen in figure 4.1.

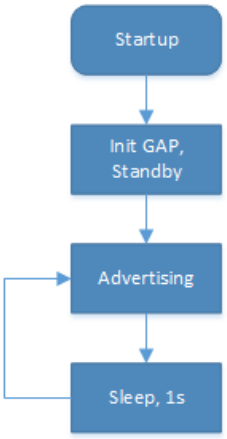

Figure 4.1: BLE SoC - simple stage

4.1.2.2 Implementation

The software for the SLE70 controller is written in the Keil Integrated Development Environment (IDE). Afterwards, the resulting HEX file can be flashed on the SLE70 by using the Infineon tool SmartcardManager. Flashing the controller is only possible via contactless interface. This means, that the prototype has to be fully assembled and connected to an antenna at the NFC interface.

4.1.2.2.1 Bluetooth Handler The BLE Handler describes the task to initialize the BLE stack and process events, which will be received from the BLE SoC. The Bluetooth Low Energy stack was developed by Infineon Technologies for the SLE70 controller, so this can be used to test the the fundamental communication to the BLE SoC. It consists of the Host part of the BLE architecture from figure 4.2 in subsection 2.1.2. For the implementation, the development view changed due to the Bluetooth Stack on the SLE70. The application and host layer from the BLE archtitecture is implemented in the SLE70 controller. Only the Controller layer rests on the BLE SoC, see figure 4.2 below. The BLE stack contains all mandatory layers from the Host part of the Bluetooth standard. A summary about the function of each layer in the BLE stack can be read in 2.1.2.2. Therefore, the L2CAP and GAP layer are required for the fundamental initialization for BLE.

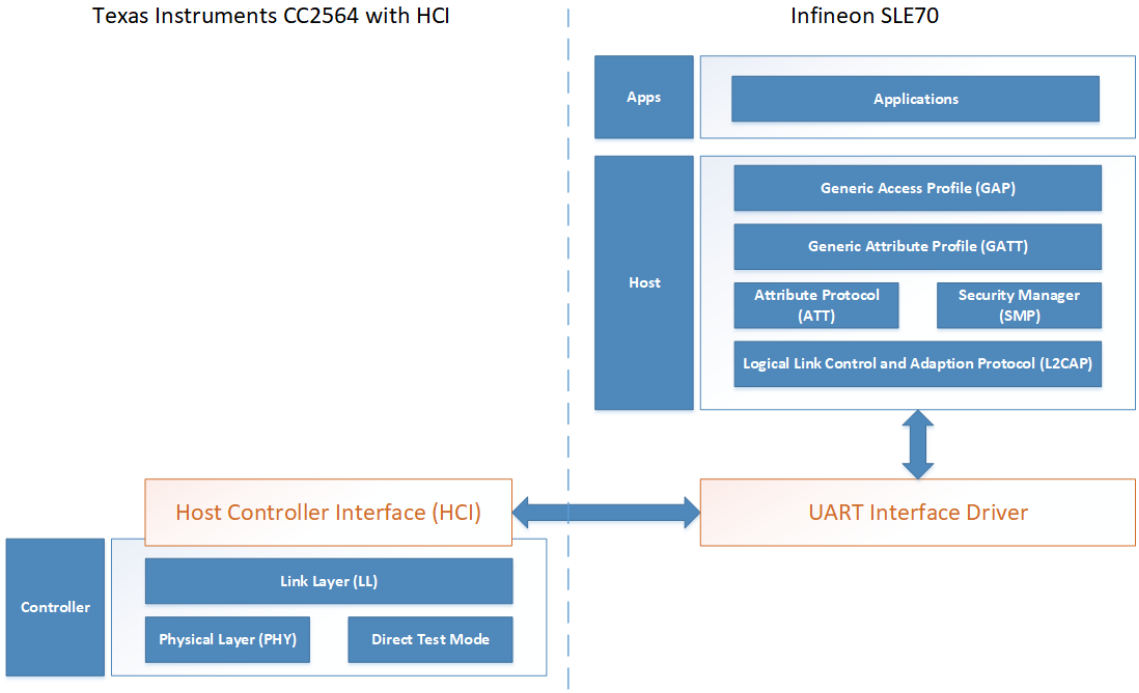

Figure 4.2: SLE70 Bluetooth Low Energy Handler

4.1.2.2.2 Heart Rate and NFC Handler The Heart Rate Handler and NFC handler were not implemented and tested due to problems with the UART communication

between the SLE70 and the Texas Instruments CC2564 BLE SoC. Unfortunately, the reason for communication failures was not found. An extensively testing of the printed circuit board PCB and on the software brought no further details. An estimation is, that the designed 4 layer PCB has issues at the inner layers because no prototype worked. The conclusion of this learnings was that a redesign of the concept is mandatory.

4.1.3 Bluetooth Low Energy SoC

Due to problems with the first design, a change between the controllers was needed as mentioned in the last section. The Texas Instruments CC2564 was replaced by the nRF52832 from Nordic Semiconductor. To simplify the system a bit and save yourself another source of issues, a BLE SoC module with included antenna and oscillator was choosen.

4.1.3.1 Flow - Diagrams

The first steps include the same tasks as mentioned in figure4.1. For the advanced application the communication between both controllers is established via 1 - Wire UART interface. In addition, an initialization of the I2C interface for data handling with the heart rate sensor should be the next step.

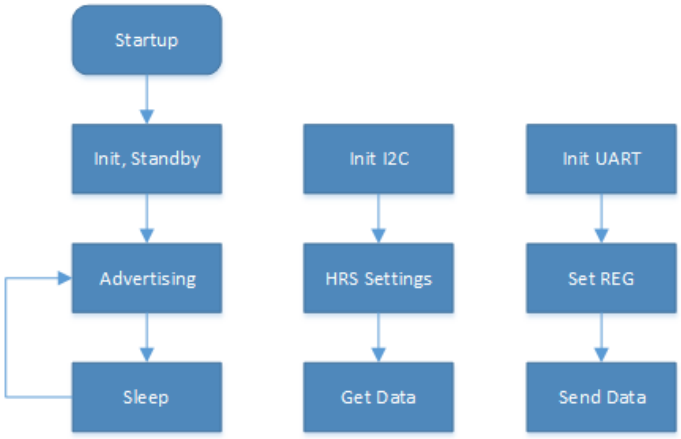

Figure 4.3: BLE SoC - advanced stage

4.1.3.2 Implementation

The IDE has changed from the Keil to the Eclipse software. By using Eclipse it is necessary to use the GNU MCU Eclipse plug-in for multi-platform embedded ARM development. The nRF52832 controller was flashed with the resulting HEX file by using the Nordic Semiconductor nRF52 development kit. By using the development kit, the nRF52 controller on the kit must be bypassed and the prototype is connected on a dedicated pin configuration, see figure 4.4.

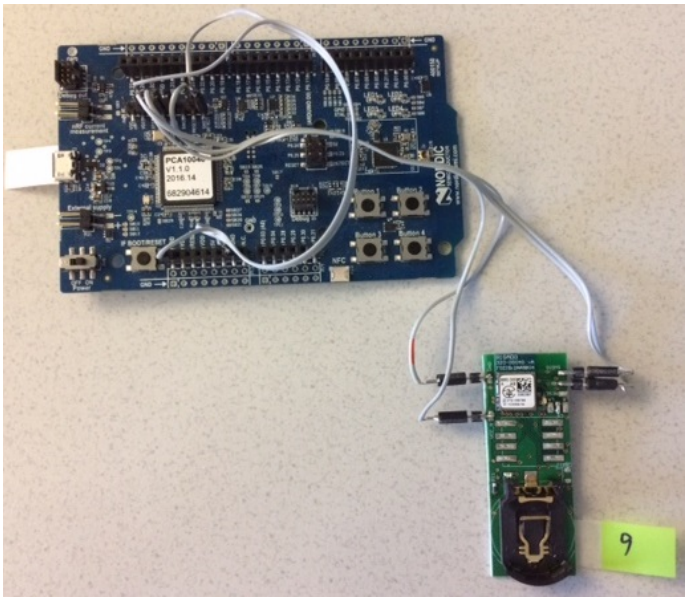

Figure 4.4: Nordic Semiconductor nRF52 development kit connected with prototype

4.1.3.2.1 Advertising Mode For an active advertising mode a few parameter settings are required. The code snippet below is only a small piece of them. It represents the struct for advertising parameters in the GAP layer.

```
uint8_t                          type
ble_gap_addr_t *                 p_peer_addr
uint8_t                          fp
ble_gap_whitelist_t *          p_whitelist
uint16_t                         interval
uint16_t                         timeout
ble_gap_adv_ch_mask_t    channel_mask
```

For the first test the advertising packet should be a non-connectable packet.

```
m_adv_params.type = BLE_GAP_ADV_TYPE_ADV_NONCONN_IND;
m_adv_params.p_peer_addr = NULL;
m_adv_params.fp = BLE_GAP_ADV_FP_ANY;
m_adv_params.interval = NON_CONNECTABLE_ADV_INTERVAL;
m_adv_params.timeout = APP_CFG_NON_CONN_ADV_TIMEOUT;
```

To set all parameters for active advertising an initialization should be done for the separatly BLE stack, all GAP parameters and also for the advertising mode and packet payload.

4.1.3.2.2 UART interface The 1-Wire UART interface solution is reduced to the absolute minimum as can be seen in figure 4.5. At the nRF52 controller a General Purpose Input Output (GPIO) pin is used as Input Output (IO). The drawback of this configuration is the small data transfer rate and the strict compliance of timings for reading and writing data. Both reasons can lead to a bottleneck for data transfer between the controllers, but this configuration is the only possible way. All bits of a data byte will be transmitted by the least significant bit (LSB) first. The packet frame consists of a start bit, one byte of payload, a parity bit and at least a stop bit.

A pullup resistor in the schematic provides a logic high on the bus passively. The nRF52832 GPIO pin configuration is open drain and acts as bus master. The cylce will be started by driving the 1-Wire bus from high to low via the GPIO pin, following by the start bit, payload, parity and stop bit. When data is send from the SLE70, the transmitted byte will also be seen on the RX pin.

For the UART implementation no further informations are available due to internal information restrictions.

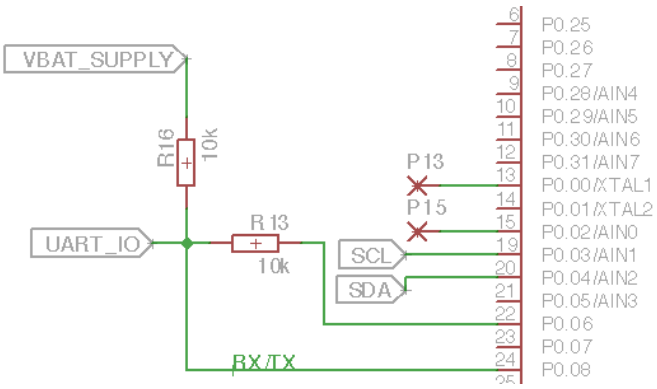

Figure 4.5: UART interface solution

4.1.3.2.3 I2C interface The heart rate sensor is connected via I2C interface to the nRF52 controller. Therefore, a clock SCL, a data SDA and a interrupt line are required for this connection. All bus lines are pulled to the power supply line VCC via resistors. The struct for the pin, frequency and interrupt configuration can be seen below.

```
uint32_t         scl
uint32_t         sda
nrf_twi_frequency_t      frequency
uint8_t          interrupt_priority
```

The clock frequency is set for the standard mode of the heart rate sensor, otherwise a fast mode can also be set with a clock of 400 kHz. The next steps include to set only those registers that are needed for the current mode. Altogehter there are twenty - seven user accessible 8 bit registers available to configure the sensor. Therefore, the proximity mode was configured to detect reflected light at close range. Since the prototype should be worn handwrapped the distance to the human skin should be as low as possible.

```
m_twi_config.scl = PIN_SCL;
m_twi_config.sda = PIN_SDA;
m_twi_config.frequency = NRF_TWI_FREQ_100K;
m_twi_config.interrupt_priority = APP_IRQ_PRIORITY_HIGH;
```

4.1.4 Raspberry Pi

The Raspberry Pi base station represents the locating system unit for a health care facility. After installing the operating system *Raspbian Jessie* on the Raspberry Pi and doing the initialization routine for the BLE and ethernet interface, the device is ready to use. The BLE interface uses the BlueZ Linux kernel-based Bluetooth stack which supports all Bluetooth protocols and layers, also including BLE. By implementing the first task, some issues occured with the initialization procedure of BLE at the device. Therefore, the scanning procedure fails all the time. After reinstalling BlueZ, updating and configuring the HCI setting with parameters, the interface works most of the time as expected. Sometimes, the HCI has issues and the Bluetooth adapter requires a restart, which was considered again in the code for the GUI application. The GUI was implemented with TKinter.

4.1.4.1 Flow - Diagrams

The first task will be described with the flow diagram in figure 4.6. A simple scan to locate all BLE devices in the detecting range and a clear listing of those devices should be done.

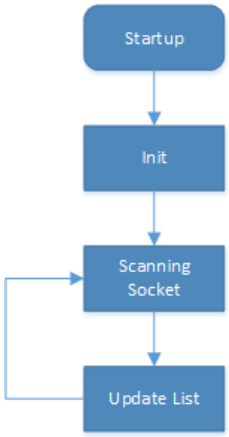

Figure 4.6: Raspberry Pi flow diagramm - simple stage

Figure 4.7 includes the next part of the software implementation. All scanned devices should be listed immediately at the GUI while scanning procedure is active. A separation should be done to see detected devices in a separate list. Furthermore, it is graphically shown, if a device to be searched was actually found in the list. This tasks are realized by using four different threads which will be controlled by different events.

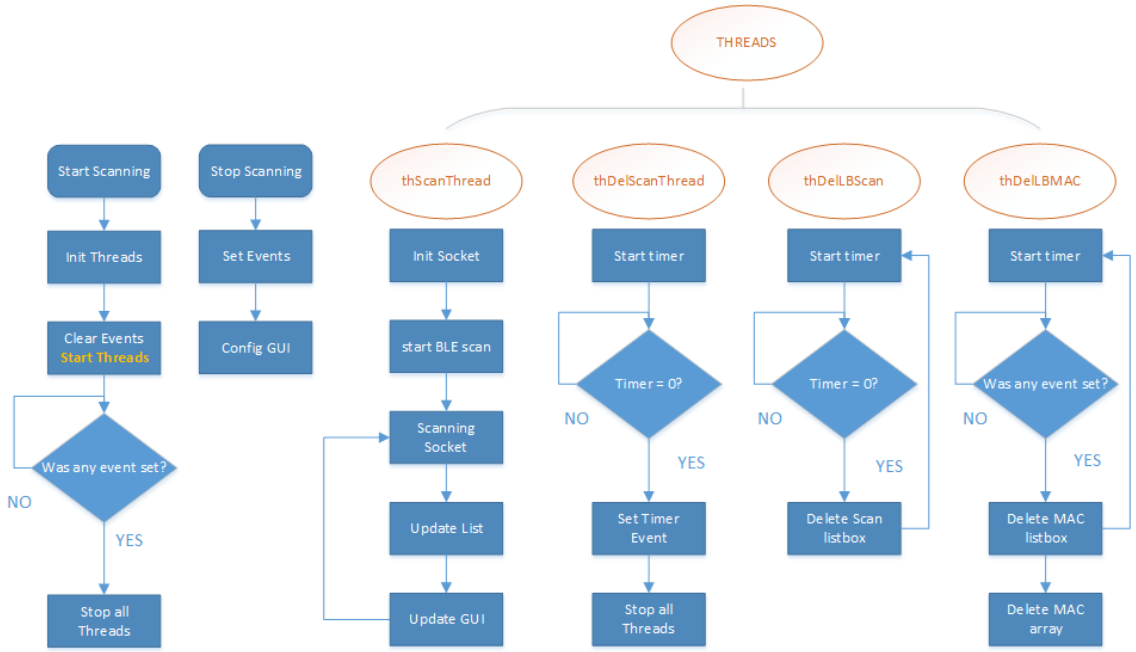

Figure 4.7: Raspberry Pi flow diagramm - advanced stage

4.1.4.2 Implementation

The implementation of the scan procedure starts with an initialization of the socket interface. At first, the socket module and all necessary address and protocol families are imported into the application, which can bee seen in the code snippet window below. All formats and options can be found in the BlueZ bluetooth stack.

4.1.4.2.1 AF_BLUETOOTH For handling Bluetooth communications, the *AF_BLUETOOTH* address family is required and includes different address and protocol formats. One of them is the *BTPROTO_HCI* format which accepts the Raspberry Pi device address.

4.1.4.2.2 SOCK_RAW This socket type provides a raw network protocol access. The receiving or sending packet structure includes custom headers which are not provided by the used operating system.

4.1.4.2.3 SOL_HCI Changing socket options can be applicable on the HCI level, which is necessary for the use of setting event filters.

4.1.4.2.4 HCI_FILTER The *HCI_FILTER* option will be used to set HCI event filters on the socket.

4.1.4.2.5 SHUT_RD Handles the shutdown of the streaming procedure of the socket. The receiving command *recv()* of the *BlueZ* bluetooth stack is set to 0 and indicates an end of the data stream.

```
from socket import (
        socket,
        AF_BLUETOOTH,
        BTPROTO_HCI,
        HCI_FILTER,
        SOCK_RAW
        SOL_HCI,
        SHUT_RD,
)
```

Furthermore, a raw HCI socket object will be created with *AF_BLUETOOTH*, *SOCK_RAW* and *BTPROTO_HCI*. It is necessary to set a timeout after this command to avoid issues with the socket. Currently, the socket object is not assigned to any address. The next step is to bind an address to the socket object before a receiving command will be started. Setting BLE scan parameters and allowing advertising events are the next tasks. Furthermore, setting or manipulate socket options is done with the types *SOL_HCI* and *HCI_FILTER*.

```
bluez = CDLL(btlib, use_errno=True)
device_id = bluez.hci_get_route("B8:27:EB:AA:CE:42") # RPi address of
    bluetooth device on hci0
sock = socket(AF_BLUETOOTH, SOCK_RAW, BTPROTO_HCI)
sock.settimeout(3) # wait 3 seconds to stop
lblStatusTxt.configure(text=sock)
sock.bind((device_id,))
```

To get the MAC address from the BLE advertising packet, it is important to know, that the most significant bit is placed in a reverse order in the packet. Therefore, the extracting data from the packet must be reversed accordingly. An advertising data packet is 0 - 37 byte long, which can be seen in figure 4.8. The first 6 bytes include the advertising address, the following byte describes the length of the advertising data struct and the second byte is the advertising type of the struct. All other bytes include the payload.

Devices in the state *LE General Discoverable Mode* and *BR/EDR Not Supported* includes a 0x01 as advertising type. The value 0x01 represents the flag type and the payload is only one byte long. So up to eight flags can be set in the last byte. All in all, summing up the Cyclic Redundancy Check (CRC) and the additional 3 bytes from the advertising payload above results in 6 bytes. [49] The code snippet below shows the withdrawal and reversal of 6 bytes representing the address by the array indices from 7 to 12 while the rest of the packet will be removed.

```
dev_addr = (':'.join("{0:02x}".format(ord(x)) for x in socket_data
    [12:6:-1]))
```

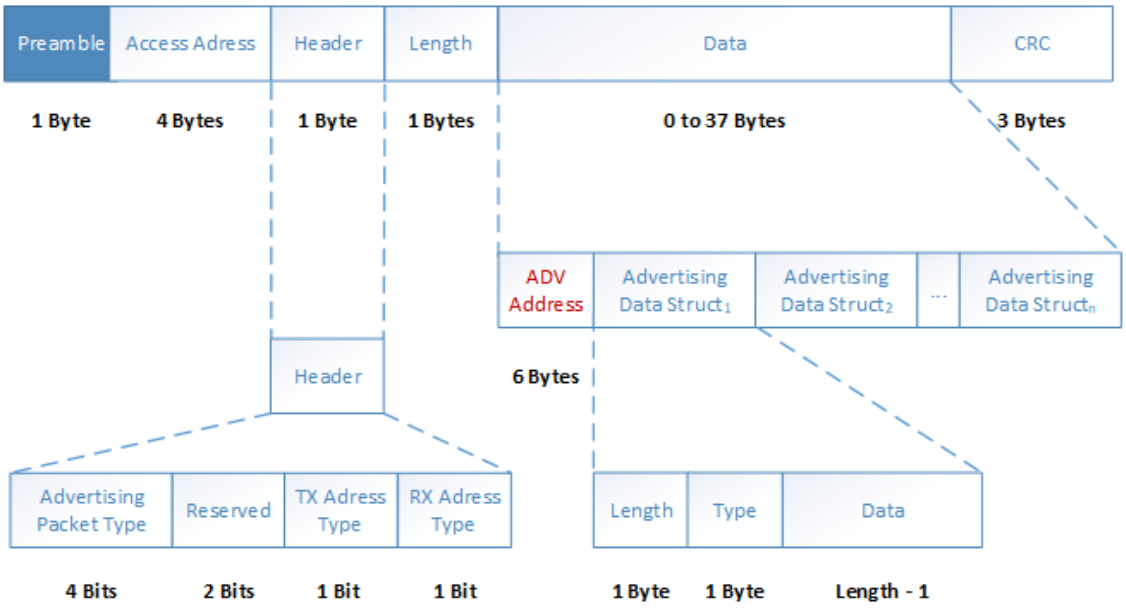

Figure 4.8: BLE advertising packet

The advanced version of the locating system should display the scanning event and the locatable devices in on the GUI. To handle these tasks all simultaneous, this can only be realized by implementing events and threads. Each thread will be handled by different events. The defined threads and their use case will be mentioned below.

```
thScanThread = threading.Thread(target=scanDevices)
thScanThread.daemon = True

thDelScanSocket = threading.Thread(target=sleepThread)
thDelScanSocket.daemon = True

thDelLBScan = threading.Thread(target=delLBScan)
thDelLBScan.daemon = True

thDelLBMAC = threading.Thread(target=delLBMAC)
thDelLBMAC.daemon = True
```

4.1.4.2.6 thScanThread This thread starts the device scanning part where socket informations will be read throughout. This procedure includes the initialization of the socket, the HCI parameter settings, scanning the socket and extracting the BLE device address from the incoming data.

4.1.4.2.7 thDelScanSocket This thread sets a timer for deleting the input buffer from the received data. All data will be transfered during the scanning procedure into the defined lists.

4.1.4.2.8 thDelLBScan To handle also the listbox content with the current scanning results, a thread is needed with the same responsibilities compared to the *thDelScanSocket* thread. The course of listed devices will be deleted after a configured timer interval as long as the scan procedure is active. This task is necessary to reduce the information content from the listbox in the GUI. The timer interval is 10 seconds.

4.1.4.2.9 thDelLBMAC The course of listed devices will be deleted after a configured timer interval as long as the scan procedure is active. This is necessary to show if the listed device is in the range of the Raspberry Pi after the timer interval. After stopping the scanning procedure, the list and the listbox with the single displayed MAC addresses should be cleared. The timer interval is 10 seconds.

4.1.4.2.10 Graphical User Interface Figure 4.9 shows the GUI while actively scanning the socket for BLE devices. With the *start BLE* button, all informations from the configured socket object are evaluated for addresses in the left listbox below. A second listbox, nearby the left listbox, includes the uniquely MAC addresses of each located device. Therefore, two different devices were found. Listing MAC addresses instead of names is confusing, but for software testing, it is a much easier way for comparing the scanned address with the known MAC address from the BLE device on the wristband. A second listbox with device names which creates references to the MAC addresses from the other listbox will be the solution for this problem.

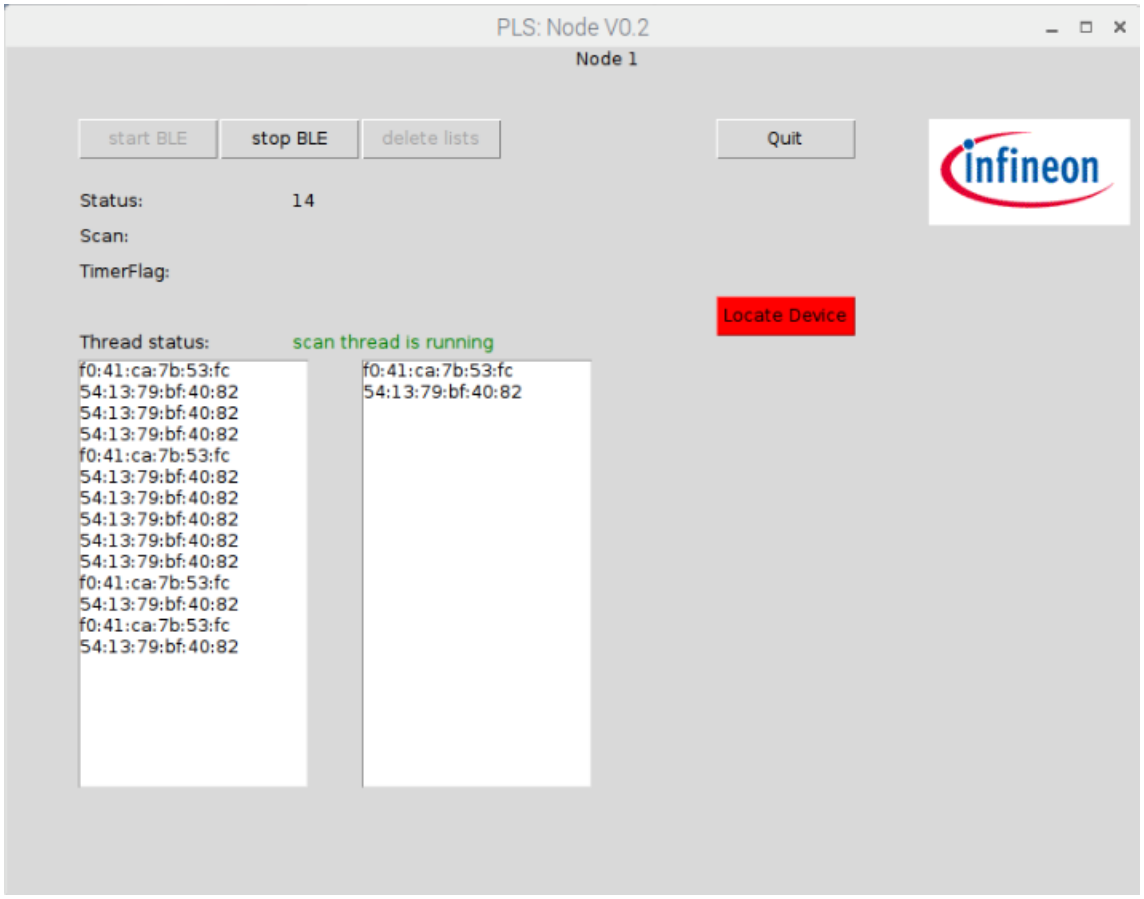

Figure 4.9: GUI on Raspberry Pi for locating Patient Locating System Devices - two detected devices

Figure 4.10 shows the results of a second node in both listboxes after another scanning run. The scanning procedure has stopped after the timer stops and shows only one located BLE device. We have now the information, that one BLE device is in the intersection of both nodes. This indicates that the patient with this device can be found in an area between both devices.

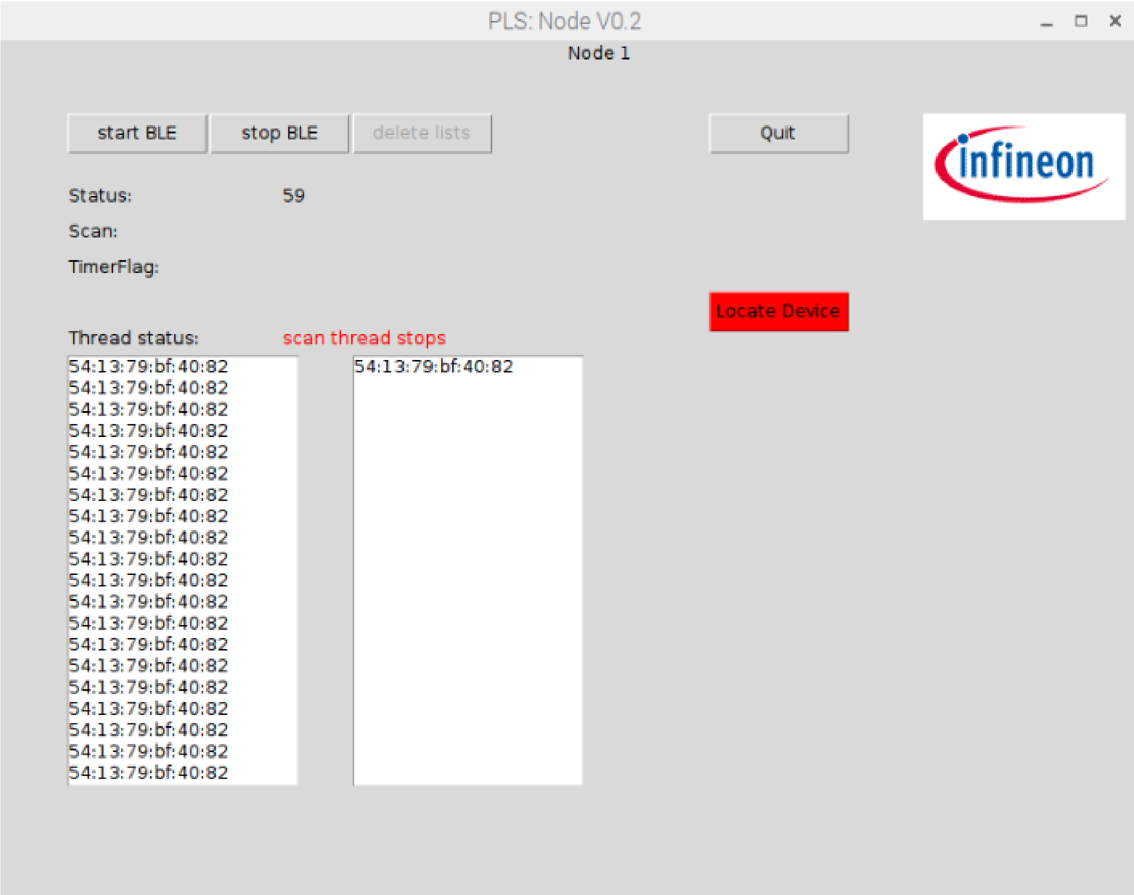

Figure 4.10: GUI on Raspberry Pi for locating Patient Locating System Devices - only one detected device

5 System Measurements, Simulations and Testing

5.1 Energy Harvesting

This chapter describes the measurement and test results of the energy harvesting block, which includes the photovoltaic cell, comparator, energy harvesting IC and battery charger IC section.

5.1.1 Photovoltaic Cell

Measuring the output voltage of the photovoltaic cell with direct incidence of sunlight results in a voltage of 0,5 V, which represents the nominal voltage of the cell. With a window glass plane in between the output voltage decreases by 50 mV. Using the cell indoor at direct fluorescent lamp light, the resulting output voltage decreases to 0,3 V. The measured waveform of the voltage is a rectified sine wave with 50 Hz, which can be seen in figure 5.1. To damp the oscillation in the output signal a parallel connected capacitor with a value of 1 μF is used.

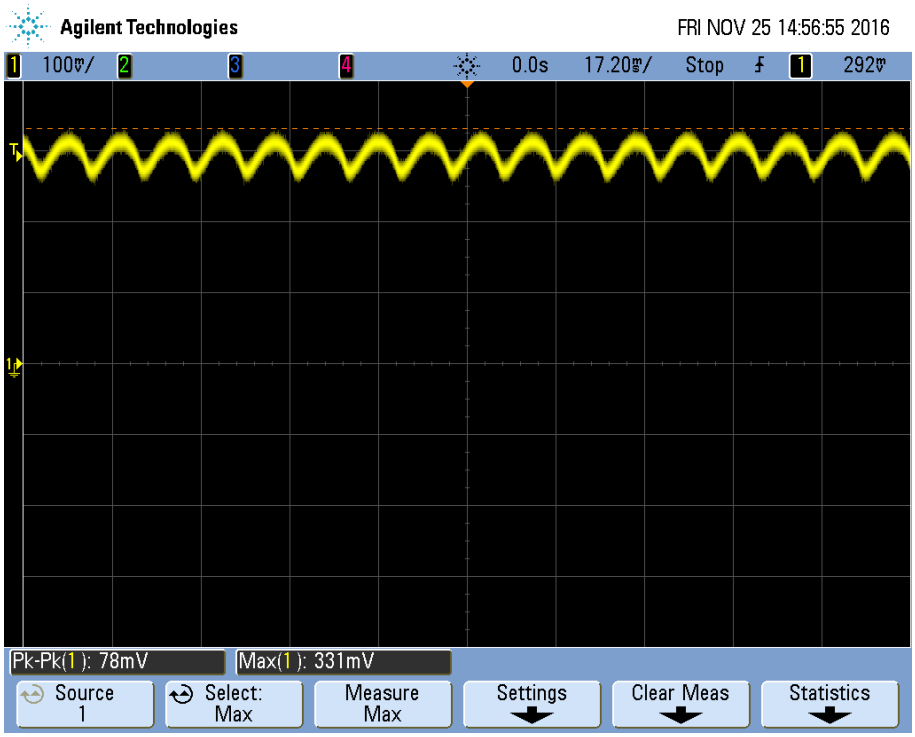

Figure 5.1: Photovoltaic cell: measurement of rectified 50 Hz oscillation

5.1.2 Comparator and Inverter Section

To test the comparator and inverter section a triangle waveform with 100 Hz from a waveform generator is applied on one input of the comparator. On the other input a constant signal is applied. The signal properties from the waveform generator are listed below:

- Triangle waveform frequency: $f = 100\,Hz$
- Peak voltage: $V_{Peak} = 500\,mV$
- Lower voltage limit: $V_{Low} = 200\,mA$
- Symmetry: 50 %

On the second input a DC signal with 451,90 mV is applied. Figure 5.2 shows the triangle waveform (blue), the DC input signal (green) and the resulting output signal (yellow) after the n-channel MOSFET section. The yellow signal represents the input signal of the energy harvesting IC. The measured spikes in the figure are the product of an unindended formed ground loop with the oscilloscope probes.

Figure 5.3 shows the measured hysteresis band with 50 mV at 100 Hz.

By increasing the frequency of the triangle waveform up to 1 kHz the measured hysteresis band is 186,88 mV, see figure 5.4. Therefore, by applying higher frequencies at the input, it

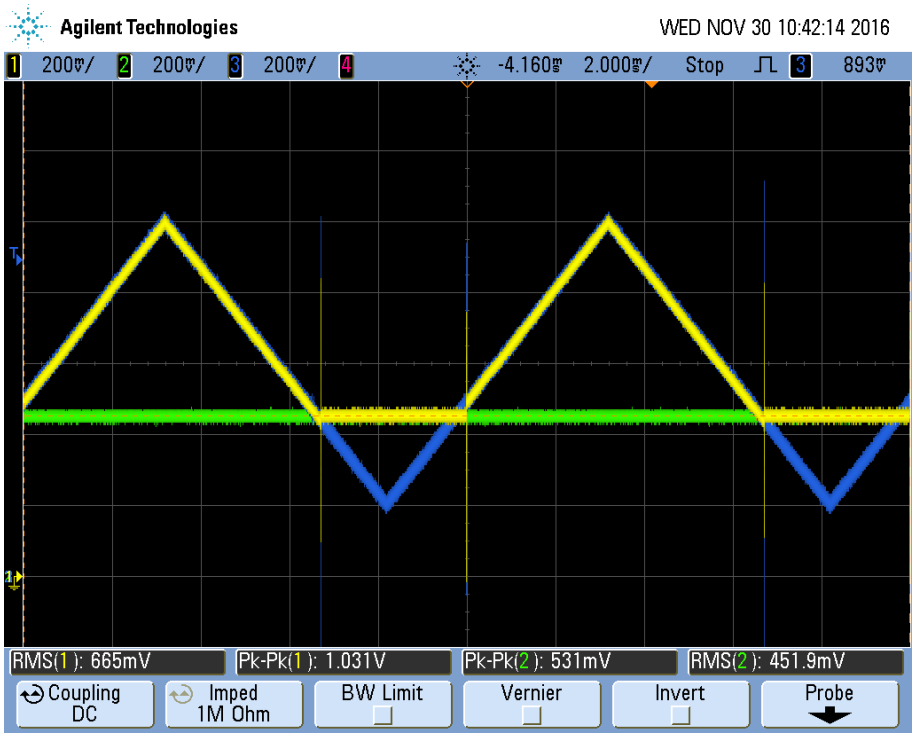

Figure 5.2: Comparator: measured output with triangle waveform and DC signal on the input

is necessary to decrease the resistor values from the circuit to narrow the hysteresis band. By applying DC signals on both inputs, the calculated hysteresis band $V_{HB} = 20\,mV$ from subsubsection 3.1.3.3 is measured.

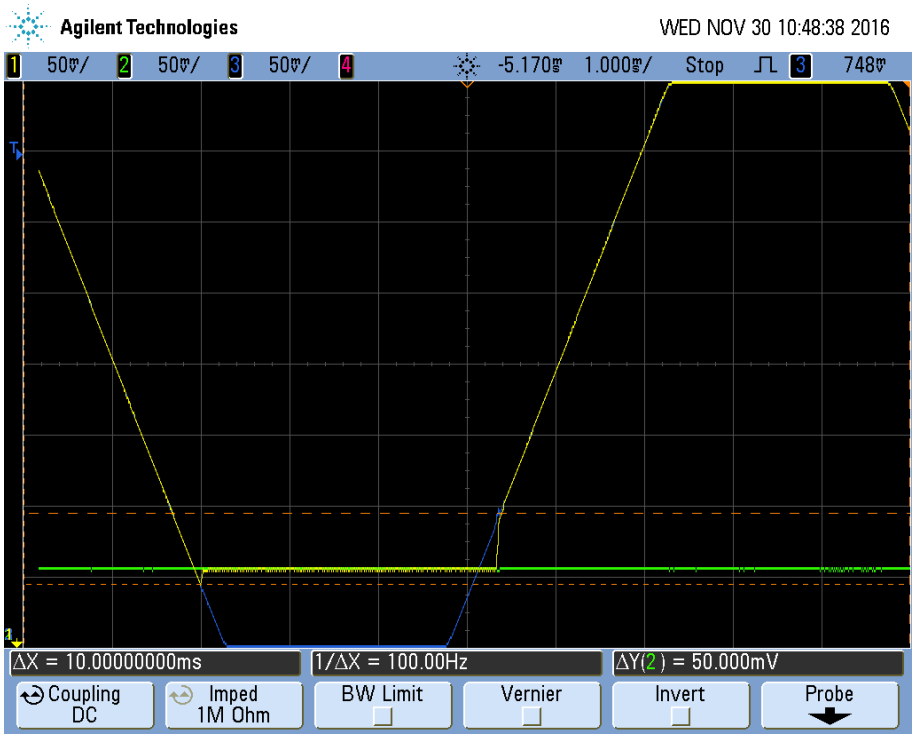

Figure 5.3: Comparator: measured hysteresis with 100 Hz triangle waveform and DC signal

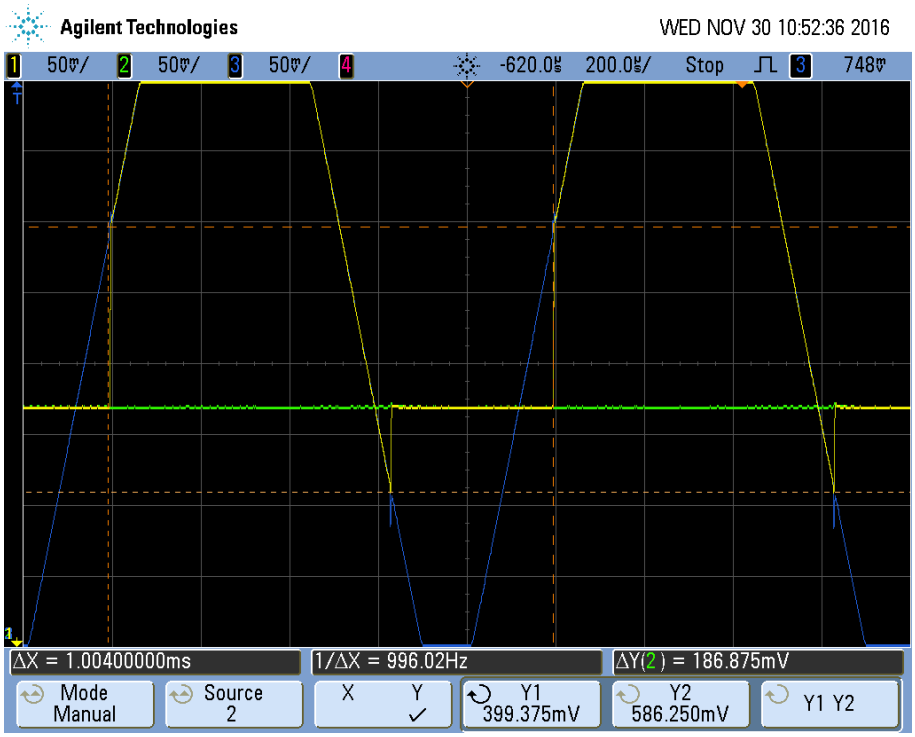

Figure 5.4: Comparator: measured hysteresis with 1k Hz triangle waveform and DC signal

5.1.3 Energy Harvesting IC

The following figures show the measurement results from the energy harvesting section. For the first measurement a power supply is connected at the input V_{cell0} connector and V_{cell1} is short circuited to ground. Additionally, the capacitor $C13 = 1\,\mu F$ from the battery charger section is utilized without assembling the charger IC itself. Using only $C10 = 30\,pF$ at the output of the energy harvesting IC results in a noisy signal 5.5.

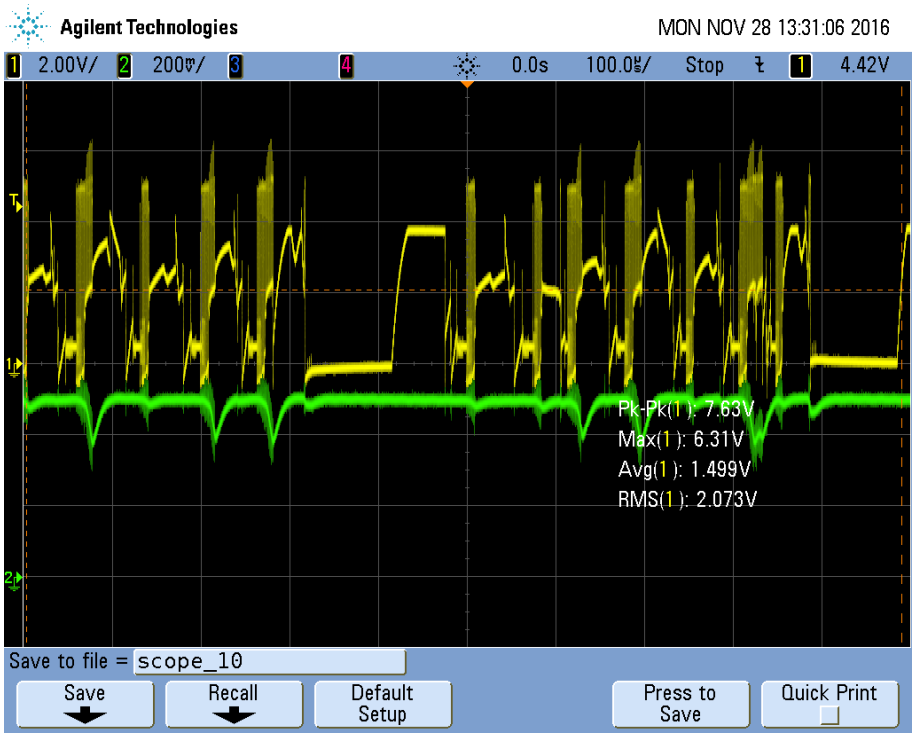

Figure 5.5: Energy harvesting IC: measured noisy signal due to form an open loop circuit

By applying $395,80\,mV$ at the input, the energy harvesting IC starts and a output voltage of 3,04 V is measured at the output pin, see figure 5.6. An increase of the input voltage to 418,00 mV results in a high current consumption of around 30 mA for one second and an output voltage of 4,19 V. A decrease of the resistor value $R10 = 1,5\,M\Omega$ to $R10 = 1,3\,M\Omega$ results that the IC starts at 0,32 V input voltage to harvest energy. The measured output voltage is 3,71 V. A high current consumption is detected as before.

By decreasing the input voltage to 0,24 V the energy harvesting IC can maintain the output voltage at nearly the same value of 3,7 V. Applying a voltage below 0,24 V at the input, the output voltage decreases and at 0,2 V the output voltage drops under 1 V.

By using the photovoltaic cell, the cell is exposed to sunlight with a window glass plane in between and an output voltage of 0,43 V. The cell is directly connected to one input of the comparator. The second input is supplied with a power supply to switch between both input signals by utilizing the comparator section. The comparator section and the inverter

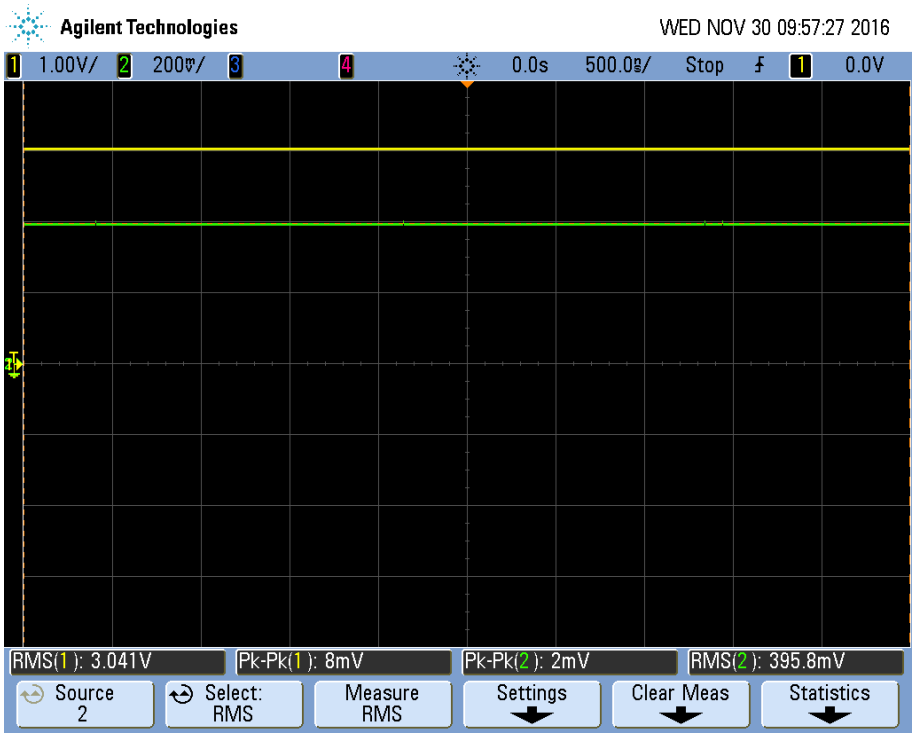

Figure 5.6: Energy harvesting IC: measured output signal by applying $395,80\,mV$ at the input by using a power supply

works as expected but the energy harvesting IC provides only 2,2 V at the ouput. After increasing the power supply voltage up to 0,45 V the current consumption increases for one second and the output voltage is 3,7 V. A decrease of the power supply voltage ensures that the cell supplies the energy harvesting section. Several measurements showed that the start threshold of the boost converter could not be exceeded with the photovoltaic cell.

The conclusion of the measurement results is that the photovoltaic cell is not capable to provide such a input voltage and current to get above the threshold of the energy harvesting IC. Therefore, the energy harvesting section will not be assembled in the next system design.

5.1.4 Battery Charger IC

Using the battery charger IC with the output voltage of 3,7 V from the energy harvesting IC results in an output voltage of 4,2 V. Due to the unsufficient results of the photovoltaic cell with the energy harvesting section, this section will not be assembled in the next design.

5.1.5 Current Consumption

The following figures show the current consumption of the board in an advertising mode and by deactivated status LED. In figure 5.7 the advertising mode with an interval of $t = 500\,ms$ and a transmission power of 0 dBm is set. An Infineon internal designed measurement board is utilized to measure the current consumption of the system. The voltage is measured via oscilloscope at a $R = 100\,\Omega$ resistor. Therefore, the voltage values on the oscilloscope has to be divided by $R = 100\,\Omega$ to calculate the current.

Figure 5.7: Current consumption of a continuous 500 ms advertising event

Figure 5.8 shows the measured advertising event in a range of 4 ms.

Figure 5.8: BLE advertising event

The current consumption of this advertising event can be calculated with the expressions below. With the time t=4 ms and the mean voltage of $V_{Adv} = 368\,mV$, the current and the charge Q of the event are calculated.

$$I_{Adv} = \frac{U_{Adv}}{R} = \frac{368\,mV}{100\,\Omega} = 3,68\,mA \tag{5.1}$$

$$Q = I_{Adv} \cdot t = 3,68\,mA \cdot 4\,ms = 14,72\,\mu C \tag{5.2}$$

$$I = \frac{Q}{t_{Adv}} = \frac{14,72\,\mu C}{501,07\,ms} = 29,37\,\mu A \tag{5.3}$$

The resulting current consumption in a range of $t = 501,07\,ms$ is $29,37\,\mu A$ without any activated LED, sensor or SE.

5.1.6 Localization Distance

In terms of wristband device localization, an indoor range of approximately 17,5 m is achieved (measured with room plan). The output power of 0 dBm is sufficient to locate the smart wristband through three walls within the measured distance.

5.2 Antenna Simulations

Figure 5.9 shows the PCD antenna and the antenna design from section 3.1 in 3 D. For this simulation design two various coordinate systems are implemented. Therefore, the coordinate system of the antenna is placed with an offset of 15 mm in z - direction from the PCD antenna.

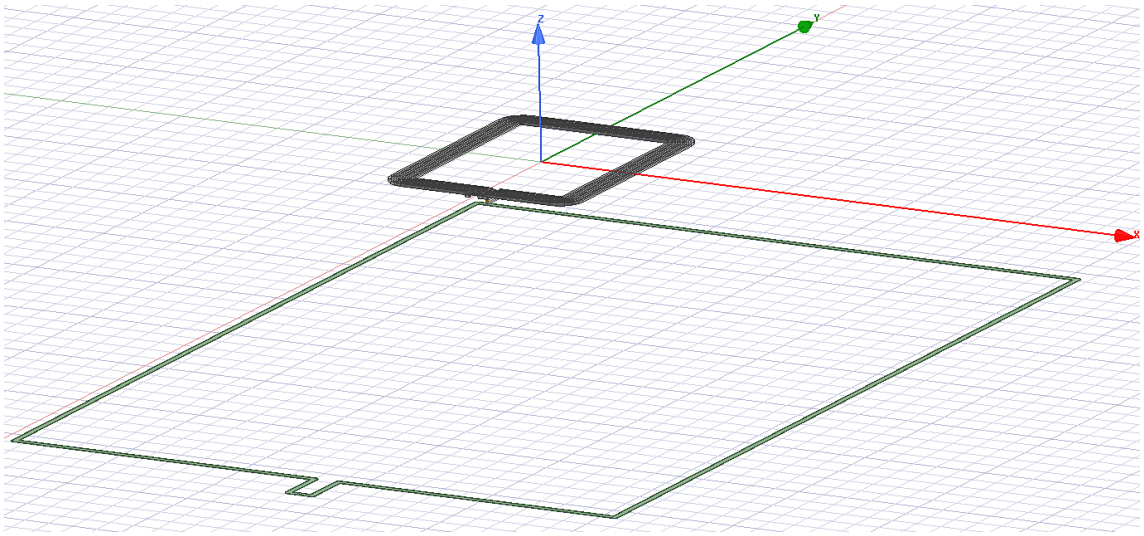

Figure 5.9: Antenna 3 D design with addtitional reader antenna below to simulate the induced voltage

Figure 5.10 shows the open circuit input impedance Z11 in a frequency sweep from 1 - 30 MHz for the antenna and the 56 pF SE. The resonant frequency can not be determined in this sweep due to the selected resolution. By using an internal created MATLAB script for equivalent circuit parameter determination, the resonance frequency can be determined, see 5.1. It can be seen that the system is not tuned to the carrier frequency of 13,56 MHz. In addition, a calculation process can be done after the simulation procedure by adding a parallel tuning capacity. With an additional capacity of $C_{P1} = 100\,pF$ and $C_{P1} = 2,2\,pF$ the whole system is in resonance, see 5.11.

Table 5.1 shows all simulated parameters of the system in untuned and tuned conditions.

Table 5.1: Calculated equivalent circuit parameters from the simulated antenna

C_{Chip}	C_p	f_{res}	R	L	C	Q
pF	pF	MHz	Ω	μH	pF	-
56	0	22,71	0,89	0,87	56,57	138,61
56	102,2	13,50	0,66	0,87	158,48	111,42

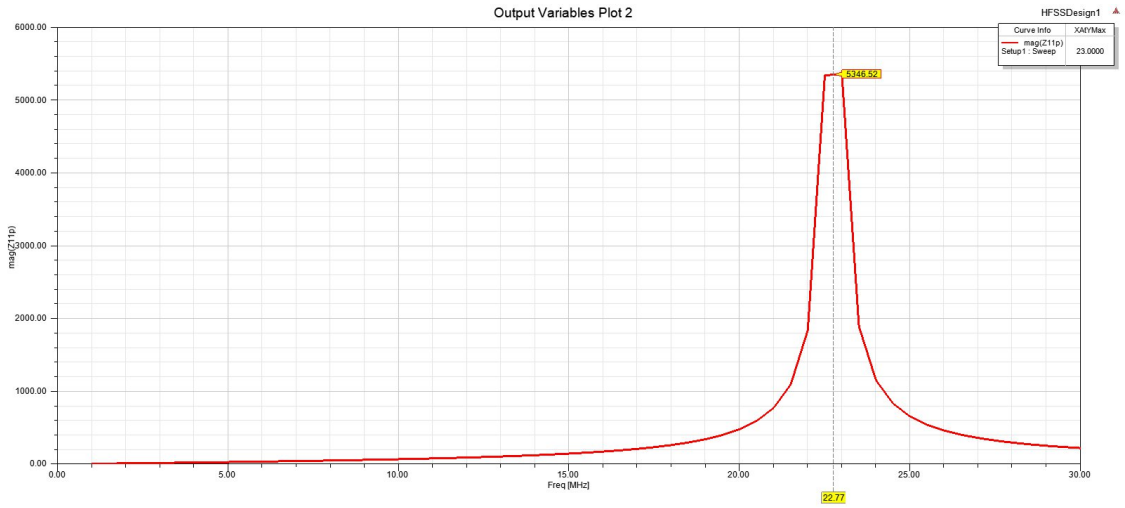

Figure 5.10: 56 pF SE and antenna: simulated frequency response of Z11

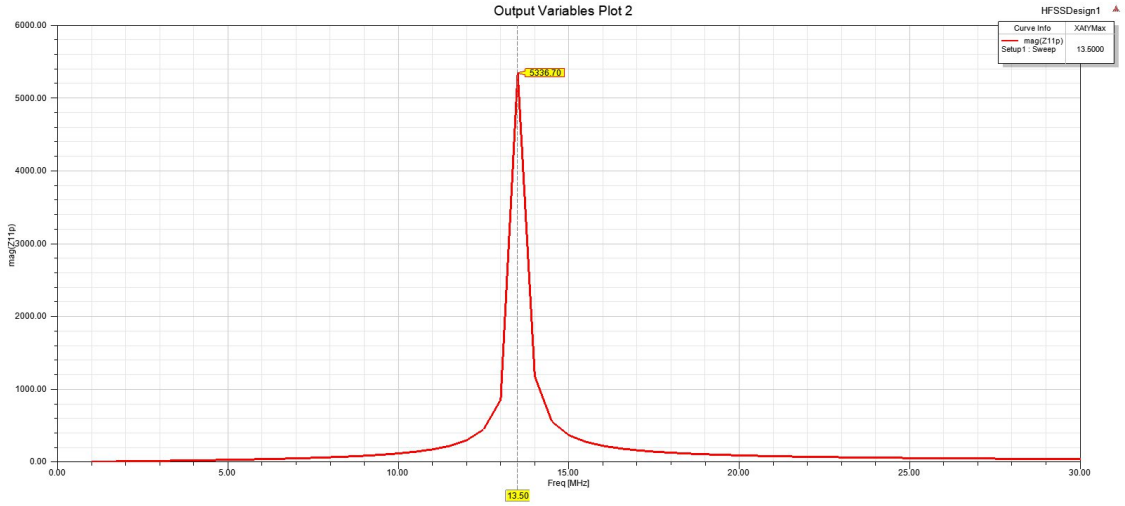

Figure 5.11: 56 pF SE, tuning capacity of 102,2 pF and antenna: simulated frequency response of Z11

The figure 5.12 shows a preprocessing circuit to determine the induced voltage in the antenna. To calculate the induced voltage V_{Ind} at various distances from the origin of the coordinate system of the antenna, a preprocessing circuit is used. This circuit contains the equivalent circuit diagram of the SE with a parallel placed capacitor and a resistor. With Port1 the PCD antenna is supplied with a sine wave of 1 V in amplitude at 13,56 MHz. The simulated parameters can be seen in table 5.2. Due to the small geometries of the antenna in comparison to the PCD antenna only a quarter of the Port1 voltage will be induced into the antenna at a offset position of 15 mm (d=0 mm).

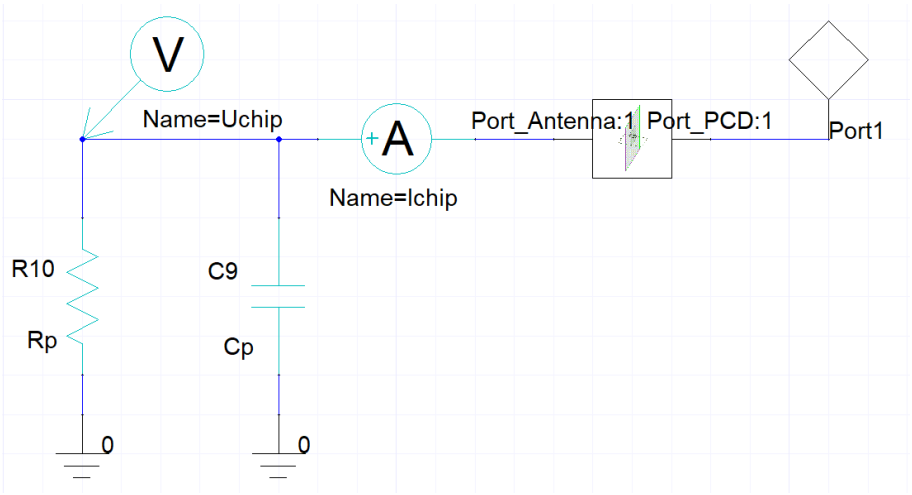

Figure 5.12: Preprocessing circuit

Table 5.2: Simulation of induced voltage in the antenna at different distances from the PCD, offset=15 mm

d	C_{Chip}	C_p	f_{res}	V_{Ind}
mm	pF	pF	MHz	mV
0	56	0	22,71	264,34
10	56	0	22,70	171,88
20	56	0	22,69	108,85
30	56	0	22,69	70,41
40	56	0	22,70	47,19
50	56	0	22,71	32,60
60	56	0	22,70	23,33
0	56	102,2	13,56	283,91
10	56	102,2	13,56	184,54
20	56	102,2	13,55	117,12
30	56	102,2	13,55	75,75
40	56	102,2	13,56	50,71
50	56	102,2	13,56	35,06
60	56	102,2	13,56	25,05

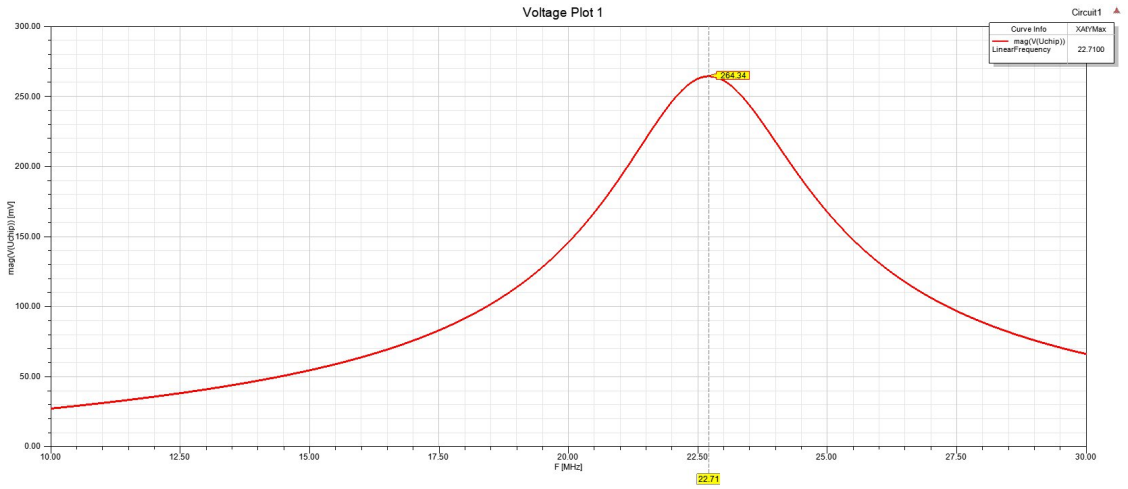

Figure 5.13: 56 pF SE and antenna: simulation of induced voltage at $d = 0\,mm$

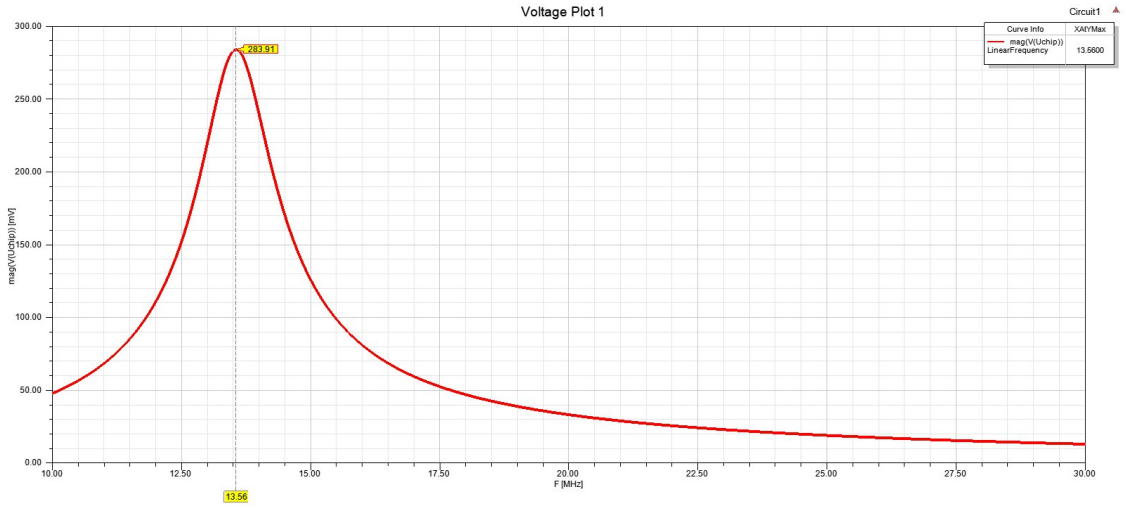

Figure 5.14: 56 pF SE, tuning capacity of 102,2 pF and antenna: simulation of induced voltage at $d = 0\,mm$

5.3 Antenna Measurements

To measure the resonance frequency of the antenna design a Bode 100 vector network analyzer from Omicron is used. The system is measured at a power of $-18\,dBm$ and at a offset distance of 20 mm. Figure 5.15 shows the frequency responce of Z11 by measuring the untuned system. The resulting resonance frequency is at 24,60 MHz which is a higher value in comparison to the simulation value of 22,71 MHz. The difference of both values results due to the drilled supply lines from the PCB to the antenna, see figure 3.22 from subsection 3.1.4, the hand - laid conductor lines of the antenna and the output power of $-18\,dBm$. At this power the SE is in an unloaded condition.

Figure 5.16 shows the system with three additionally parallel implemented capacitors

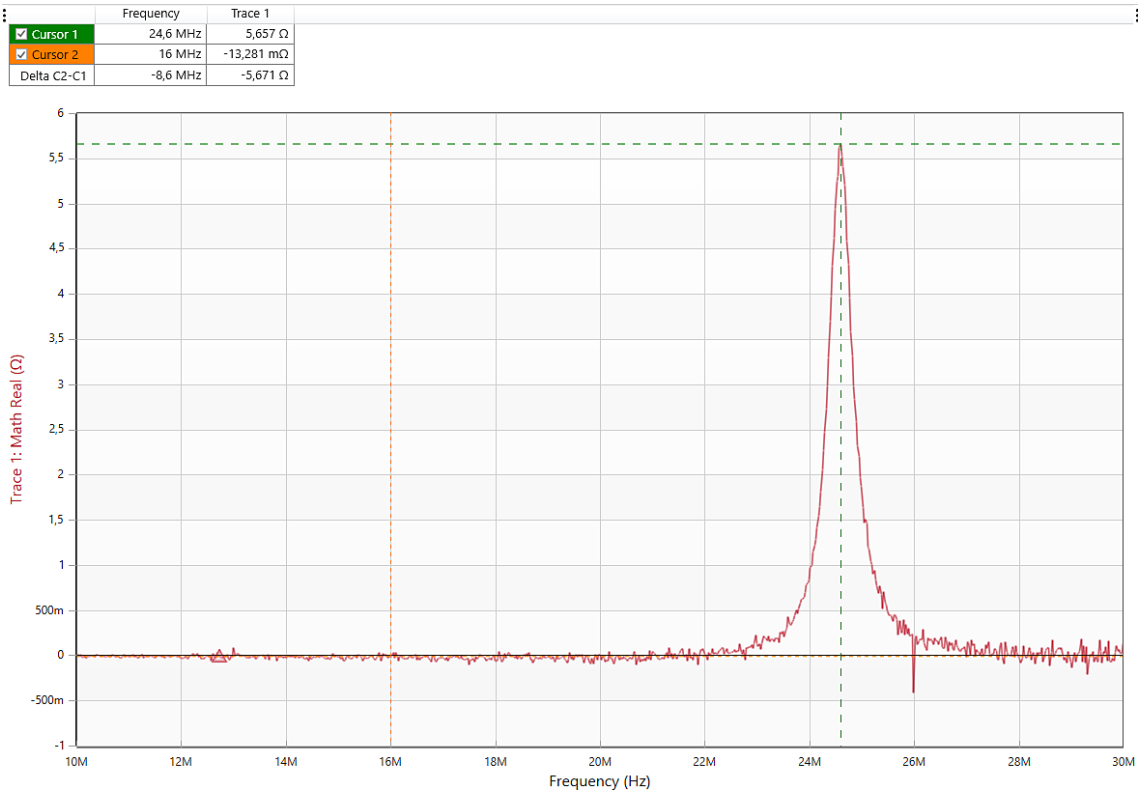

Figure 5.15: 56 pF SE and antenna: measured frequency response of Z11

with values of $C_{P1} = 100\,pF$, $C_{P2} = 10\,pF$ and $C_{P3} = 4,7\,pF$, which results in $C_P = 114,7\,pF$. The measured resonance frequency is 13,57 MHz. Additionally, the quality factor Q is 69,1 which is lower than the simulated value.

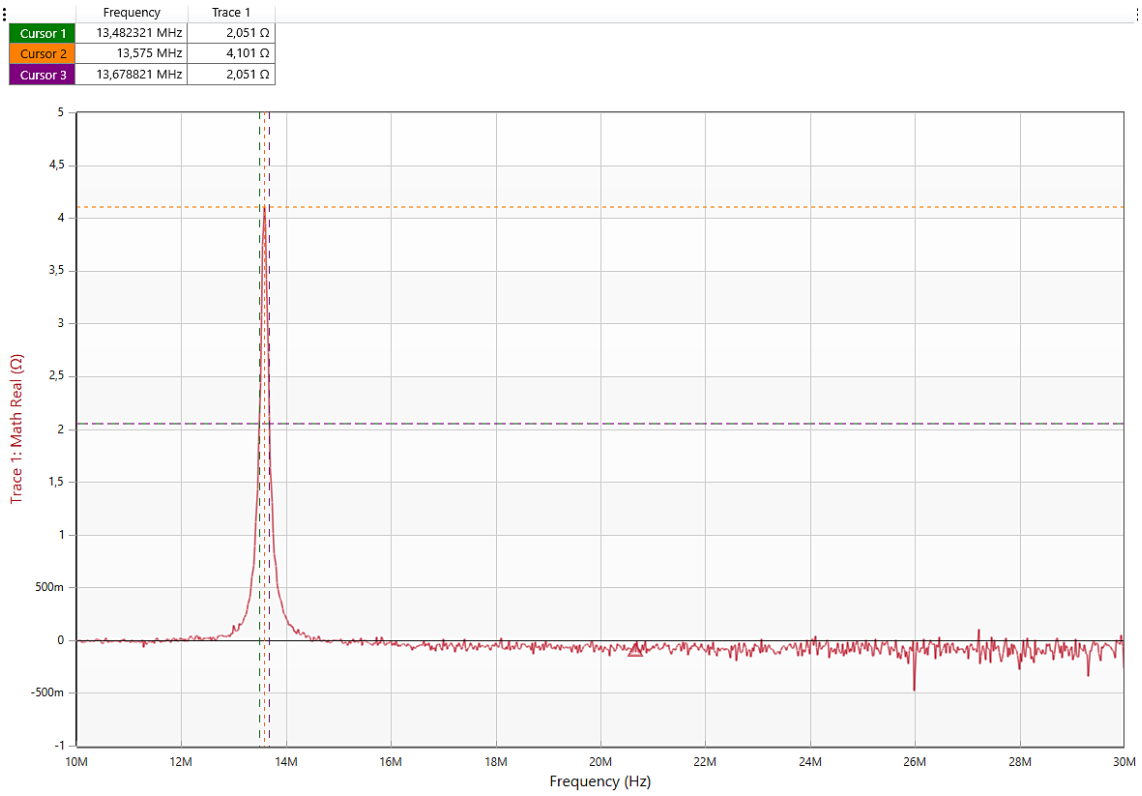

Figure 5.16: 56 pF SE, tuning capacity of 102,2 pF and antenna: measured frequency response of Z11

5.4 Reading Distance

With the current antenna tuning values a maximum reading distance of 2 cm on a Ingenico and ViVOpay payment reader is measured. For the given antenna geometry the value of 2 cm can be considered quite acceptable. A better performance can be achieved by an additional matching circuit or at least with a larger antenna.

6 Conditions for Classification as Medical Device

The classification for medical devices has consequences in comparison to non-medical devices, such as wellness devices. Therefore, a distinction is made between legal, administrative and organizational obligations. This includes risk and quality management, a safe design and production, a documentation and a market approval and surveillance. All of these obligations are associated with higher effort and costs. According to the international generic standard for electromedical devices *EN IEC 60601-1*, the classification of a product has to be done by the manufacturer itself. Since only the manufacturer knows the intended purpose of the device. If the manufacturer is not entirely sure about the classification, European Notified Bodies can give an advice to his product.
Medical devices can be separated into three different categories and each category is governed by a specific EU directive. Accordingly, a distinction is made between the following categories:

- *Medical Device Directive (MDD) 93/42/EEC*
- *In Vitro Diagnostic Medical Devices 98/79/EEC*
- *Active Implantable Medical Devices 90/385/EEC*

Furthermore, each medical device can be characterized into four different conformity classes I, IIa, IIb and III. Each conformity class includes different risk profiles. The risk reaches from no or insignificant risk in class I, to small risk in class IIa, elevated risk in class IIb and in high risk in class III. [28]

According to the smart wearable wristband which is designed and developed in this master's thesis, the medical intended purpose with the current tasks is not given. The wristband has the ability to locate patients, support connection handling to other devices of the IT infrastructure via BLE and stores patient data securily. Therefore, the device can be classified as non-medical device and also as medical device. The highest conformity class that this device can achieve in the MDD 93/42/EEC is class I, comparable to a current medical plastic wristband in the hospital sector.

If the heart rate sensor is implemented and the data of the sensor can be used for a medical purpose, like alarming the hospital staff by low heart rates, the constraints will changed. Therefore, the device can be classified as conformity class IIa device.

7 Conclusion

7.1 Conclusion

Nowadays, smart wearable devices combine many communication technologies and will play an important role in the future for the consumer and for the health care market. Even, there are only a few medical devices designed as a smart wristband available, the outlook, however, looks promising for the future. Innovations in this sector will not stop and the diversity is increasing, which can be seen in devices like smart contact lenses, eyeglasses, stents and wristbands. Understanding the capabilities of energy harvesting methods and communication interfaces like BLE and NFC in combination with sensors are important components for future systems.

According to the prototype, the smart wristband contains technologies for various applications. For patient locating, the BLE interface is a common technology which also can be used for small data transfers between two devices and can operate in different states like acting as a beacon or a transceiver. According to the distance of localization, the measured distance is 17,5 m with an output power of 0 dBm. The possibility for secure data storage to keep patient-related data save is enabled by the inclusion of application software which is developed in conformance with the CIPURSE standard. Additionally, the NFC interface of the SLE70 SE provides a close communication range for secure data transfer between the wristband and a reader device. By using the NFC interface a maximum reading distance of 2 cm is measured with two different payment reader. Encrypted data can be send also contact-based to other devices, like the BLE controller. Adding different sensors to the existing system is as well possible, thanks to the various interface types of the BLE controller from Nordic Semiconductor. According to the energy harvesting aspect and the utilized method with photovoltaic cells, the approach should be reconsidered due to its inefficiency. Selecting other photovoltaic cells for indoor applications or other harvesting IC's can may be solve the energy harvesting issues for this wearable.

According to the various findings at the prototypes, the extended software was skipped due to lack of time. Therefore, the final wearable device only provides the basic features.

7.1.1 Outlook

Further improvements could include a redesign by adding gyroscopes and accelerometers to enhance moving artefact elimination by using the heart rate sensor. Also, a miniaturization of the PCB can be applied. Therefore, the compromise solution with a

smart card chip module on the top layer instead of the package chip solution can be eliminated. Currently, the assembled chip offers all requirements for interfaces and software applications. An extension of the software can be done by implementing connection handling, encrypting and data analysis from the heart rate sensor. Increasing the base station structure with the Raspberry Pi's can be changed or enhanced with a third device, which acts as master to collect all informations about wristbands from all the other nodes in a room or a building.

According to the performance, future work could include further software implementation, hardware analyzation and testing to improve the power management to extend the life time of the wristband. If this device should be used in any way as a medical device, a redesign of the hardware and also a change in software would be in order to fulfill the European MDD 93/42/ EEC and the standards of the EN-60601.

Appendix

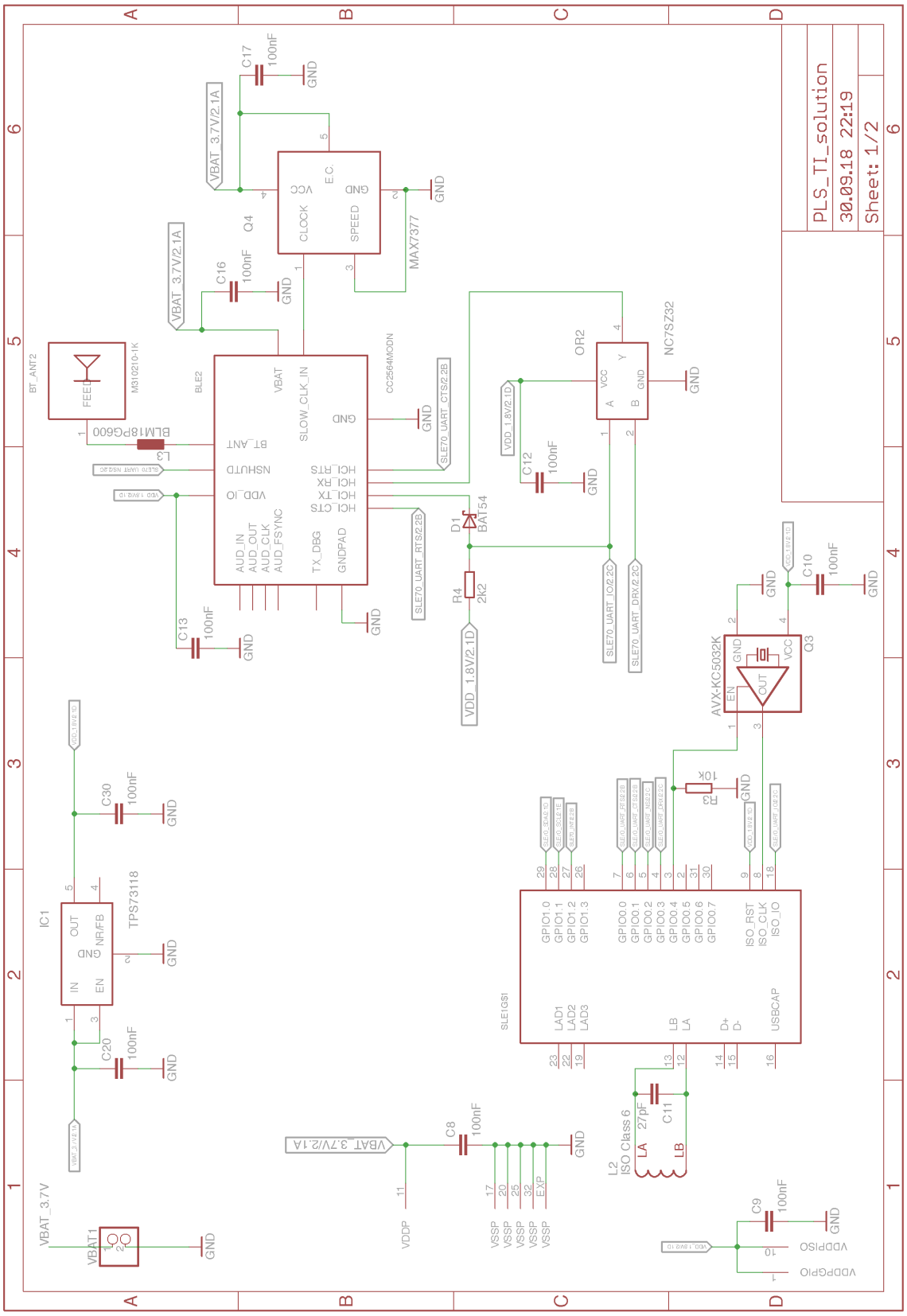

Figure .1: First concept

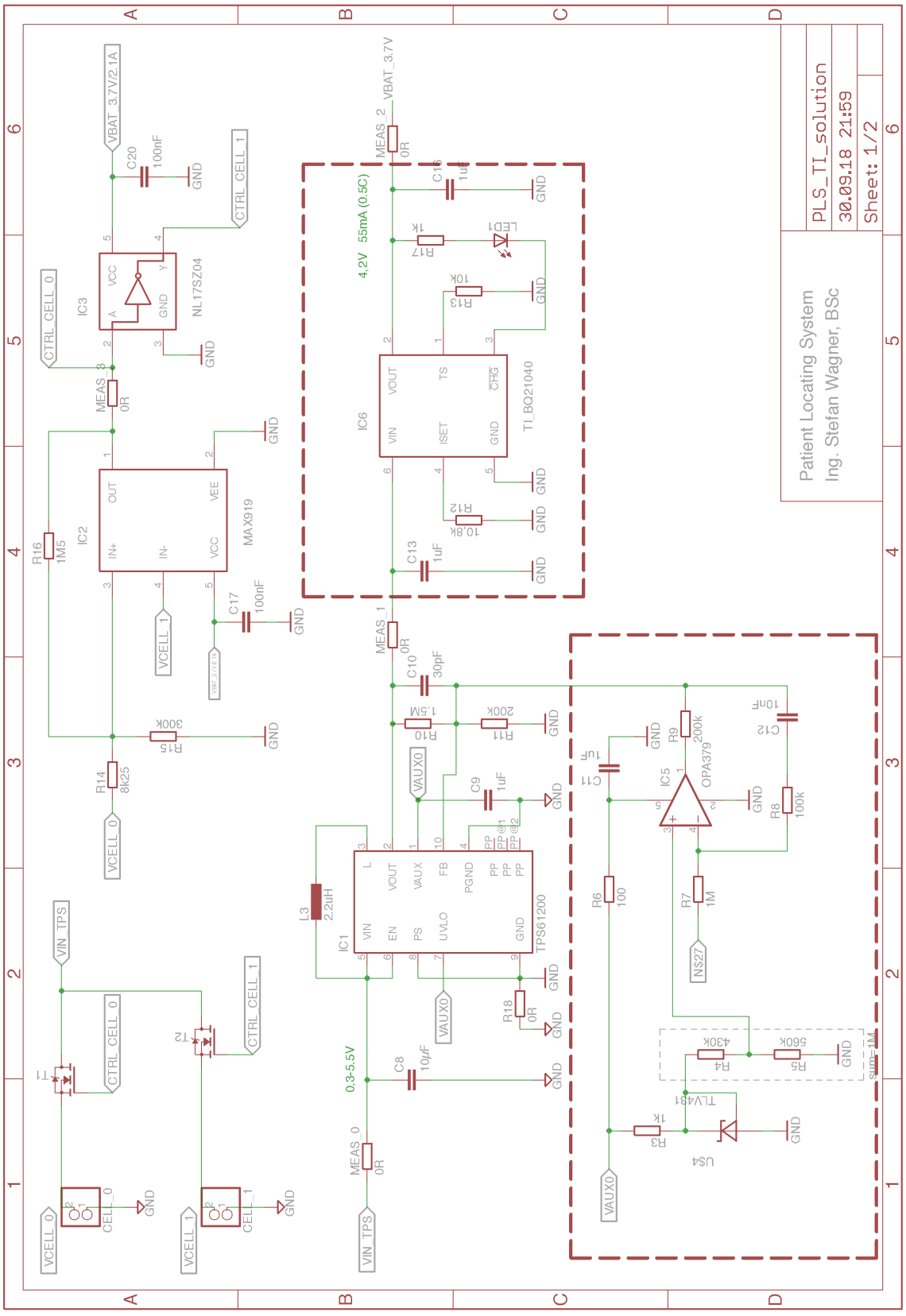

Figure .2: First concept

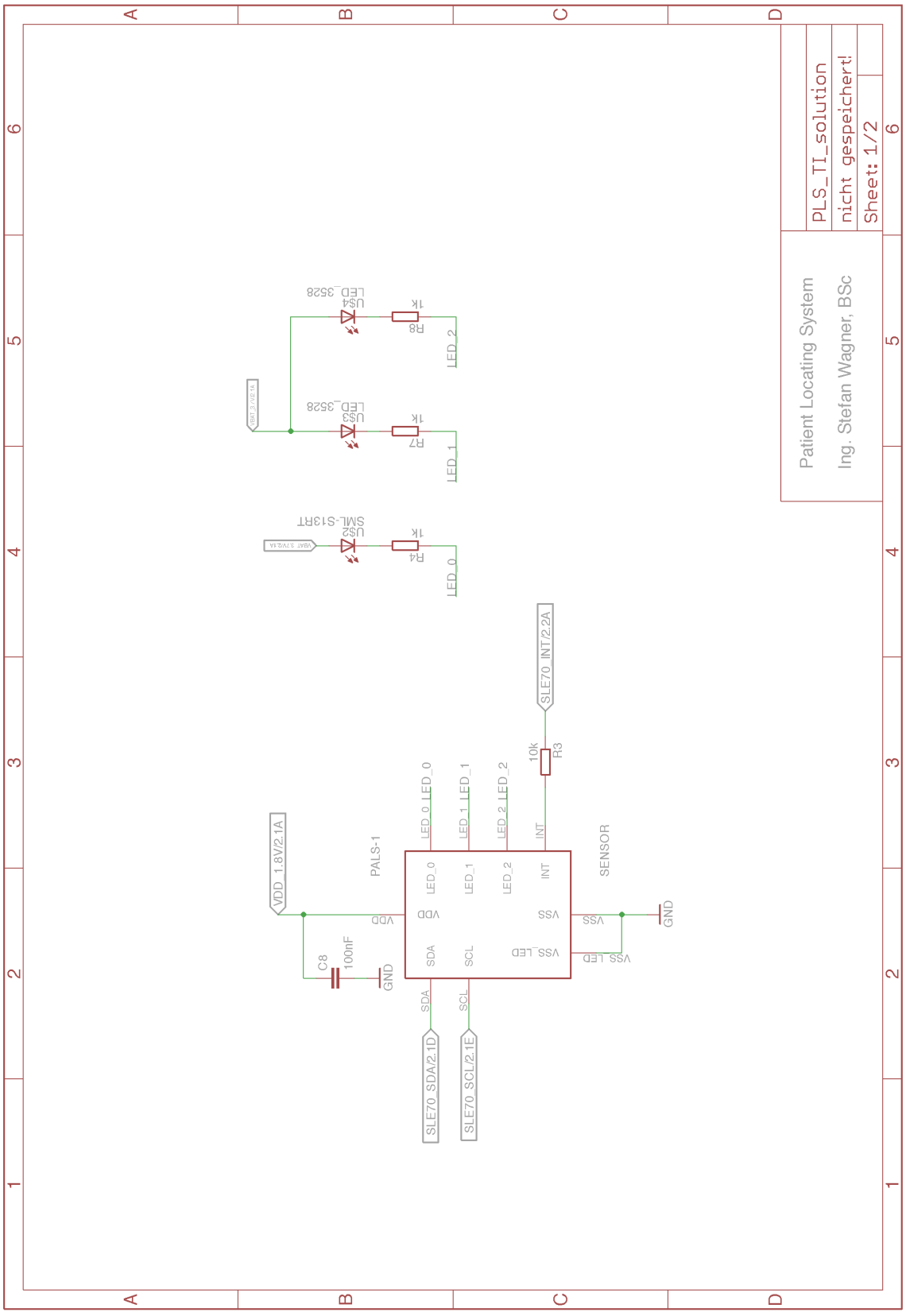

Figure .3: First concept

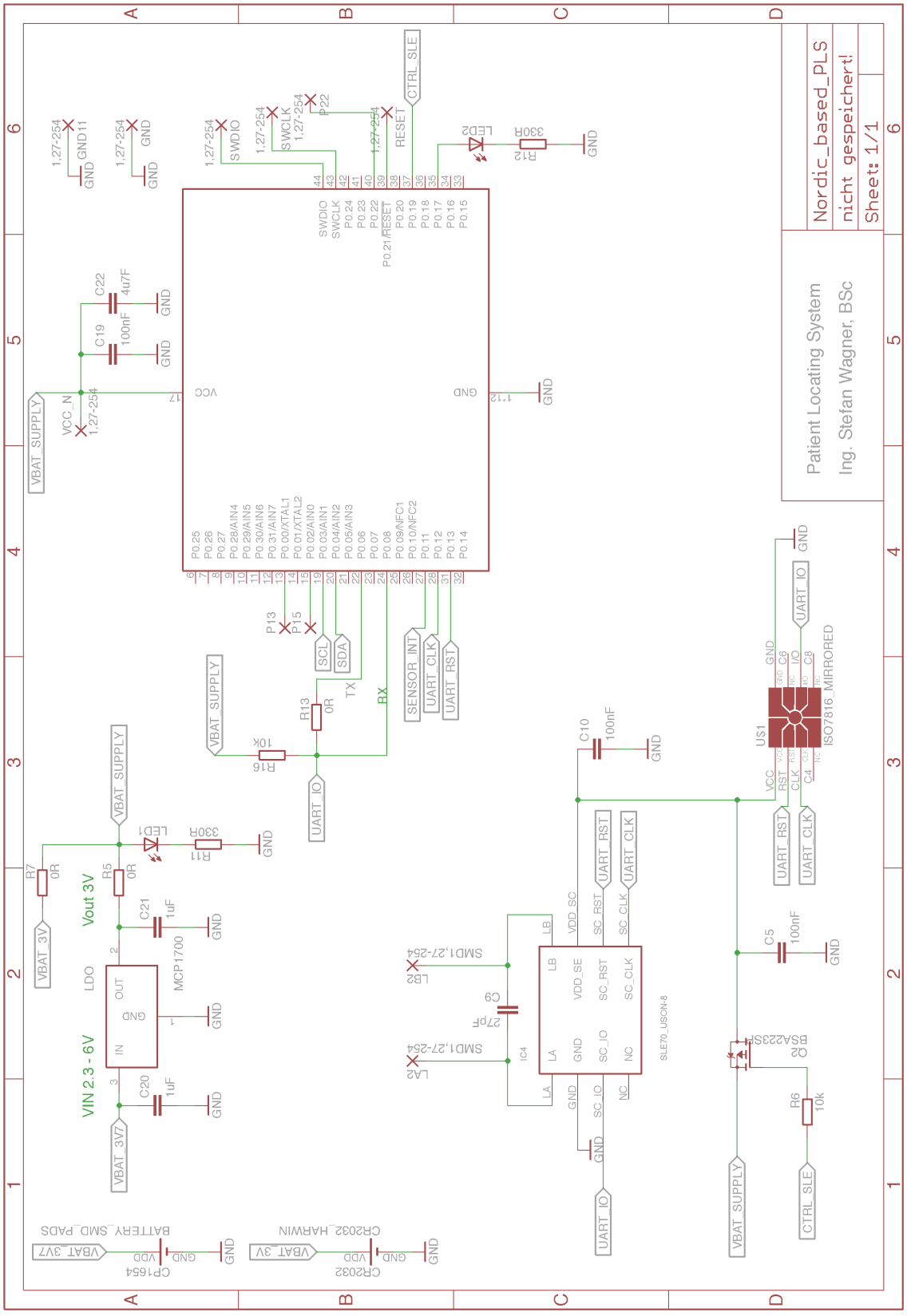

Figure .4: Second concept

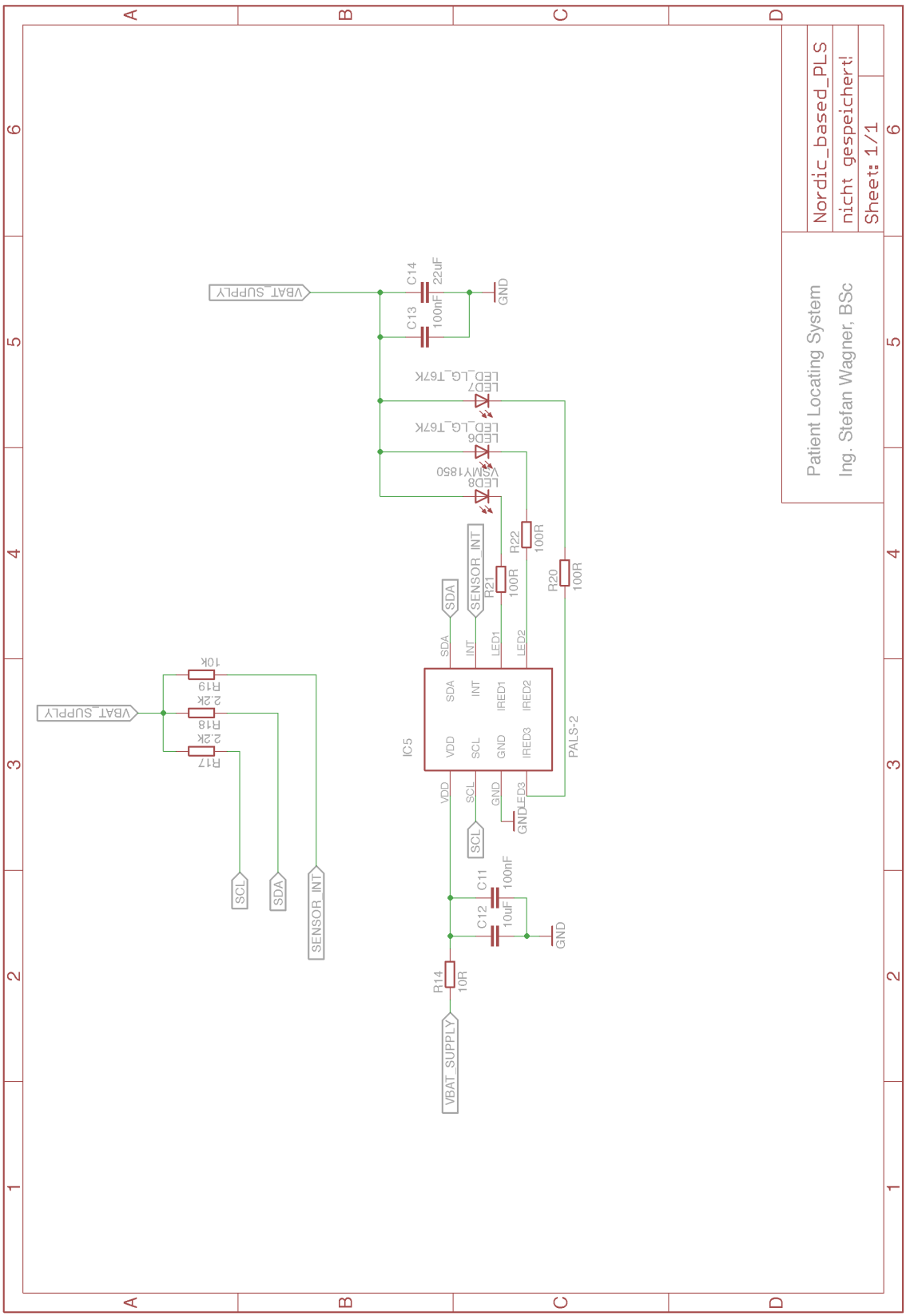

Figure .5: Second concept

Bibliography

[1] M. Alhawari et al. *Energy Harvesting for Self-Powered Wearable Devices*. Springer, 2018 (cit. on pp. 27, 28, 30–33).

[2] Zigbee Alliance. *Official Zigbee Alliance Website*. Sept. 2018. URL: https://www.zigbee.org (visited on 09/09/2018) (cit. on p. 5).

[3] Apple. *Official Apple Website*. Sept. 2018. URL: https://www.apple.com/at/watch/ (visited on 09/09/2018) (cit. on p. 2).

[4] CARE Medical History Bracelet. *CARE Medical History Bracelet*. 2018. URL: http://medicalhistorybracelet.com (cit. on p. 2).

[5] D. Briand, E. Yeatman, and S. Roundy. *Micro Energy Harvesting*. Wiley-VCH, 2015 (cit. on pp. 28–30).

[6] Cabot. *BLE vs Wi-Fi: Which is Better for IoT Product Development*. Sept. 2018. URL: https://www.cabotsolutions.com/2018/02/ble-vs-wi-fi-which-is-better-for-iot-product-development (visited on 09/09/2018) (cit. on p. 6).

[7] L. Cadmus-Bertram et al. "Use of the Fitbit to Measure Adherence to a Physical Activity Intervention Among Overweight or Obese, Postmenopausal Women: Self-Monitoring Trajectory During 16 Weeks." In: *JMIR Mhealth Uhealth* 3.4 (Nov. 2015), e96. ISSN: 2291-5222. DOI: 10.2196/mhealth.4229 (cit. on p. 2).

[8] R. Caliò et al. "Piezoelectric Energy Harvesting Solutions." In: *Sensors (Basel).* 14.3 (Mar. 2014), pp. 4755–4790. ISSN: 1424-8220. DOI: 10.3390/s140304755 (cit. on p. 28).

[9] S. Chakkor et al. "Comparative Performance Analysis of Wireless Communication Protocols for Intelligent Sensors and Their Applications." In: *International Journal of Advanced Computer Science and Applications* 5.4 (Sept. 2014). ISSN: 2156-5570. DOI: 10.14569/IJACSA.2014.050413 (cit. on p. 5).

[10] Cisco. *IEEE 802.11 - The Internet Protocol Journal - Volume 5, Number 1*. July 2015. URL: https://www.cisco.com/c/en/us/about/press/internet-protocol-journal/back-issues/table-contents-21/ieee.html (visited on 09/09/2018) (cit. on p. 5).

[11] IEC- International Electrotechnical Commission. *IEC white paper - internet of things: wireless sensor networks*. [Online; accessed 29. Sep. 2018]. Sept. 2018. URL: https://www.iec.ch/whitepaper/pdf/iecWP-internetofthings-LR-en.pdf (cit. on p. 5).

[12] A. Dementyev et al. "Power consumption analysis of Bluetooth Low Energy, ZigBee and ANT sensor nodes in a cyclic sleep scenario." In: *2013 IEEE International Wireless Symposium, IWS 2013* (Apr. 2013), pp. 1–4. DOI: 10.1109/IEEE-IWS.2013.6616827 (cit. on pp. 5, 6).

[13] L. Dhakar. *Triboelectric Devices for Power Generation and Self-Powered Sensing Applications*. Springer, 2017 (cit. on pp. 28, 29).

[14] K. Finkenzeller. *RFID Handbook: Fundamentals and Applications in Contactless Smart Cards, Radio Frequency Identification and Near-Field Communication*. third edition. John Wiley & Sons, 2010 (cit. on pp. 14–24).

[15] fitbit. *Fitbit Official Site for Activity Trackers & More*. 2018. URL: https://www.fitbit.com/home (cit. on p. 2).

[16] Raspberry Pi Foundation. *Raspberry Pi — Teach, Learn, and Make with Raspberry Pi*. 2018. URL: https://www.raspberrypi.org (cit. on p. 49).

[17] C. Garcia-Perez et al. "Improving the efficiency and reliability of wearable based mobile eHealth applications." In: *Pervasive Mob. Comput.* 40 (Sept. 2017), pp. 674–691. ISSN: 1574-1192. DOI: 10.1016/j.pmcj.2017.06.021 (cit. on p. 1).

[18] *Gartner, Gartner Says 8.4 Billion Connected "Things" Will Be in Use in 2017, Up 31 Percent From 2016*. [Online; accessed 29. Aug. 2018]. Sept. 2018. URL: https://www.gartner.com/en/newsroom/press-releases/2017-02-07-gartner-says-8-billion-connected-things-will-be-in-use-in-2017-up-31-percent-from-2016 (cit. on p. 1).

[19] M. Gebhart. *RFID Systems (Lecture notes)*. Graz University of Technology, 2016 (cit. on pp. 21, 25).

[20] M. Haghi, K. Thurow, and R. Stoll. "Wearable Devices in Medical Internet of Things: Scientific Research and Commercially Available Devices." In: *Healthc. Inform. Res.* 23.1 (Jan. 2017), pp. 4–15. ISSN: 2093-3681. DOI: 10.4258/hir.2017.23.1.4 (cit. on pp. 2, 3).

[21] R. Heydon. *Bluetooth Low Energy: The Developer's Handbook*. Prentice Hall, 2012 (cit. on pp. 5, 9–13).

[22] Honeywell. *Medical Wristbands Ensure the Security of Patients Info | Honeywell - medical-wristbands-application-brief-en-a4.pdf*. Aug. 2015. URL: https://country.honeywellaidc.com/CatalogDocuments/medical-wristbands-application-brief-en-a4.pdf (visited on 09/09/2018) (cit. on p. 2).

[23] *ISO standards catalogue, 35.040.50 - Automatic identification and data capture techniquesn*. [Online; accessed 29. Sep. 2018]. Sept. 2018. URL: https://www.iso.org/ics/35.040.50/x (cit. on p. 14).

[24] R. S. H. Istepanian and T. M. Al-anzi. "m-Health interventions for diabetes remote monitoring and self management: clinical and compliance issues." In: *Mhealth* 4 (Feb. 2018), p. 4. ISSN: 2306-9740. DOI: 10.21037/mhealth.2018.01.02 (cit. on p. 4).

[25] E. Kleitsch. *Solarzellen*. [Online; accessed 14. Sep. 2018]. Sept. 2018. URL: https://lemo-solar.de/shop/solarzellen.php (cit. on p. 41).

[26] *Kyocera, Clock Oscillators - Surface Mount Type - Clock K-Series*. [Online; accessed 24. Sep. 2018]. Sept. 2018. URL: https://global.kyocera.com/prdct/electro/product/pdf/clock_k_e.pdf (cit. on p. 37).

[27] H. Lehpamer. *RFID Design Principles*. second edition. Artech House, 2012 (cit. on pp. 16, 17, 19, 20, 26, 27).

[28] N. Leitgeb. *Sicherheit von Medizingeräten: Recht - Risiko - Chancen*. Springer-Verlag, 2010 (cit. on p. 87).

[29] J. A. Mallow et al. "Using mHealth Tools to Improve Rural Diabetes Care Guided by the Chronic Care Model." In: *Online J. Rural Nurs. Health Care* 14.1 (2014), pp. 43–65. ISSN: 1539-3399. DOI: 10.14574/ojrnhc.v14i1.276 (cit. on p. 3).

[30] *Maxim Integrated, MAX7377*. [Online; accessed 24. Sep. 2018]. Sept. 2018. URL: https://www.maximintegrated.com/en/products/digital/clock-generation-distribution/silicon-crystal-oscillators/MAX7377.html (cit. on p. 37).

[31] *Maxim Integrated, MAX919 SOT23*. [Online; accessed 24. Sep. 2018]. Sept. 2018. URL: https://www.maximintegrated.com/en/products/analog/amplifiers/MAX919.html (cit. on p. 37).

[32] Mediaform. *Armilla Patientenarmbaender*. Nov. 2016. URL: https://www.mediaform.de/fileadmin/medizinprodukte/dokumente/kataloge/11-16-016_Katalogauskopplung_Armilla_BMM00201_WEB_Schutz.pdf (visited on 09/09/2018) (cit. on pp. 1, 2).

[33] *Microchip, MCP1700*. [Online; accessed 24. Sep. 2018]. Sept. 2018. URL: http://ww1.microchip.com/downloads/en/DeviceDoc/20001826D.pdf (cit. on p. 37).

[34] P. D. Mitcheson et al. "Energy Harvesting From Human and Machine Motion for Wireless Electronic Devices." In: *Proc. IEEE* 96.9 (Sept. 2008), pp. 1457–1486. ISSN: 0018-9219. DOI: 10.1109/JPROC.2008.927494 (cit. on p. 27).

[35] S. C. Mukhopadhyay. "Wearable Sensors for Human Activity Monitoring: A Review." In: *Sensors Journal, IEEE* 15.3 (Mar. 2015), pp. 1321–1330. ISSN: 1530-437X. DOI: 10.1109/JSEN.2014.2370945 (cit. on p. 27).

[36] K. Nair et al. "Optimizing power consumption in iot based wireless sensor networks using Bluetooth Low Energy." In: *2015 International Conference on Green Computing and Internet of Things (ICGCIoT)* (Oct. 2015), pp. 589–593. DOI: 10.1109/ICGCIoT.2015.7380533 (cit. on pp. 5, 6).

[37] *Nordic Semiconductor, nRF52 Online Power Profiler*. [Online; accessed 29. Sep. 2018]. Sept. 2018. URL: https://devzone.nordicsemi.com/b/blog/posts/nrf52-online-power-profiler (cit. on p. 5).

[38] *ON Semiconductor, NC7SZ32*. [Online; accessed 24. Sep. 2018]. Sept. 2018. URL: http://www.onsemi.com/PowerSolutions/product.do?id=NC7SZ32 (cit. on p. 37).

[39] *ON Semiconductor,NL17SZ04: Single Inverter*. [Online; accessed 24. Sep. 2018]. Sept. 2018. URL: http://www.onsemi.com/PowerSolutions/product.do?id=NL17SZ04 (cit. on p. 37).

[40] M. T. Penella-López and M. Gasulla-Forner. *Powering Autonomous Sensors: An Integral Approach with Focus on Solar and RF Energy Harvesting*. Springer Netherlands, 2011 (cit. on p. 32).

[41] Philips. *Philips Health Watch DL8790/00*. Sept. 2018. URL: https://www.usa.philips.com/c-p/DL8791_00/health-watch (visited on 09/09/2018) (cit. on pp. 4, 5).

[42] S. Priya and D. J. Inman. *Energy Harvesting Technologies*. Springer, 2008 (cit. on pp. 28, 31).

[43] P. P. Ray. "A survey on Internet of Things architectures." In: *Journal of King Saud University - Computer and Information Sciences* 30.3 (July 2018), pp. 291–319. ISSN: 1319-1578. DOI: 10.1016/j.jksuci.2016.10.003 (cit. on pp. 1, 3, 5).

[44] *Rigado, BMD-300 - Rigado*. [Online; accessed 24. Sep. 2018]. Sept. 2018. URL: https://www.rigado.com/products/modules/bmd-300 (cit. on p. 37).

[45] Samsung. *Official Samsung Website*. Sept. 2018. URL: https://www.samsung.com/at/wearables/ (visited on 09/09/2018) (cit. on p. 2).

[46] *Samsung SDI, Wearable Device Li-ion(Lithium ion) Battery Cell | Samsung SDI*. [Online; accessed 22. Sep. 2018]. Sept. 2018. URL: http://www.samsungsdi.com/lithium-ion-battery/it-devices/wearable-device.html (cit. on p. 40).

[47] G. Schreier. *Predictive Healthcare Information Systems (Lecture notes)*. Graz University of Technology, 2017 (cit. on p. 4).

[48] Verily Life Sciences. *Study Watch - Verily Life Sciences*. June 2018. URL: https://verily.com/projects/sensors/study-watch (visited on 09/09/2018) (cit. on p. 3).

[49] Bluetooth SIG. *Bluetooth Specification Version 4.2*. 2014 (cit. on pp. 10, 12, 66).

[50] *Texas Instruments, BQ21040*. [Online; accessed 24. Sep. 2018]. Sept. 2018. URL: http://www.ti.com/product/BQ21040 (cit. on p. 37).

[51] *Texas Instruments, CC2564*. [Online; accessed 24. Sep. 2018]. Sept. 2018. URL: http://www.ti.com/product/CC2564 (cit. on p. 37).

[52] *Texas Instruments, OPA379*. [Online; accessed 24. Sep. 2018]. Sept. 2018. URL: http://www.ti.com/product/OPA379?keyMatch=OPA379&tisearch=Search-EN-Everything (cit. on p. 37).

[53] *Texas Instruments, TPS61200*. [Online; accessed 24. Sep. 2018]. Sept. 2018. URL: http://www.ti.com/product/TPS61200 (cit. on p. 37).

[54] *Texas Instruments, TPS73118-EP*. [Online; accessed 24. Sep. 2018]. Sept. 2018. URL: http://www.ti.com/product/TPS73118-EP (cit. on p. 37).

[55] D. Thomas, E. Wilkie, and J. Irvine. *Comparison of Power Consumption of WiFi Inbuilt Internet of Things Device with Bluetooth Low Energy*. [Online; accessed 21. Aug. 2018]. 2016. URL: https://www.semanticscholar.org/paper/Comparison-of-Power-Consumption-of-WiFi-Inbuilt-of-Thomas-Wilkie/73cb7616c46a37df9db3783a51ddee4a059856 (cit. on pp. 5, 6).

[56] K. Townsend, R. Davidson, and C. Cufí. *Getting Started with Bluetooth Low Energy*. O'Reilly, 2014 (cit. on pp. 10–13).

[57] M. Usama bin Aftab. *Building Bluetooth Low Energy Systems*. Packt, 2017 (cit. on pp. 9, 13).

[58] *Varta, CoinPower CP 1654 A2*. [Online; accessed 22. Sep. 2018]. Sept. 2018. URL: https://products.varta-microbattery.com//applications/mb_data/documents/data_sheets/DS63165.pdf (cit. on p. 40).